ELELCTROOSMOTIC SEPARATION OF DOUBLE STRANDED DNA BY STEADY AND PULSED ELECTRIC POTENTIALS IN A MICROCHANNEL

A Thesis

Presented in Partial Fulfillment of the Requirements for the

Degree of Master of Science

with a

Major in Chemical Engineering

in the

College of Graduate Studies

University of Idaho

by

Keith Christopher

May 2014

Major Professor: Aaron M. Thomas, PhD

Authorization to Submit Thesis

The thesis of Keith Christopher, submitted for the degree of Master of Science, with a major in Chemical Engineering and titled "**Electroosmotic Separation of Double Stranded DNA by Steady and Pulsed Electric Potentials in a Microchannel**" has been reviewed in final form. Permission, as indicated by the signatures and dates given below, is now granted to submit final copies to the College of Graduate Studies for approval.

Major Professor:	_____	Date: _____
	Eric Aston, PhD	
Committee Members:	_____	Date: _____
	Aaron M. Thomas, PhD	
	_____	Date: _____
	Wudneh Admassu, PhD	
Department Administrator:	_____	Date: _____
	Wudneh Admassu, PhD	
Discipline's College Dean:	_____	Date: _____
	Larry Stauffer, PhD	

Final Approval and Acceptance

Dean of the College of Graduate Studies:	_____	Date: _____
	Jie Chen, PhD	

Abstract

Electroosmotic Separation of Double Stranded DNA by Steady and Pulsed Electric Potentials in a Microchannel

Here, the enhancement of the overall mass transfer and separation of double stranded DNA (dsDNA) in a microchannel using steady and pulsatile flow is studied. The degree of separation was seen to increase with oscillatory flow as compared to steady conditions. It was also observed that the separation improved with increasing oscillation amplitude until reaching a certain critical point when the oscillations were large enough to begin promoting mixing. The study achieves the initial goal of proof-of-concept of microscale separation through electroosmotic flows and furthers the effort of building a handheld 'lab-on-a-chip' device that could be used to rapidly analyze a variety of biomolecules.

Microchannel castings were made using polydimethyl siloxane (PDMS). A mixture of 10mer and 50mer dsDNA along with another mixture of 10mer and 100mer dsDNA were used to visualize the separations using epifluorescence microscopy. The observations were characterized using a spectrophotometer which utilized a program known as Avasoft 8. The peak-to-peak separation distance between the dsDNA species demonstrated a dependence on the microchannel geometry, the electrical double layer, and the amplitude of the oscillations. Numerical velocity profiles and concentration tracking plots were generated with COMSOL Multiphysics to provide further insight and understanding of the dependency of these characteristics on the separation process.

Acknowledgements

First, I would like to thank my major professor Dr. Aaron Thomas for his patience, support, guidance and overall assistance throughout the course of my Master's degree.

I would also like to thank Dr. Eric Aston and Dr. Vivek Utgikar for their assistance and advice through the complex circumstances that accompanied this project.

I have been fortunate to have the guidance of Gail Bergman and Margaret Baker with a special thanks to Dr. Wudneh Admassu who has been nothing but helpful throughout my time in the department of Chemical and Materials Engineering.

I am appreciative for the work that Dr. Cornelius Ivory for his help in developing the numerical model based on the experiment.

I would also like to direct another special thanks to Shawn Murphy and Jacob R. Bow for their assistance during the project and efforts in researching the parts necessary to construct the experimental apparatus, my gratitude knows no bounds.

I am also very grateful for the help I received from Dr. Dave Macpherson and Charles Cornwall, without them, the apparatus would have never been built.

Lastly, to my family, for their support throughout this project.

Table of Contents

List of Figures

List of Tables

Chapter 1: Introduction

Microfluidic systems were a topic of mild discussion when they first emerged in the 1970s but it was not until the development and integration of micro-electromechanical systems (MEMS) that the field became one of substantial interest. MEMS is the basis for 'lab-on-a-chip' technologies that seek to miniaturize chemical analytical systems [1-5]. These small wonders received even greater consideration upon the completion of the Human Genome Project (HGP) in 2001. Since then, the application of MEMS has flourished in the fields of biotechnology and medicine, being successfully implemented in both the detection of food-borne pathogens and in genetic diagnostics [6,7]. Humans have approximately 100,000 genes that could be tested to identify various diseases. There are currently hundreds of these diseases that are diagnosable by the analysis of nucleic acids, with the number rapidly rising [6,8]. The technological setup for such a 'lab-on-a-chip' would consist of nucleic acids on the scale of microns, which leads to the importance of characterizing the fluid flow on the microscale in these devices.

The implementation of microfluidics has several advantages [3] such as (1) a lightweight and compact design, (2) increased precision of operation, (3) high throughput per unit volume, (4) advanced heat and mass transfer, (5) laminar flow profile, (6) smaller amount of sample required per experiment, and (7) a lower cost of operation.

An obvious benefit of miniaturization is the reduction in the size of a device. On the microscale there is an almost complete eradication of turbulent flow thus enhancing the viscous effects needed to cause a discernible separation. Recently, there have been enormous developments made in the fabrication of MEMS equipment such as micropumps and valves [9]. These devices facilitate incorporating multiple operations on a singular chip such as the flow control, separation, and characterizing equipment necessary for "lab-on-a-chip" systems. However, this introduces a dependence on the performance of these mechanical aspects of the design, which are prone to failure due to small fabrication defects and fatigue [10]. In this case, an array with no physically moving components would be the

most robust system. Such a system can be achieved with the integration of an applied electric field to pump the fluid in the microchannel using electrokinetic phenomena [11,12].

In the case of fluid flow in microchannels, electrokinetic phenomena refer to the interactions of the applied electric field and the movement of the colloidal fluid system that can be separated into four discernible categories: electroosmosis, electrophoresis, streaming potential, and sedimentation potential. Electroosmosis is defined as the motion of fluid flow produced by the applied electric field on an ionized fluid. Electrophoresis is the motion of charged particles in reference to a stationary fluid. Streaming potential is the potential induced by the movement of fluid near an interface. Sedimentation potential is the potential induced by the movement of charged particles [12] in a gravity or inertial field. The focus of this thesis is the application of electroosmotic flow (EOF) for the separation of biomolecules. However, since DNA is inherently negatively charged, there is still an application of electrophoretic transport. The electroosmotic-electrophoretic flows work in tandem to achieve the electrokinetic transport; however, the electroosmotic flow is often the dominant force since the resultant flow is cathodic.

Electrical Double Layer

Although the phenomenon of electroosmosis has been known for over two centuries, its application in the microscale transport of biological species has only recently been studied [13]. The process is known to be driven by the effect of the electrical double layer (EDL) which is caused by the surface charge induced when a polar medium is introduced into the system due to either ionization, ion adsorption, or dissolution. This imposes an ion distribution in the medium and forms the EDL through the net effects of electroneutrality and chemical potential gradient constraints [14,15]. In the present study, when glass or polydimethylsiloxane (PDMS) comes into contact with an aqueous solution there is a net negative surface charge due to ion adsorption and the dislocation of hydroxyl groups, which can be seen in Figure 1.1.

The EDL, illustrated in Figure 1.1, is the region closest to the charged surface where co-ions and counter-ions are distributed such that the net charge density is not equal to zero locally, even though the net charge is zero in the bulk medium. The negatively-charged wall attracts positive ions that are then fixed to the surface and are collectively known as the Stern layer. It has a thickness roughly equivalent to the diameter of the adsorbed ions. The next layer contains mobile ions that are susceptible to electrokinetic transport and is known as the diffuse layer. This layer stretches from the edge of the Stern layer and ends once the net charge density is equal to zero. The electric potential imposed by the nonzero charge density at the slip plane of the Stern layer is known as the zeta potential (ζ).

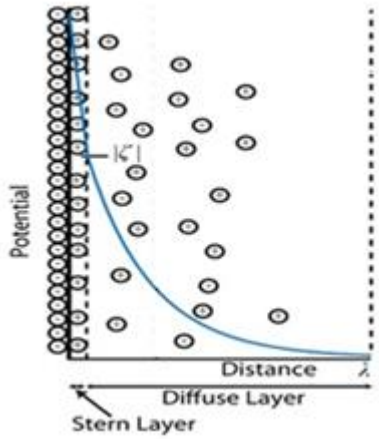

Figure 1.1 The electric double layer (EDL) and the corresponding zeta potential trend.

The surface potential is at a maximum at the wall due and the potential in the fluid decreases exponentially to zero at the end of the diffuse layer. The distance from the wall to the edge is characterized in thickness by the Debye length (λ) . Past this point the zeta potential no longer influences the arrangement of the positive and negative ions, meaning that the rest of the solution is electrically neutral. When the electric field is applied across the system (orthogonal to the walls in this thesis), a force is exerted on the ions in the diffuse layer resulting in the electrokinetic motion. The fluid motion results in the movement of the entire solution as the bulk material is “dragged” along due the friction from viscous forces. This motion is the principle result of electroosmosis [15].

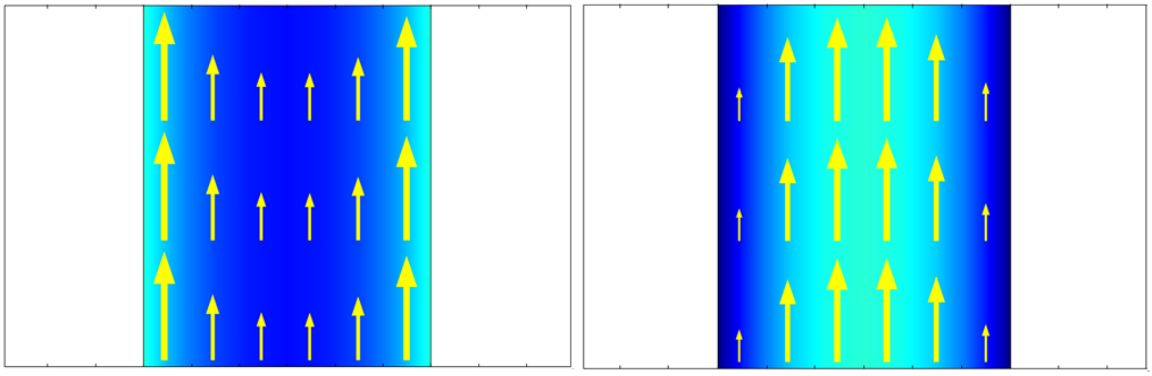

Figure 1.2 EOF velocity profile (left) and the pressure driven flow velocity profile (right) with scaled velocity arrows.

As shown in Figure 1.2, electroosmotic flow differs from pressure-driven flow in that the driving force for EOF originates in the EDL near the wall, while in pressure-driven flow the driving force applies normally across the entire cross-section.

Background

Before discussing the more recent developments in electrokinetic phenomena, it is worth reviewing briefly the origins of the subject. The first example of flow induced by the application of an electric field was reported by Reuss in 1808 [16]. Nearly half a century later, Wiedmann [17] performed several sets of experiments and postulated a theory that still serves as a fundamental basis for electrokinetics: the volumetric electroosmotic flow is proportional to the current that is applied to the system. It was not until 1879 that Helmholtz developed the electrical double layer model [18]. Later in 1910, Gouy [19] introduced a more realistic concept of the potential and charge distribution in the fluid directly adjacent to the capillary wall. Debye and Hückel expanded on this notion in 1923 when they determined the ion distribution in low ionic energy solutions by means of the Boltzmann ion energy distribution [20]. Finally, the last major development came the year following when Stern unified the theories put forward by Helmholtz and Gouy [21]. The Stern model suggested that some of the ions adhere to the capillary wall or electrode, yielding the Stern layer, and some compose the diffuse layer, which is free to move.

Since these disciplinary breakthroughs, the field of electrokinetics has had little progress except for some minor improvements in theory. However, there have been a number of developments in the application of electrokinetics to microfluidic separations and phenomena that develop in such a system. The separation of species in a microfluidic system is not straightforward. Dispersion or band-broadening will reduce the relative separation of the process, especially in an electroosmotically-driven situation [22,23]. Dispersion in pressure-driven flows, both steady and oscillatory, have been studied extensively since the works of Aris [24] who developed the dispersion coefficient of an inert solute using the method of moments. Work pioneered by Taylor who studied the increased diffusion of a solute in laminar flow through a tube [25]. Taylor, a pioneer in the matter of dispersion [26, 27], studied the effects further and conceptualized the basic mechanism that contributes to the enhanced diffusion, now known as Taylor dispersion. The mechanism itself consists of molecular diffusion occurring across lateral concentration gradients created by nonuniform velocity gradients, meaning that a sharper velocity gradient across the channel can result in a greater dispersion effect. This explains why the dispersion is typically seen to increase with the electric field since the stronger the applied potential, the broader the EDL, which in turn decreases the span of the plug flow.

Another extensively studied phenomena of EOF in microchannels is that of Joule heating and viscous dissipation. The driving force of electroosmosis is produced by the application of a high external electric field across the channel. This results in Joule heating that arises from two effects: the convective electric current and the conductive electric current. However, the significance of the Joule heating effect depends on the volume of the channel itself. Lim et al. [28] demonstrated that improving the heat dissipation of the system, by implementation of fins or simple changes in the topology, reduced the temperature gradient across the channel. Later, Swinney and Bornhop [29] showed that for a system involving capillary electrophoresis, even for low electric field strengths (≈475V/cm), resulted in an overall temperature increase of nearly 3^{o}C above the ambient. The other aforementioned form of energy generation within the system is viscous dissipation, which is when the work

done by a fluid is transformed from action due to shear forces into heat. This led to the evaporation of the fluid in the microchannel and also caused a hindrance in the fluid flow, thus slowing the transport of the species. The effect of the viscous dissipation in microchannels was characterized by Koo and Kleinstreuer [30] with various working fluids. Their numerical analysis revealed that in the situation with pressure-driven flow, fluids with low specific heat capacities and high viscosities were more prone to considerable viscous dissipation effects. The consequences of viscous dissipation can lead to extensive fluctuations in the separation of biomolecules due to the possibility of evaporating the working fluid and causing pressure heads throughout the microchannel. However, for situations involving electroosmotic flow, which is seen in the experimental work in this thesis, there is a small amount of work done on the viscous dissipation in the system due to the typically small EDL compared to the channel width [31] thus eradicating this issue.

The field of DNA electromigration separations in capillaries has become one of the most investigated applications for microfluidic devices especially due to the fact that it is one of the most viable methods for rapid DNA sequencing [32]. To understand the relationship between DNA migration and various experimental parameters, such as applied voltage biased or the dependence on mobility, Ling et al. [33], Duong et al. [34], and Allison et al. [35] investigated the migration of DNA. Ling et al. theorized that at high voltage, the velocity of the species is a linear function with respect to the applied electric field, while at lower voltages there are deviations from this trend. Duong et al. investigated the size dependency of the electrophoretic migration of DNA while in a free solution where it was seen that the smaller of the two species (48,000 base pairs) migrated faster than the larger (164,000 base pairs). Allison et al. modeled the migration of DNA based on varying elements such as the translational diffusion and electrophoretic mobility for a rigid rod model of DNA. The understanding of these properties in various systems has assisted in the endeavor to construct the ‘lab-on-a-chip’ devices that this thesis strives toward, an example being a microfluidic DNA sequencing device to be implemented in the field of forensic genetics [36], or another for the diagnosis of skin diseases [37].

Although much of microchannel development was innovative, the application of oscillatory flow was taken from prior examples where it was demonstrated to enhance the mass transfer and was originally used to separate gaseous species in larger tubes instead of microchannels. The first example of this application was demonstrated by Harris and Goren in 1967 [38]. An example was later developed by Kurzweg and Jaeger in 1987 [39] and showed that with the addition of sinusoidal oscillations, the separation of gaseous mixtures can be enhanced using what can be classified as "cross-over" phenomena, where the species that typically diffuses slower is shown to travel faster (with respect to net total displacement) than the traditionally "fast diffusing" species under certain frequencies and amplitudes. This concept was further expanded in the works of Thomas [40,41] and Thomas and Narayanan [42,43] who constructed a system to separate gases for air revitalization processes that could be utilized in life-support systems in space. They also demonstrated the effects of oscillations in boundary layer-driven and pressure-driven flows. In their studies, they identified three dimensionless parameters that are fundamental in the understanding of oscillatory flow trends: the Womersley number (W), which is the ratio of viscous diffusion time scale to the oscillatory time scale, the Schmidt number (Sc), which is the ratio of species diffusion to viscous diffusion time scales, and the length ratio of the oscillation amplitude to the channel width. Unfortunately, with the exception of the works by Chen et al. [44], Erickson and Li [45], and Ramon et al. [46], little work has been committed towards the understanding of the fundamentals of the use of oscillatory flow in EOF.

This leads to the present study that is a continuation of the works by Timothy Aldridge [47] and Parameswara Subramanian [48]. Mr. Aldridge's thesis was on the use of oscillating EOF in microchannel separations of various dye mixtures, laying the basic groundwork for future projects. He also utilized polydimethylsiloxane (PDMS) as a means of microchannel fabrication, explored the possibility of using enhanced separation of biomolecules, and developed theoretical velocity and mass transfer profiles that were further refined by Mr. Subramanian. Mr. Aldridge demonstrated that the separation of dye mixtures was increased

utilizing an AC field over a pure DC field. This then led to the exploration of the separation of other species, specifically biomolecules.

Parameswara Subramanian furthered Mr. Aldridge's work in researching the separation of ssDNA (10mer and 50mer). His results showed that for certain voltage-frequency combinations, the separation of the ssDNA did increase as compared to some of the steady flow situations, whereas other combinations faltered. He also noticed that the efficacy of the separation was dependent on the width of the microchannels used, meaning that the smaller the channel width, the better the separation of the species.

Mr. Subramanian made several suggestions for future projects in the endeavor to better understand the fundamentals of the utilization of oscillatory flows to enhance the separation of biological species in microchannels via electroosmotic flow, the first being that the departure of the oscillatory trends be investigated. It was never determined why some of the frequency-voltage combinations became less efficient than others; the only suggested solution was that there was an increase in the dispersion of the biological species. His second suggestion was that the separation trends of variously sized species be tested (i.e. a 10mer and a 50mer and another set of experiments with a 10mer and a 100mer) or that the separation is tested with a strand of ssDNA and a strand of dsDNA so as to understand the effect on the combination of different biomolecules being very different in configuration. It was also recommended that the testing apparatus should be further optimized for the application of these specific experimental studies rather than using several programs to analyze data to reduce the error associated with his system. Finally, he suggested that a numerical model be generated for the purpose of visualizing the simultaneous interactions of the velocity profile, concentration progression, and the mass transfer within the system. All of these suggestions were taken into account when designing the current project and all were addressed. This thesis discusses the construction of the numerical model (Chapter 2), the assembly of a new experimental apparatus (Chapter 3), the separation of variously sized dsDNA, and the study to explain the decline in separation efficacy in the oscillatory trend.

Chapter 2: Theoretical

Previous work by Parameswara Subramanian developed an analytical model of electroosmotic flows by deriving the velocity profile and overall mass transfer assuming that DNA was an uncharged species. This means that the only part of the solution that carried an electrical charge was the buffer itself. This is sufficient to demonstrate the characteristics of the electroosmotic flow since the charged DNA does not appreciably affect the diffuse layer and zeta potential near the walls of the microchannel. There are multiple plots in Subramanian's data; all are dependent on the variation of two parameters, the dimensionless Debye length (λ^*) and the Womersley number (W). The dimensionless Debye length provides a means to describe the thickness of the diffuse layer in relation to the overall height of the channel. The Womersley number describes the magnitude of the oscillatory flow behavior. The larger the Womersley number, the greater the pulsatile behavior.

$$\lambda^* = h \cdot \sqrt{\frac{2z^2e^2n_\infty}{\varepsilon k_B T}} \qquad 2.1$$

$$W = h \cdot \sqrt{\frac{\omega}{\nu}} \qquad 2.2$$

Where,

h – Channel height

z – Species valency

e – Charge of a single electron

n_∞ – Ionic concentration

ε – Permittivity of the medium

k_B – Boltzmann constant

T – Absolute temperature (K)

ω – Oscillation frequency

ν – Kinematic viscosity of the buffer

The next progression was to build a numerical model that more closely describes the sequence of events in the experimental procedure, which is found in its entirety in Appendix E. The software used to produce the model was the finite element program COMSOL Multiphysics version 4.3. For the purpose of this thesis, a 2D model was sufficient to generate the data necessary for a velocity profile, the concentration progression over time, and a model of the expected changes in mass transfer from steady flow to oscillatory flow. The model was constructed to simulate the separation of an oligonucleotide with 10 base pairs (the 10mer) and a second oligonucleotide with 50 base pairs (the 50mer).

It should be mentioned that the COMSOL simulation does not take into account the shape of the dsDNA. The 10mer is small enough to be considered a rigid rod in reality, and the 50mer is long enough to exhibit conformational folding into a tertiary structure due to hydrogen bonding interactions. In the case of a nucleic acid with a length longer than the 50mer (i.e. the 100mer), the structure may even become deformed enough to fold into itself which may result in various geometries: cylindrical, spherical, elliptical, etc. COMSOL approximates the species to essentially be spherical. However, this may have a significant influence on the migration of the species, specifically if the larger dsDNA is on the same order of magnitude as the Debye length, it may prevent the species from sampling the rapidly changing velocities near the wall that a smaller species could more easily sample in the oscillating flow. The movement into an out of varying flow velocities is what will dictate the mass transfer and separation of species as has been seen by previous authors in gas separations.

Assumptions

The system considered is a 2D, rectangular microchannel which is illustrated in Figure 2.1, and the geometric parameters pertaining to the system are listed in Table 2.1. It was assumed that the flow of the DNA in the main channel was governed by EOF. This is due to the electroosmotic force that carries the DNA to the anode (which is situated in the bottom buffer well, whereas the cathode is situated in the top buffer well).

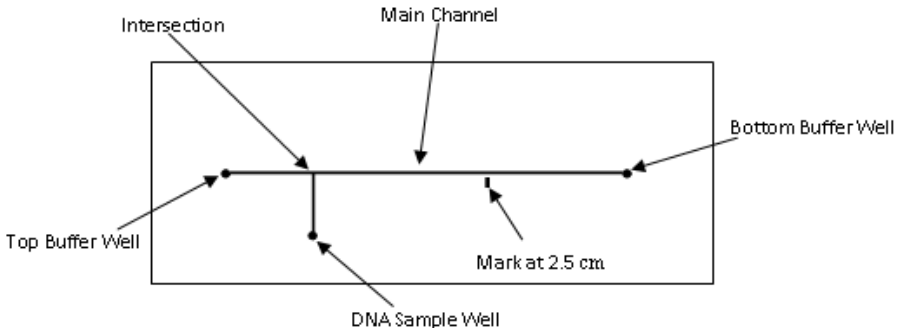

Figure 2.1 Illustration and nomenclature of the microchannel components used in this thesis.

Parameter	Value	Description
Lmain	5 [cm]	Length of main channel
W	60 [µm]	Width of main channel
depth	60 [µm]	Width of sample arm
Lside	1 [cm]	Length of side channel

Table 2.1 Dimensional values of the microchannel used in the numerical model.

The system was assumed to be isothermal, and the Reynolds number to be very small $(Re \ll 1)$ so that the creeping flow module was applicable. The assumption of creeping flow is valid due to both the low velocity of the species and the small (on the order of microns) diameter of the microchannel. There was also the assumption of the shallow channel approximation since it was the basis of the main driving force of the electroosmotic flow. The pressure head was assumed to be equalized once plug flow had developed in the main channel so that the only driving force was the EOF.

COMSOL Multiphysics Numerical Model

In order to understand the numerical model, a brief description of the experimental procedure is necessary. The experimental procedure developed for this project is very similar to that used by Mr. Subramanian with the exception that there were two sample arms in his microchannel design instead of one. This geometrical change allowed the procedure to remain similar while allowing for a reduction of the amount of required sample, while also minimizing the potential pressure gradient from sample well to sample well. An illustration of the channel that Mr. Subramanian used can be seen in Figure 2.2.

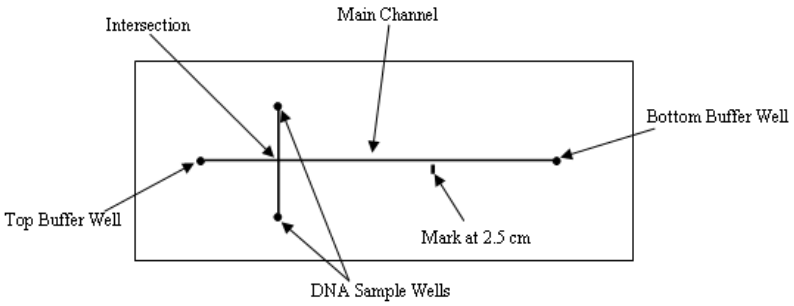

Figure 2.2 Illustration and nomenclature of the microchannel components used by Mr. Subramanian's.

First, the experiment begins with the entire microchannel filled with a 1xTE buffer. The DNA is then added to the DNA sample well, forming a slight pressure head that is needed to force the DNA into the main channel. Once there is a sufficient amount of DNA in the main channel, an additional amount of TE buffer is injected into the top sample well. This step forces the DNA down the main channel slightly and pushes the residual DNA back up the side channel, illustrated in Figure 2.3. If the residual DNA was left in the main channel, it would cause the plug to be continuous which would prevent the formation of a single plug for separation study.

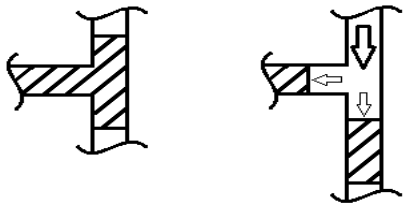

Figure 2.3 Plug formation step.

After the pressure head equalizes, the electric current is applied across the main channel and the sample starts to migrate towards the cathode via the electroosmotic force. A timeline over which these events occur are listed in Table 2.2. The observation point to analyze the separation of the species is found 2.5cm from the intersection of the main channel and the sample arm. This point was chosen so that the plug had enough distance to sufficiently separate consistently. Also, since the plug formation was not always at the same starting position (error was roughly ±2mm); the distance was long enough to minimize the

error in migration time and migration length. If the analyzation point was any further down the main channel, there was an inherent risk of the buffer wells drying out due to the added time associated with a longer migration distance; this adds a pressure gradient across the channel that alters the results. After roughly 3-6 minutes under the influence of the EOF, both species passed through the analyzation point and had their concentrations recorded continuously. Further discussion of the software and procedure can be found in Chapter 4.

Time (s)	Event
0-305	DNA seeps into main channel
305	Pressure head added to top sample well to form plug
305-335	Plug forms in main channel, residual DNA force back to DNA sample well
335	Pressure assumed to be equalized, electric current turned on
335-900	Electroosmotic force carries and separates DNA down the main channel

Table 2.2 Timeline for events in numerical model.

During the course of the construction of the numerical model, several properties had to be calculated, including the mobilities of each species and the zeta potential. These property values were derived from the experimental results in order to create the most realistic simulation possible. Other properties such as the initial pressure heads in each well had to be approximated in order to coincide with the formation of the plug for the experiment. Properties such the diffusivities of the species were calculated using existing values. The values for these properties can be found in Table 2.3. It should be mentioned that in an ideal situation, there would not be a pressure difference in the main channel and in the future, this type of approximation should be avoided. However, for this situation in which computer processing power was limited, it was the most efficient way to form the plug in the main channel and yielded a situation that was within the approximation of the model. Since the pressure head was relieved from the numerical model once the electromigration began, the pressure head bears no influence on the results after the 335s time step.

Parameter	Value	Description
sigma	975 [µS/cm]	Conductivity of TE buffer
zeta	0.1 [V]	Zeta potential
hDNA	1.5 [mm]	Pressure head in DNA sample well
hends	1 [mm]	Pressure head in bottom buffer well
htop	1.25 [mm]	Pressure head in top buffer well
hadd	4.9 [mm]	Pressure head added to form plug
epsilonr	75	Relative permitivity of medium
z10mer	1	Valency of 10mer
z50mer	1	Valency of 50mer
D10mer	120*10^-12 [m^2/s]	Diffusion coefficient of 10mer
D50mer	45*10^-12 [m^2/s]	Diffusion coefficient of 50mer
C10mer	15.15*10^-6 [mol/L]	Concentration of 10mer in DNA sample well
C50mer	4.55*10^-6 [mol/L]	Concentration of 50mer in DNA sample well
U10mer	2.052e-8 [1/T]/F_const	Calculated mobility of 10mer
U50mer	2.144e-8 [1/T]/F_const	Calculated mobility of 50mer

Table 2.3 Values and descriptions of properties used in simulation.

The numerical model depicted was for the simulation of the DC potential (steady flow) at a value of +125V. The results of the model are shown in varying time steps to show a representation of how the experiment progressed. The first few figures, (Figures 2.4, 2.5 and 2.6) show a “zoomed in” view to better articulate the formation of the plug in the main channel. Following that, the other images, (Figures 2.7, 2.8 and 2.9) show the progression of the two species through the channel. The view is skewed so that the main channel is the only visible area since there is no process occurring in the side channel. The image has also been stretched to better show the progression of the plug down the channel. It is however difficult to distinguish the two species since their concentration regimes overlap while they are separating down the channel. Although, in Figure 2.9, the separation of the species can be partially visualized as one of the species has progressed past the other where the overlapping region defaults to the background color in the microchannel.

It should be mentioned that for the simulations of the AC potential (oscillatory flow), Figures 2.3 through 2.5 are still applicable since the only difference between the models is the

electric potential applied across the channel at 335s into the simulations. The progression of the plug in AC potential is not shown; this is due to the large computing time necessary to simulate each time step when the potential changes continuously. For this reason, the simulated studies for the AC potentials were only done until the time step at 350s. The image depicting this time step is not shown since the AC model still appears identical to the DC model due to the small amount of time for the process to fully develop. However, this point proved to yield sufficient evidence of the difference in the mass transfer in the separation of the species which is discussed later on in this chapter.

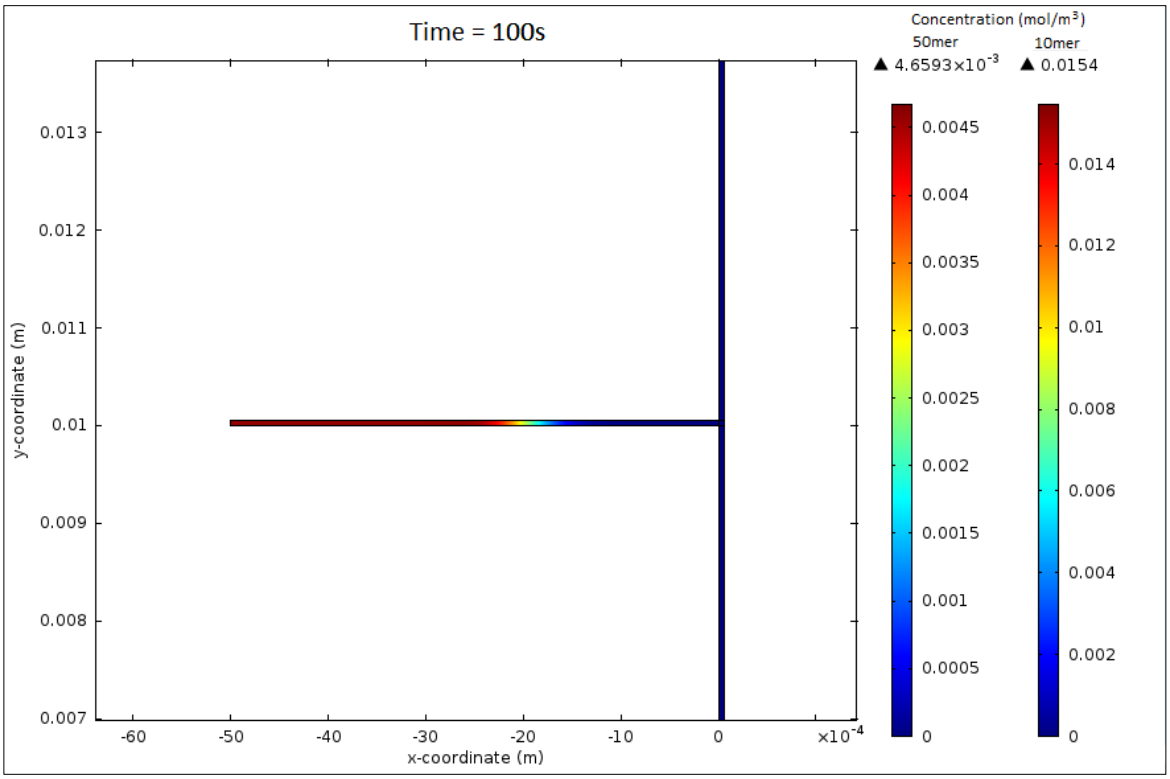

Figure 2.4 Concentration plot at t=100s.

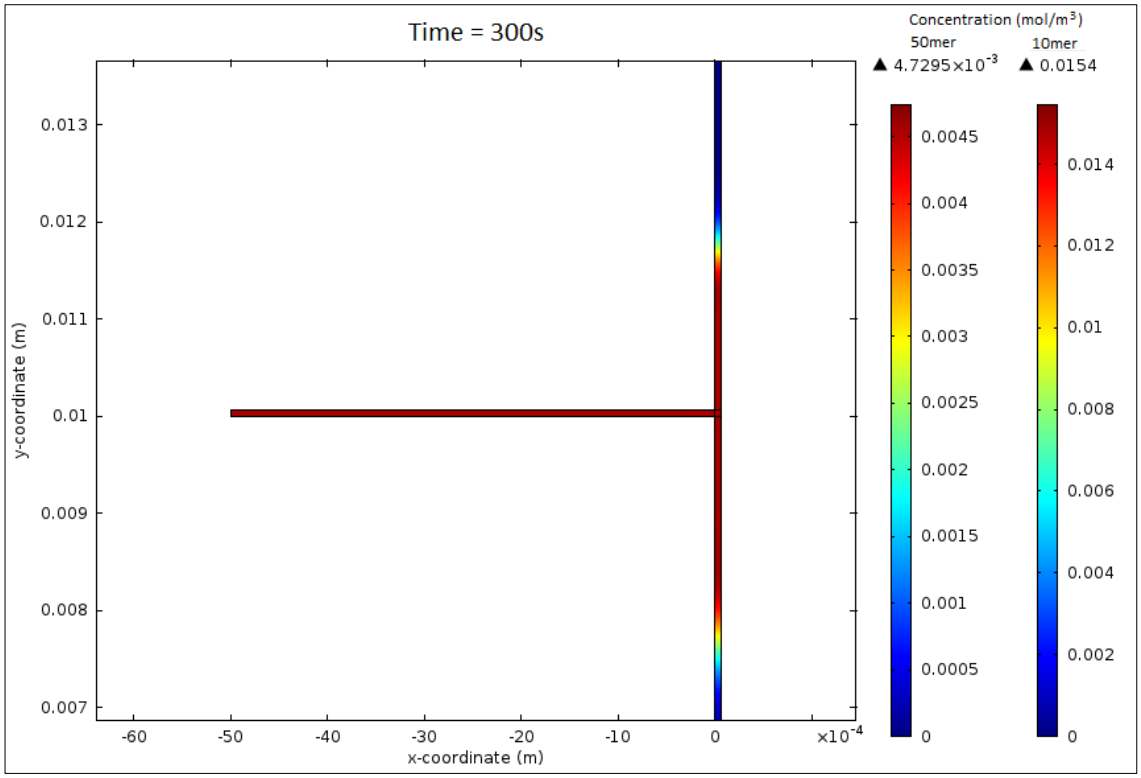

Figure 2.5 Concentration plot at t=300s.

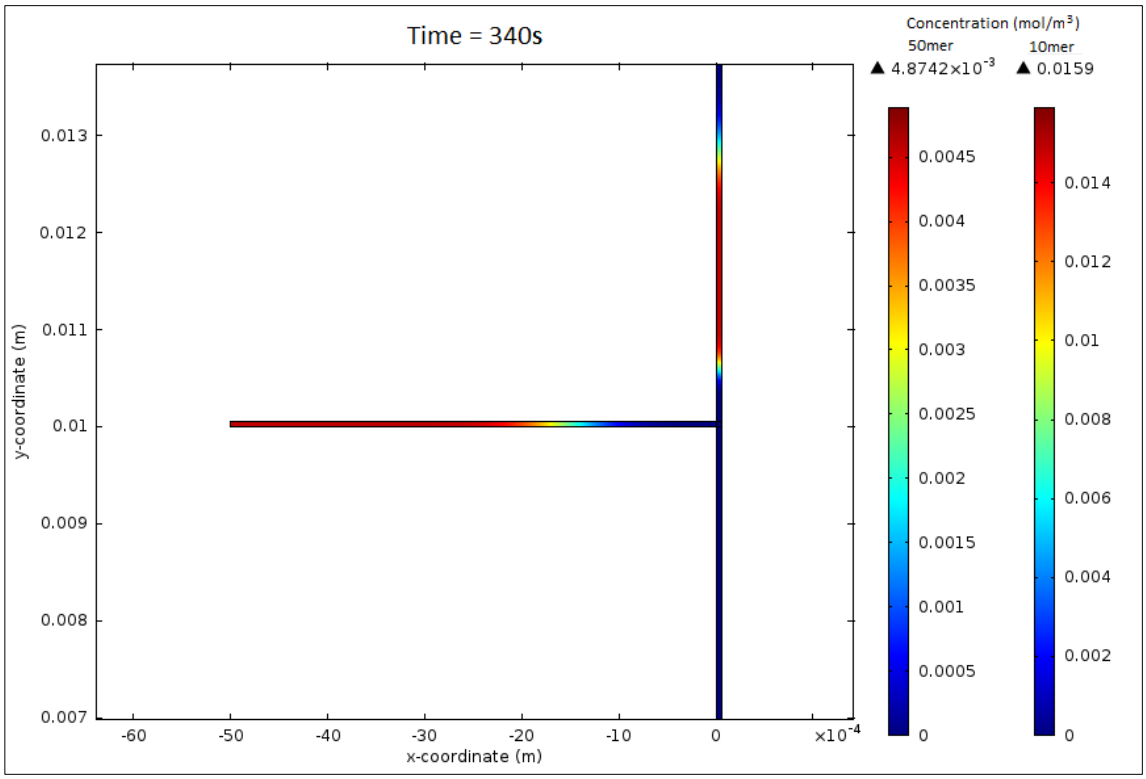

Figure 2.6 Concentration plot at t=340s.

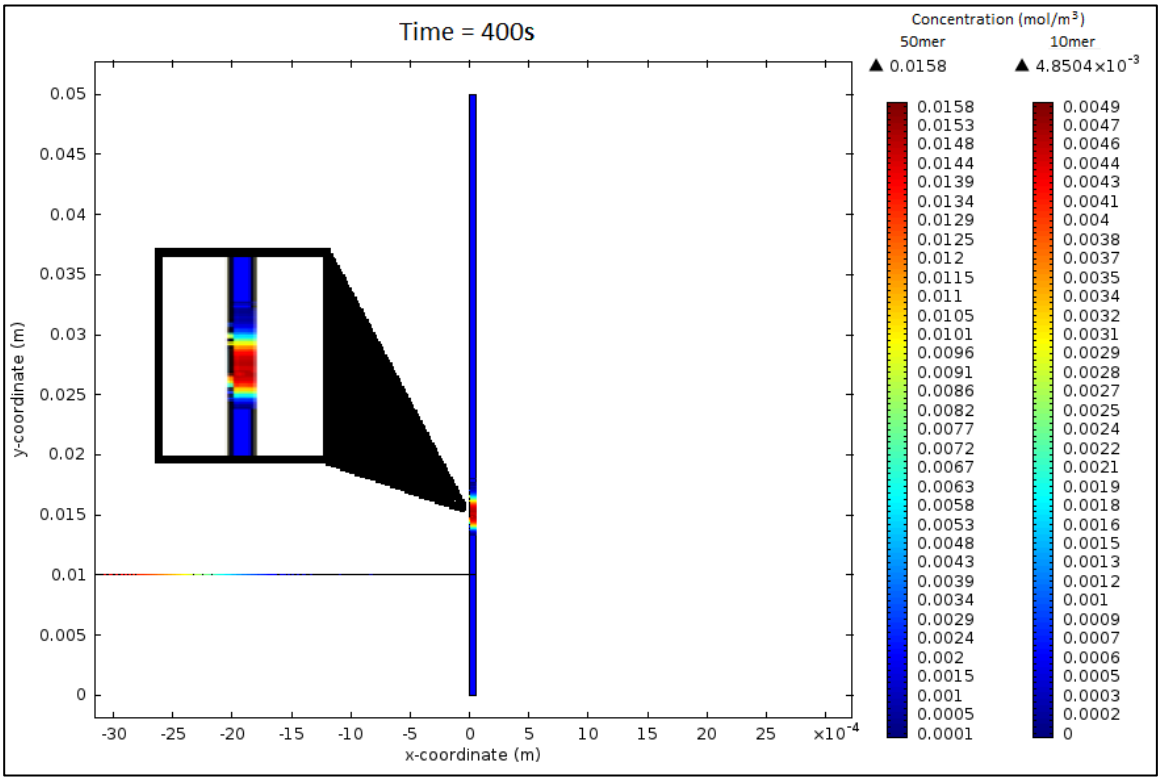

Figure 2.7 Concentration plot at t=400s.

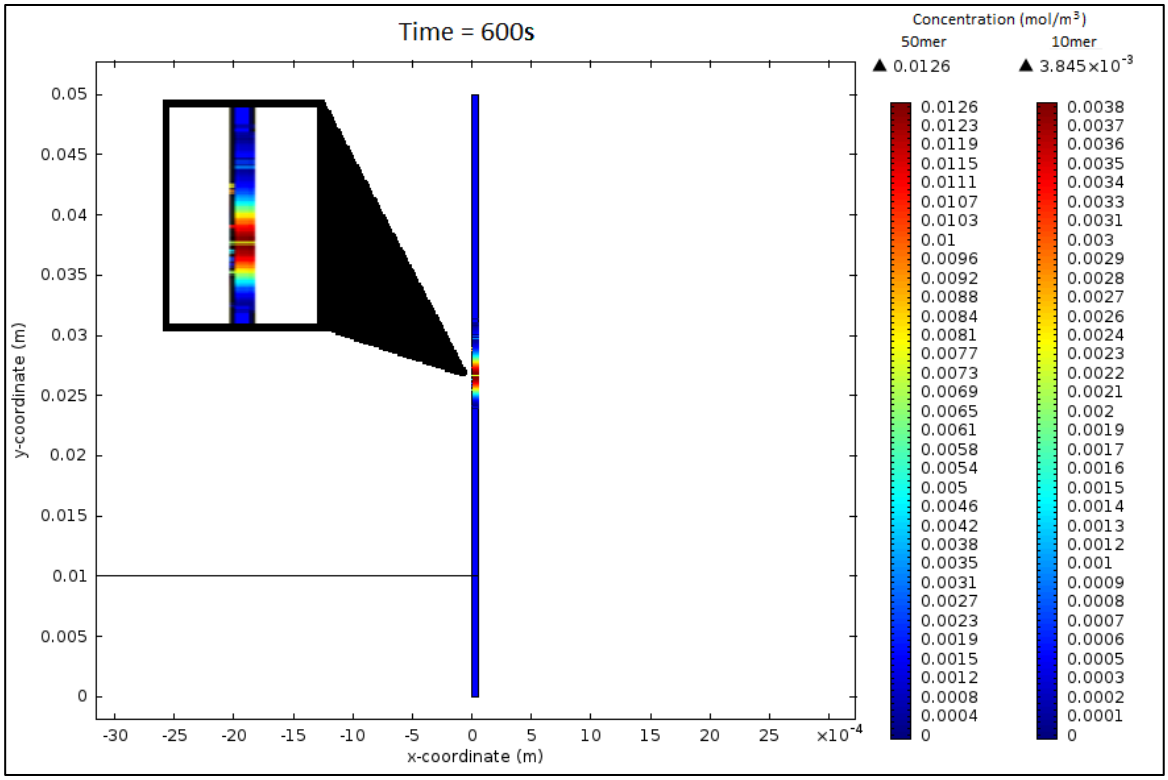

Figure 2.8 Concentration plot at t=600s.

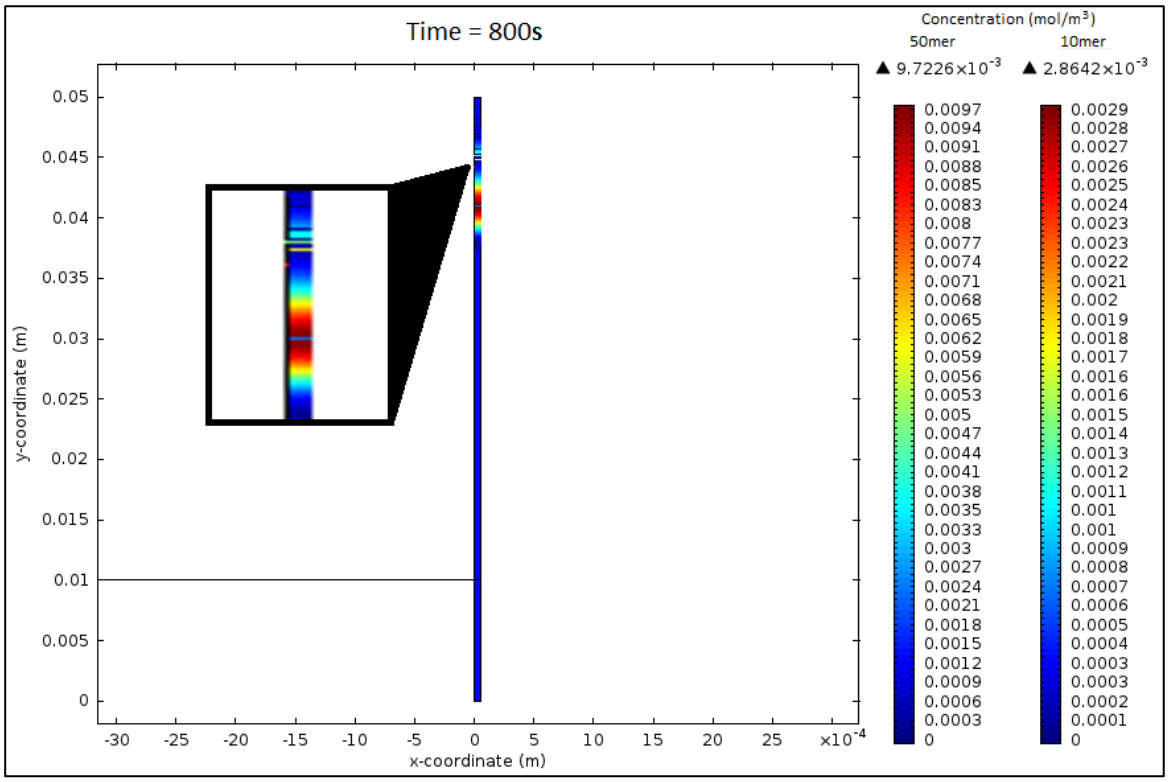

Figure 2.9 Concentration plot at t=800s.

COMSOL Output Solutions

One of the objectives of the numerical model was to develop a velocity profile. As shown in Figure 2.1, the mark made 2.5cm used to denote the observation point for the DNA separation efficacy served as the observation point of the velocity characteristics as well. The velocity profile shown in Figure 2.11 was generated across the channel at that point, which in the COMSOL model corresponds to the 0.035m point of the y-coordinate.

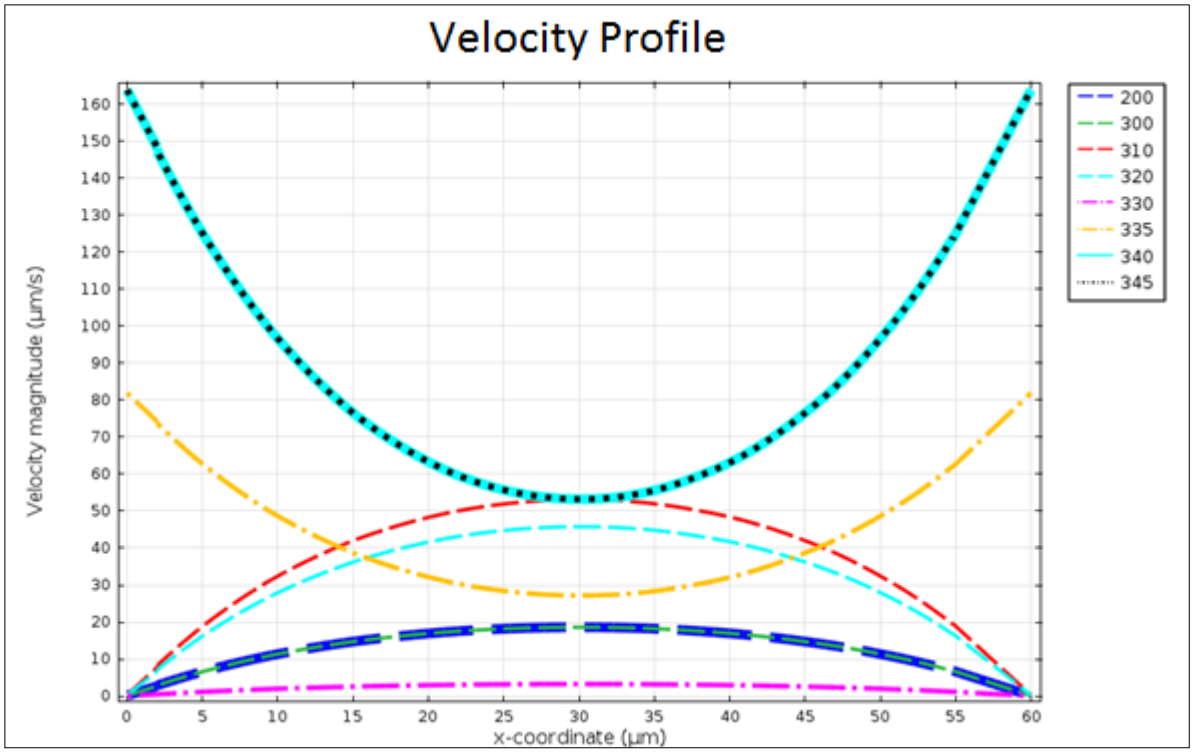

Figure 2.10 Velocity profile of the DC model taken across the width of the channel at the 2.5cm mark at various times.

The times for the plot were chosen to demonstrate the characteristics or the flows during different points in the process. The points at 200s and 300s show the pressure driven flow while the DNA was seeping into the main channel. Then, during the formation of the plug, there was a dramatic increase in the flow due to the newly created pressure head to for the plug. The time at 330s shows how the pressures equalized, thus signaling that the experiment was ready for the start of the electroosmotic flow. Starting at 335s, when the current was applied, the velocity profile finally shows the characteristics of the

electroosmotic flow showing that the fluid moves fastest along the channel wall while the fluid in the center is carried along by the viscous forces.

Another observation of interest in the DC model is the progression of each species as they migrate down the main channel. Figure 2.11 shows the concentrations of each species and their relative positions at various times. The key aspect in determining the separation distance is the difference in the peak concentration locations. The plot exemplifies how the 50mer migrates down the channel at a faster rate than that of the 10mer, characterizing the separation of the DNA by the utilization of the difference in the mobilities.

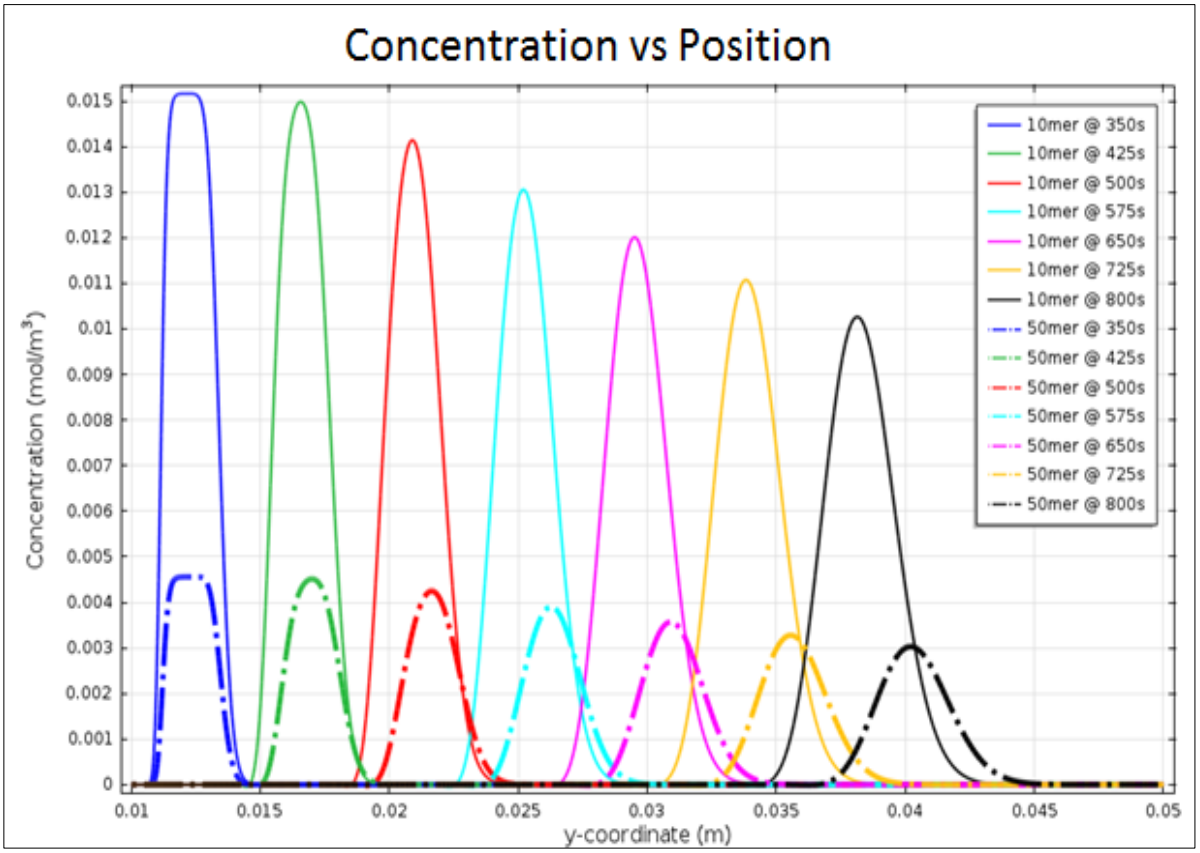

Figure 2.11 Concentration plot characterizing the progression and separation of the 10mer and 50mer through the main channel.

Since the observation point for the experiment was the 2.5cm mark from the intersection, another plot was generated to represent the expected data that was taken from each trial. Figure 2.12 shows the concentration of both species over time but only at the 2.5cm observation point. Again, the 50mer is the first to exhibit a peak in concentration, shortly followed by that of the 10mer.

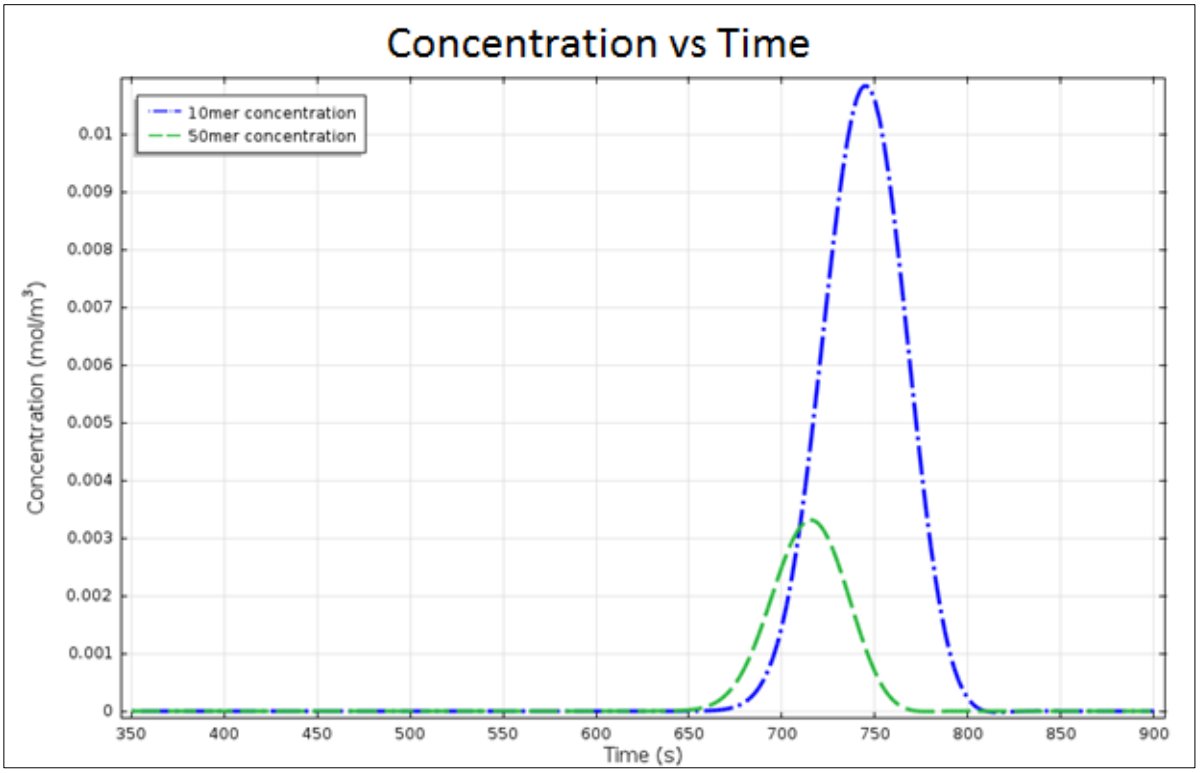

Figure 2.12 Plot of the concentration over time taken at the experimental observation point, the 2.5cm mark.

The primary purpose of the numerical model was to generate a comparison of the mass transfer of the steady flow and various oscillatory flows. Unfortunately, as previously mentioned, the simulations for the oscillatory flow were too complex to run to completion. In order to acquire the necessary data needed for the proposed mass transfer comparison, the simulations were halted at the 350s time step and the data was compiled up to that point. This was due to the insufficient availability of a high speed computer capable of simulating a system in which the electric potential is continuously changing which increased the simulation time from 4 hours for the DC model to several months in the case of the AC model. The comparison of the mass flux for the steady flow at a constant potential of

+125V, oscillating flow with a potential of +300/-50V, 4Hz, and another oscillating flow with a potential of +350/-100V, 4Hz can be seen in Figure 2.13 for the times when the pressures begin to equalize to the 350s time step.

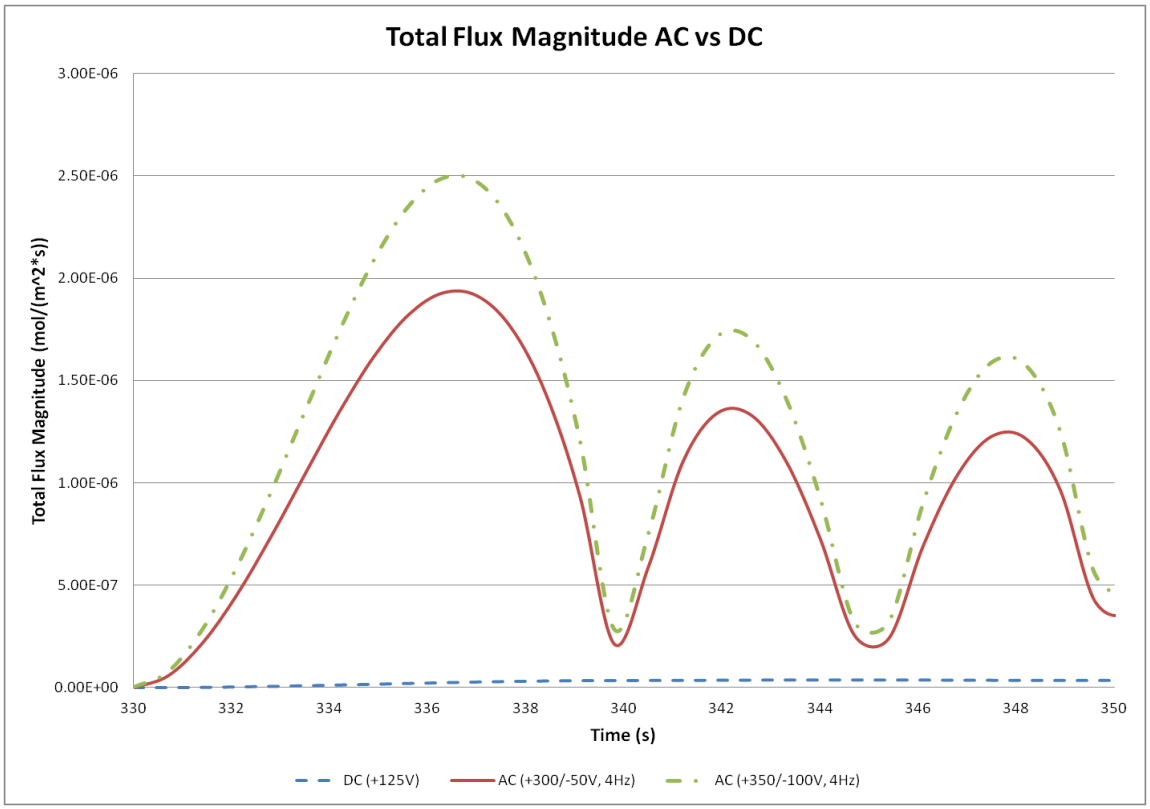

Figure 2.13 Total flux magnitude of the 50mer species from numerical model for AC and DC simulations.

The plot demonstrates the expected trend, namely that the oscillatory flow has a higher mass flux than that of the steady flow. Another expected trend that can be observed is that upon increasing the amplitude of the oscillations, the mass flux is also increased. However, due to the oscillations, the magnitudes of the mass flux follow a dampening sinusoidal wave. An assumption made from this point is that as the simulation continues past the 350s time step, the mass flux of the oscillatory flow slowly approaches a value that is roughly the average of the center point about the amplitudes. This is in agreement with the expected trends previously discussed which stated that the oscillatory flow would enhance the overall mass transfer and that as the amplitude of the oscillations increased, the overall mass transfer would be enhanced to an even greater extent.

Chapter 3: Experimental

This chapter will detail the fabrication of the microchannels and the techniques involved in the preparation of the buffer and the dsDNA samples. The experimental apparatus used for the experiments and the software used for gathering the necessary data will also be discussed in detail. Appendix E has a detailed walkthrough of the step-by-step process of each aspect of an experiment.

The microchannels used for the separation of the dsDNA were imprinted on polydimethylsiloxane (PDMS) which was cured on a silicon wafer that had an imprinted reversed copy of a microchannel on its surface. The raised pattern had a thickness on the order of roughly 15µm and was formed using photolithography. The channel was then plasma cleaned to render the PDMS hydrophilic and produce a stronger electric double layer via surface ionization. This step also irreversibly seals the PDMS onto a glass slide which forms the bottom portion of the microchannel. The ends of the microchannel have holes that serve as buffer and DNA reservoirs. These procedures are explained in further detail in the following sections of this chapter.

The fabrication brings up an interesting issue in regards to the zeta potential at the top and bottom of the microchannel. The top and bottom of the microchannel are composed of different materials, the top being PDMS and the bottom being glass; this causes the obvious dissimilarity in the zeta potentials. However, this disparity of the two zeta potentials is likely to be quite small and should not inordinately affect the separation.

Microchannel Fabrication

The process of photolithography, also known as photoetching, utilizes the photosensitivity of a material to accurately emboss a pattern onto a surface. In this case, the pattern of the aforementioned microchannel design was printed on a photomask. The pattern was then embossed on to the silicon wafer by exposure to intense UV light through the photomask on to a thin layer of photoresist that is placed upon the wafer using the spincoater. The

thickness of the photoresist, and thus the thickness of the channel, is dependent on the spin rate of the spincoater. Using an angular speed of 3000rpm, this produces a thickness of about 15 microns. Exposure to UV light causes the photoresist becomes insoluble in a developer solution. This means that after the printing of the design, the developer solution washes away any excess photoresist that was not exposed to the etching process and leaves only the pattern printed on the photomask.

From the raised pattern, replica molding can be formed by curing the predesignated polymer on the surface of the silicon wafer, thereby leaving the impression of the microchannel design in the polymer. The polymer is then baked at 100^{o}C for 45 minutes for hardening. It is then removed and prepared for plasma cleaning to remove contaminants from surfaces using energetic plasma created from gaseous particles. There are three advantages [49] to plasma cleaning; first, it produces less chemical waste than cleaning with conventional solvents. The second advantage is that when the PDMS is plasma cleaned, the surface becomes hydrophilic which causes the reduction in surface tension of the water where the EDL forms on the channel walls. This allows for the optimal alignment of the ions along the wall once the electric potential is applied and minimizes the frictional losses in the system. Lastly, there is an irreversible bonding effect with the PDMS and the glass slide which seals the microchannel. After the plasma cleaning, the microchannel is ready for use in experimentation.

Epifluorescence Microscopy

Building on the work done by Parameswara Subramanian, epifluorescence microscopy was the technique chosen for the detection of DNA separation due to its high sensitivity. For this reason, it was again chosen for the use in the current experimentation but with a further optimized system mainly based on the recommendations by Mr. Subramanian for a reduction in the sources of error that he encountered. The recommendations addressed were those pertaining to the impractical analyzation technique which involved recording a video of the separation process and using a MATLAB program to detect the levels of the colors red, blue, and green only. The other limitation was that since only one color filter

could be used at a time, species of similar colors reduced the flexibility of the species that could be analyzed in the apparatus.

In order to address Mr. Subramanian recommendations, a spectrophotometer (AvaSpec ULS3648) was utilized for fluorescent detection of the three different strands of DNA used (10mer, 50mer, and 100mer), it is also the same spectrophotometer that Mr. Aldridge used in his experimentation. There were two light sources, a custom combination of lasers which consisted of 405nm, 532nm, and 647nm wavelength laser sources. Each of these lasers roughly corresponded to the peak absorption of a specific strand of DNA that had been fluorescently marked. The 10mer dsDNA was labeled with Alexa Fluor 405 (peak absorption at 402nm and peak emission at 421nm) in the 5' end, the 50mer was labeled with Alexa Fluor 532 (peak absorption at 531nm and peak emission at 554nm) in the 5' end, and the 100mer labeled with Cy5 (peak absorption at 650nm and peak emission at 670nm) in the 5' end. The fluorescent markers were chosen for their close relations to the common wavelengths of handheld lasers and the availability of notch filters to eliminate the appearance of the peak of the light sources. The absorption/emission spectrums can be seen in Figure 3.1, which was taken from the "Fluorescence Spectra Viewer" found on the Life Technologies website where the fluorescently labeled dsDNA was purchased.

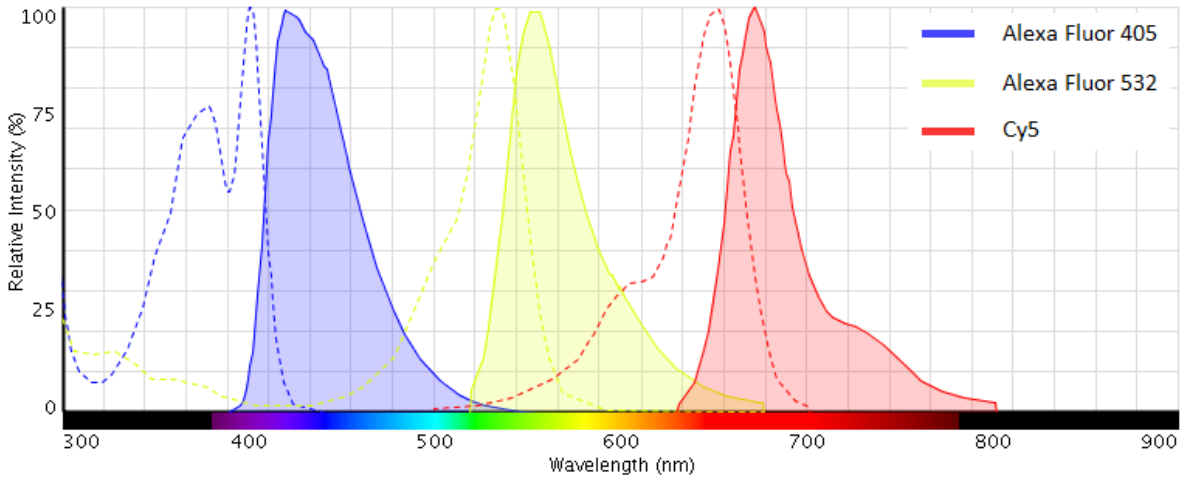

Figure 3.1 Absorption and emission spectra for the chosen fluorescent dyes.

Buffer and Sample Solution

Tris-EDTA, or simply TE, is a commonly used buffer in the case of biological species, especially for DNA and RNA, and was chosen for these experiments for that reason.. A stock solution was made from Tris-HCl and EDTA disodium salt. 100mL of 1M Tris-HCl was mixed with 20mL of 0.5M EDTA and diluted with 880mL of DI water to make 1L of 10X TE buffer stock solution. This solution was then further diluted to make the 1X TE buffer used in the experiments. When necessary, drops of 5mM NaOH was used to maintain a pH of roughly 8 since DNA is best stored in a neutral pH.

The dsDNA ordered from Life Technologies and Sigma Aldrich arrived in a dried primer solution to prevent degradation before arrival. The dried primer was then dissolved using the 1X TE buffer to make 50µM concentrations according to the specifications sheets of the respective dsDNA. Tests were conducted to find the find ratios to mix the strands based on the peak intensities so that one peak may not overwhelm the other during the process of the experiment which will be discussed later in this chapter. It was determined that the optimal ratio for the 10mer/50mer and 10mer/100mer experiments was 20:3 respectively. There were no experiments contrasting the separation of the 50mer vs 100mer due to time constraints and theory that there would be a greater amount of entanglement between the species with such large oligonucleotides together.

Experimental Apparatus

The apparatus used to conduct the experiments was based on the concepts used in Parameswara Subramanian's work, but with some improvements. The system had potential for further optimization and in doing so allowed for greater customization and ease of operation such as the ability to choose a specific laser source allows for more accurate data and the ability to vary the combinations of the dsDNA. Another improvement was the analyzation process. Before, it was required that a video of the experiment was taken and then ran through a program for determining light intensities. However, the implementation of the spectrophotometer allowed for real-time analysis. The experimental apparatus can be seen in Figure 3.2 and the overall lab area can be seen in Figure 3.3.

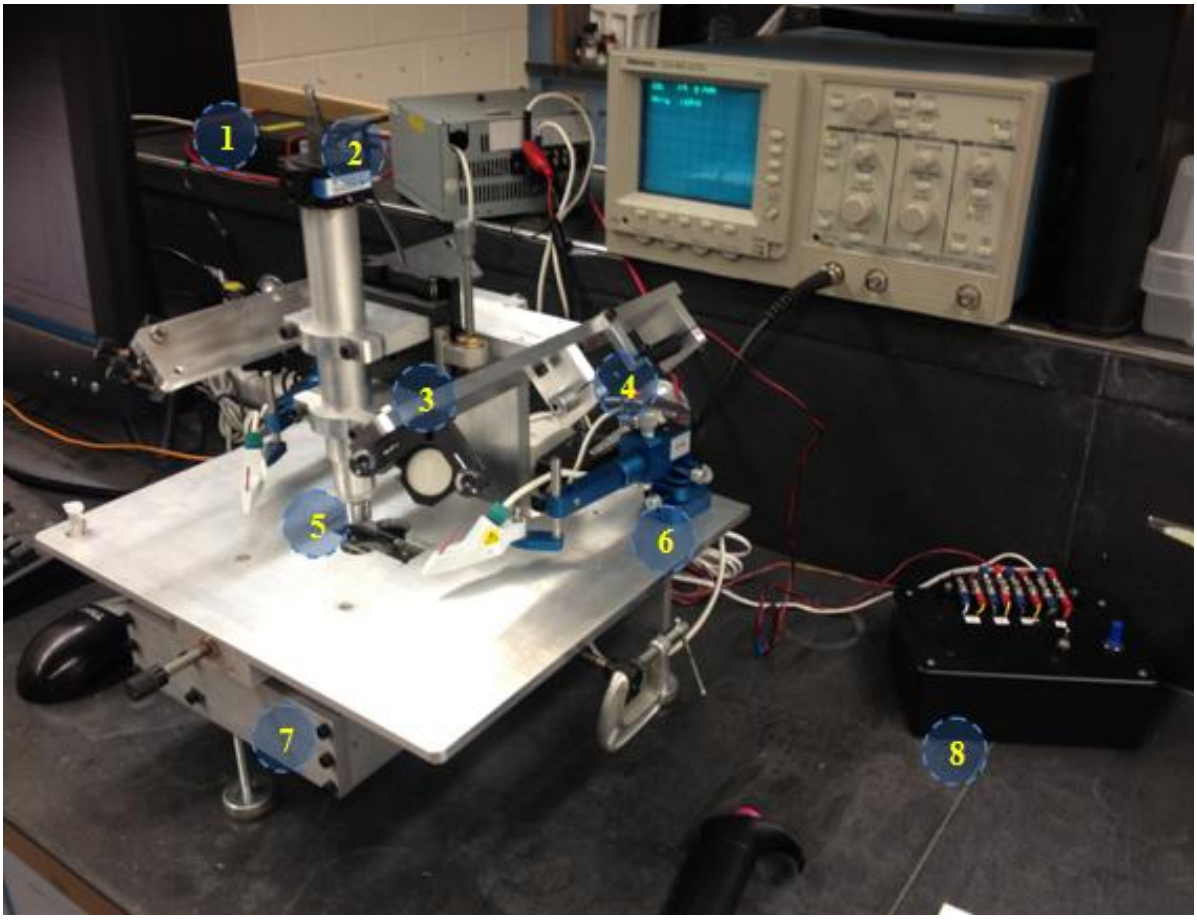

Figure 3.2 Experimental apparatus.

1 – Spectrophotometer

2 – Observation camera

3 – Mirror

4 – Laser

5 – Microchannel

6 – Electrodes

7 – Housing for lamp and optical fibers

8 – Power supply for lasers and lamp

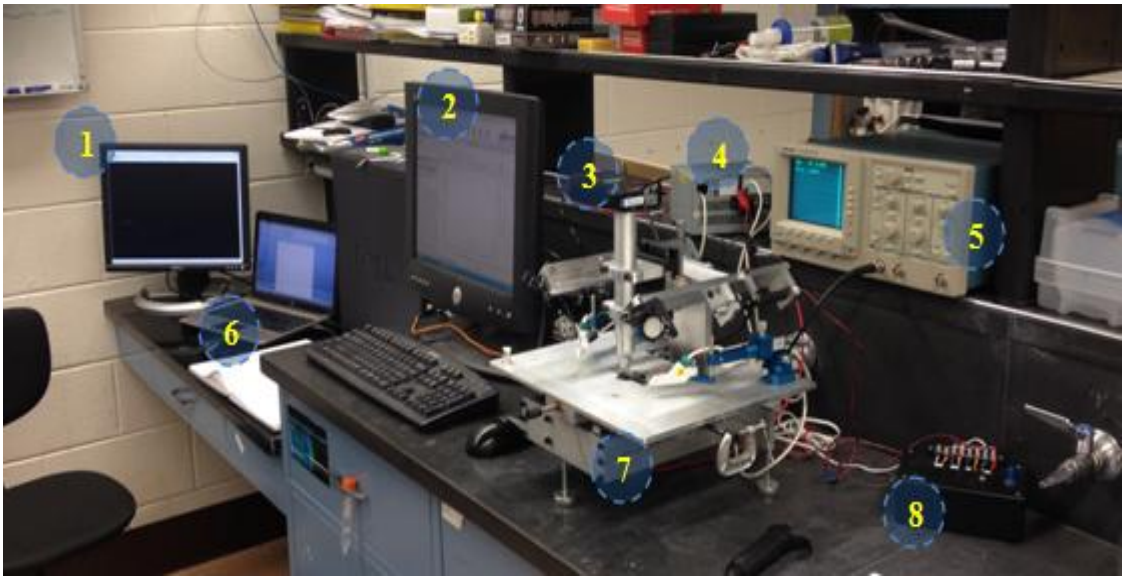

Figure 3.3 Overall layout of lab area.

1 – Monitor for camera observations

2 – Monitor for Avasoft readings

3 – Spectrophotometer

4 – AC and DC power supply

5 – Oscilloscope

6 – Notes for observations of experiments

7 – Experimental apparatus

8 – Power supply for lasers and lamp

The program used to monitor the experiment was Avasoft 8, a software specific to the spectrophotometer. There were two sets of data collected simultaneously from the program in order to provide sufficient feedback for analysis. The first tracks the wavelength with the greatest intensity; a screenshot of the graph after an experiment is shown in Figure 3.4. This shows which species has the greatest concentration at the analysis point at a given time since the intensity is a function of the concentration. For example, in the image, after the 190s time step the peak with the greatest intensity has a wavelength of 540nm. This indicates that the 50mer, which has an emission wavelength of 540nm, has the highest concentration at that point and continues to be the dominant species until 232s when the peak with the greatest wavelength is 430nm. This corresponds to the 10mer emission wavelength and indicates that it is the species with the greatest concentration which continues for the duration of the experiment.

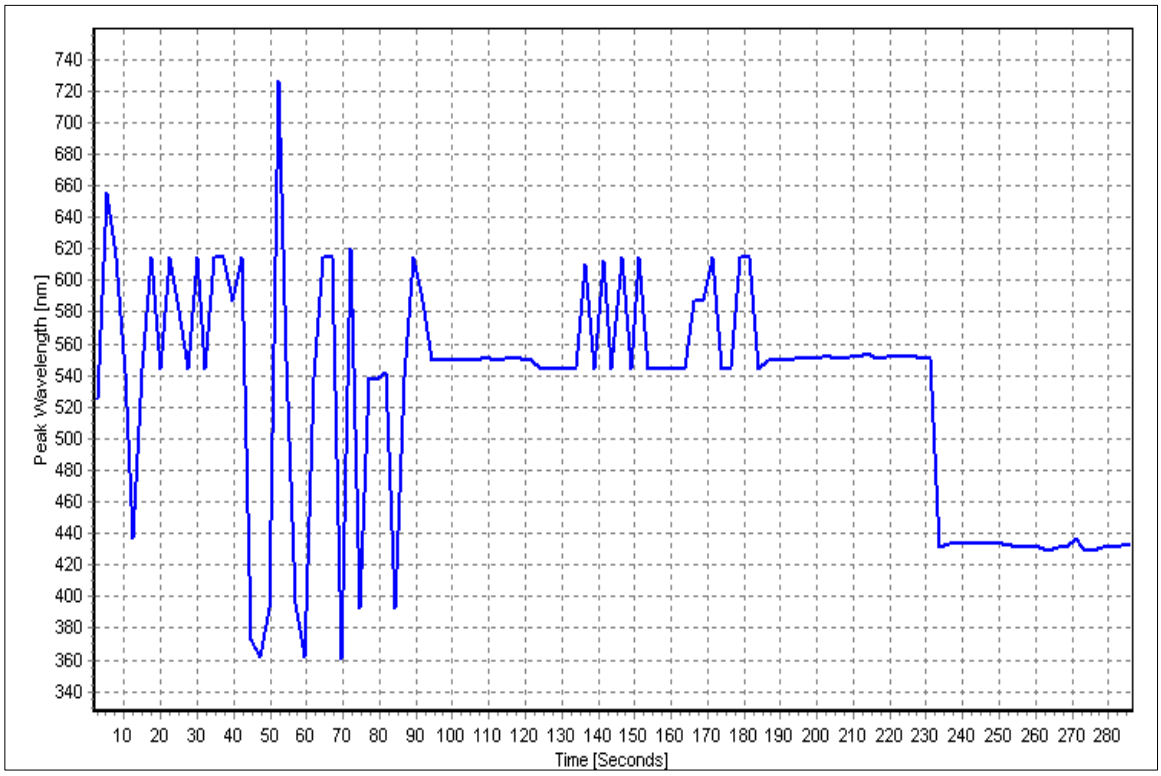

Figure 3.4 Graph of the peak wavelength data set from Avasoft.

The second piece of information was the ability to discern the actual intensity of that peak. This indicates when the species is most abundant and thus allows for a distinct peak to be observed; a screenshot of this can be seen in Figure 3.5. This observation is used to quantify the separation distance between the peaks of the species. An important attribute of the graph is the small peak of the 50mer that appears far in advance of the actual analytical data. This peak appears due to the residual ssDNA strands that were annealed to make the dsDNA while hybridizing the complimentary ssDNA strands.

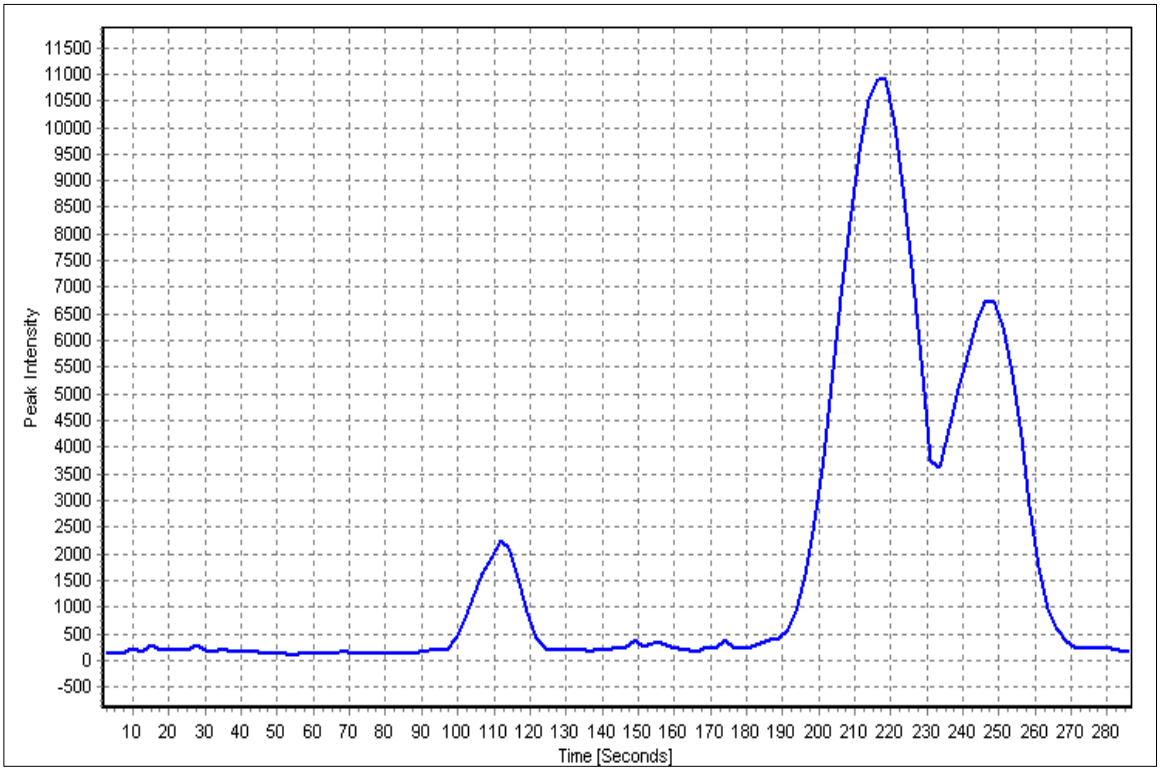

Figure 3.5 Graph of the peak wavelength intensity from Avasoft.

Dr. Dave Macpherson, Chemical Engineering Senior Research Associate at the University of Idaho, constructed the high voltage power supply needed to deliver the electric field necessary for the development of the electroosmotic flow and the program to run the power supply whose waveform can be seen in Figure 3.3 and in Figure 3.6 respectively. There were two voltage options required for experimentation: the first was the basic DC output, which could be specified in the lower left hand corner of the program. The other option was the AC

output which involved the addition of two sinusoidal waves, one positive (blue in image) and one negative (brown in image), to produce the necessary biased AC wave (green in image). The biased wave is necessary to promote the flow towards anode; if the voltage was nonbiased the DNA would separate but with no overall migration towards either the anode or cathode. The frequency of the oscillations could also be adjusted up to 7.7Hz; however, 4Hz was chosen throughout the experiments to minimize heating effects.

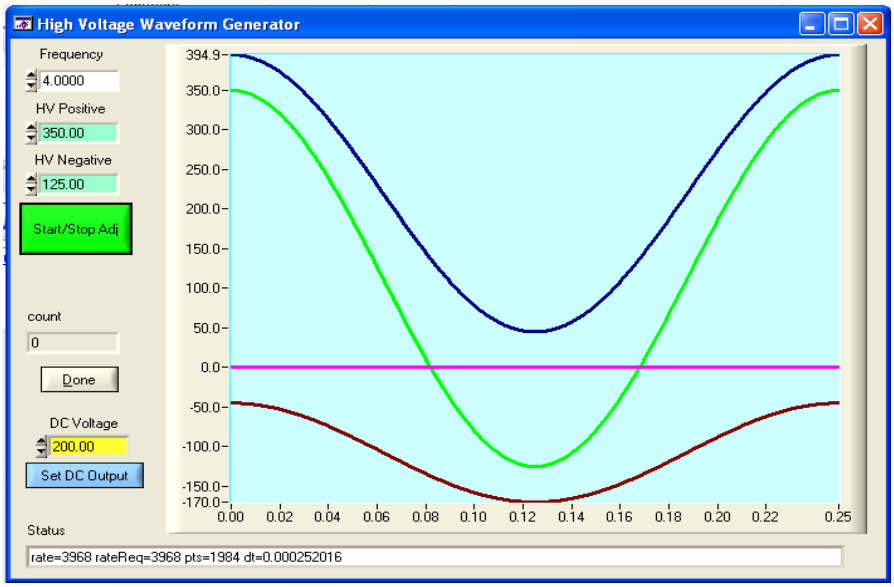

Figure 3.6 High voltage waveform generator used to control the power supply.

Another aspect that was essentially unchanged from the prior experimental setup was the ability to visually monitor the DNA in the channel by using a microscope and a camera (DFK42 from The Imaging Source). This was advantageous because it enabled the operator to know when enough DNA had seeped into the main channel, signaling the time to initiate the plug flow to begin the experiment. Figure 3.7 is a screenshot of the channel just prior to the start of the plug flow. After the start of the plug flow and the application of the electric field, the camera was moved to the experimental observation point to monitor progress. Figures 3.8 through 3.10 shows the 50mer (yellow) entering the observation point first, then the transition to the 10mer (blue), then finally the 10mer as it flows through the observation point respectively. Monitoring the migration of the DNA allowed for faulty runs to be detected rapidly, minimizing wasted time and resources.

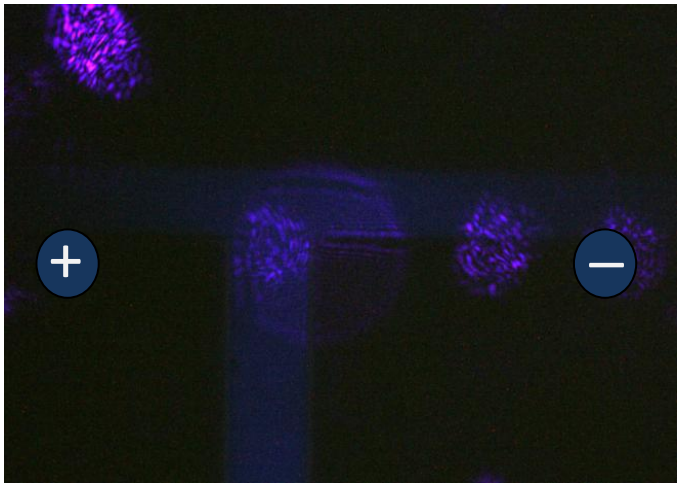

Figure 3.7 Screenshot of the DNA seeping into the main channel prior to plug flow.

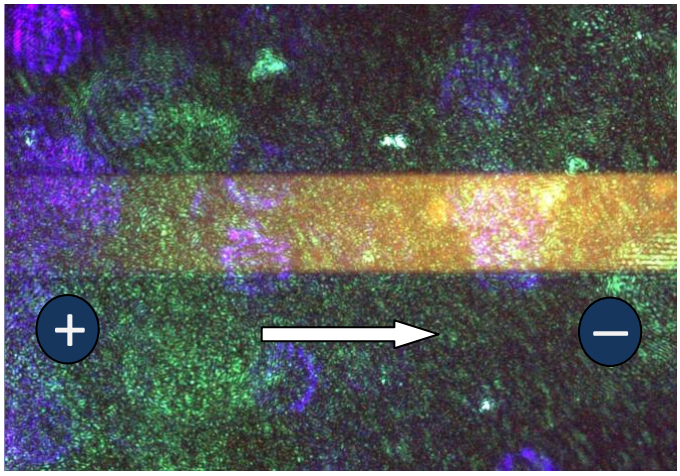

Figure 3.8 Screenshot of the 50mer entering the experimental observation point.

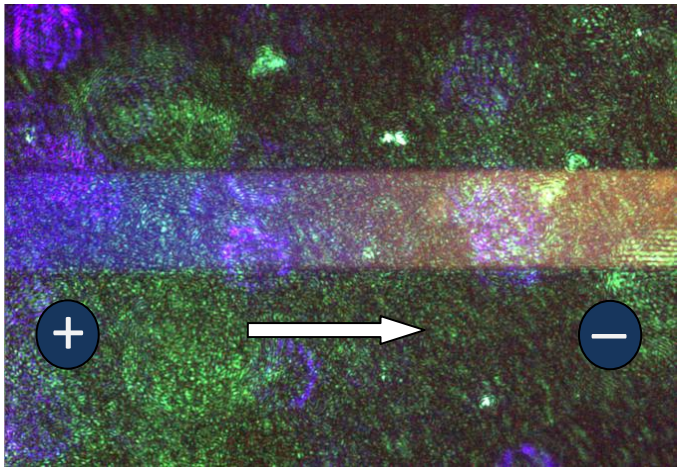

Figure 3.9 Screenshot of the transition of the 50mer to 10mer at the experimental observation point.

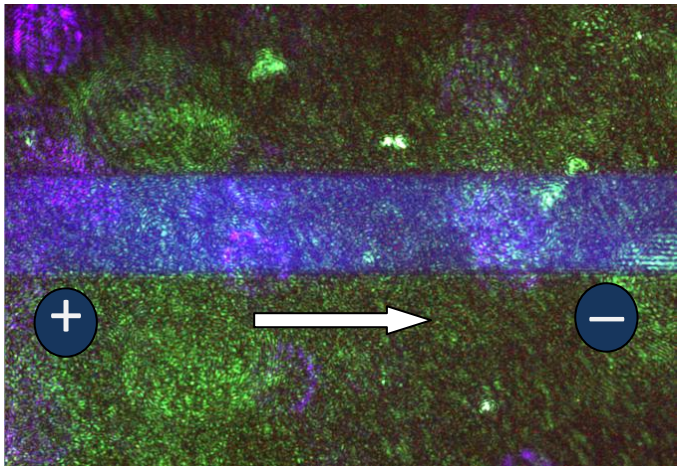

Figure 3.10 Screenshot of the 10mer entering the experimental observation point.

Using the software and protocols detailed in this chapter, the separation of multiple species of dsDNA in the PDMS-glass microchannels made from photolithographic techniques was quantified under steady and pulsatile flow conditions. The data was compiled to determine the separation of the fluorescently labeled dsDNA. The results of these experiments are discussed in the subsequent chapter.

Chapter 4: Results & Discussion

The results in this section will include the comparison of the separation for oscillatory current to the separation for steady current for both series of experiments (the 10mer vs 50mer and the 10mer vs 100mer). Another noteworthy observation was that of the sudden variation in the trending separation patterns. Further studies were conducted to find the possible cause of the intriguing results.

Preliminary Results

The first series of experiments was conducted using the 10mer labeled with Alexa Fluor 405 at the 5' end and the 50mer labeled with Alexa Fluor 532. A second series was conducted on the 10mer and the 100mer labeled with Cy5. Both series were used to test the steady and pulsatile electroosmotic flows as a method of separation for the dsDNA species. Both series were conducted using the same procedures so as to ensure consistency throughout the data analysis. The data from the spectrophotometer outputs were combined into a single file to allow the wavelength tracking and intensity data sets to be compared directly as shown in the figures below. Figures 4.1 and 4.2 are the combined datasets for some of the steady and pulsatile flow experiments, respectively, for the separation of the 10mer and 50mer. The resulting intensity peaks can be seen to correspond to a particular wavelength which is the identifying characteristic for a specific dye.

Another important feature that should be discussed is the shape of the intensity peaks. The intensity corresponds to the concentration of the dsDNA at that particular point. As it can be seen, the plug of each species is initially less concentrated as it passes the sample point before reaching the maximum and slowly decreasing, which forms the approximately Gaussian distribution. The distance between the peak concentrations of the two species serves as the characteristic separation distance between the two species.

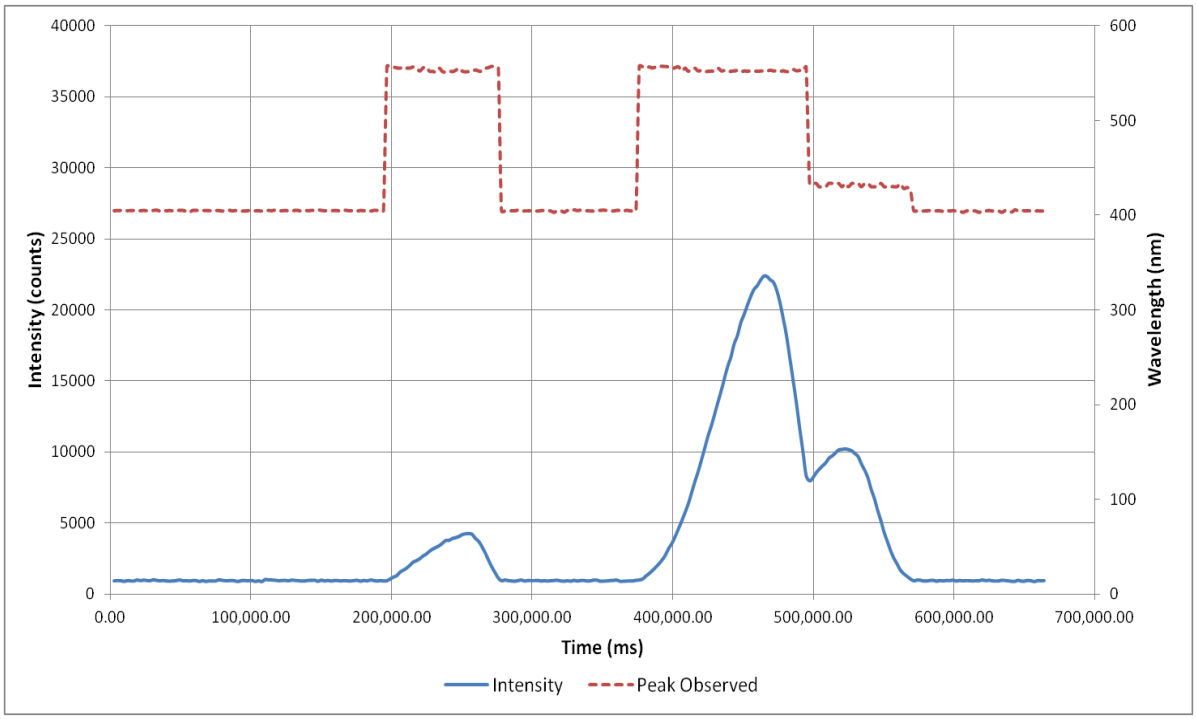

Figure 4.1 Avasoft data from a 10v50mer steady flow experiment at a voltage of +125V.

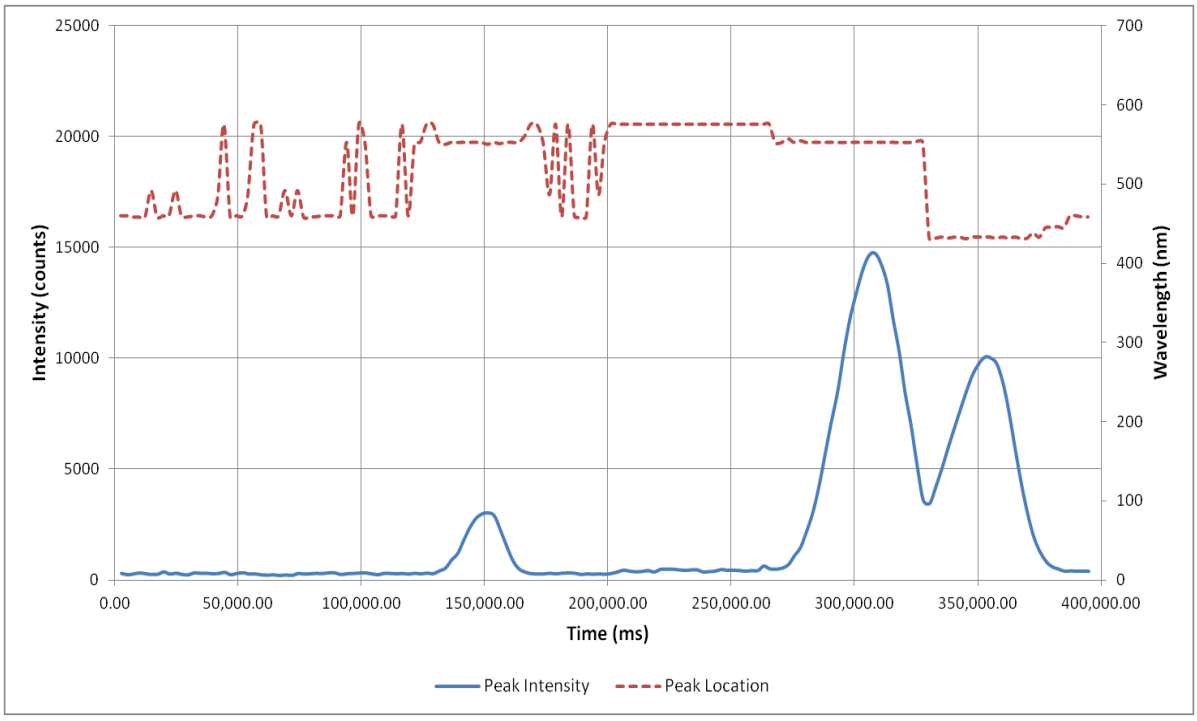

Figure 4.2 Avasoft data from a 10v50mer pulsatile flow experiment at a voltage of +325/-75V, 4Hz.

Data Analysis

After the spectrum data was compiled for an experiment, an approximation of the plug migration speed was calculated. Using the inter-peak distance (i.e. the time between the appearance of the two concentration peaks), a conversion to the separation distance was made. Although the sample point was at the 2.5cm mark along the channel, sometimes there were obstructions, typically dust, lying on top of the PDMS or underneath the glass slide. The sampling was then sometimes made at 2.4cm or 2.6cm to circumvent these errors. Since changing the sampling point would alter the comparison the samples made at the 2.5cm, the separation distance was non-dimensionalized with respect to the distance from the intersection to the sampling point. This parameter will be referred to as the "separation per distance" for the duration of this thesis. Since the migration time of the dsDNA was not always the same due to minor variations when the TE buffer was added to the system, another analytical comparison implemented was the separation per distance per residence time, the residence time being the amount of time from the application of the electric field to the mean analyzation time of the separating species. It can be easily inferred that the longer the dsDNA was in the channel, the longer the separation process was in effect. Contrasting the separation to the residence time proved to be effective in accounting for these variations. It was determined that the analysis of 10 sample runs per voltage set was sufficient to provide reliable data for the averages and standard deviations. A sample of the calculation and analysis tables can be seen in Table 4.1.

Distance from Intersct. (cm)	AF 532 Peak (s)	AF 405 Peak (s)	Inter-Peak Distance (s)	Averaged speed (microns/s)	Separation Distance (mm)	Separation per Distance (mm/mm)	Sep. Dist./ Residence Time
2.5	271.1	298.3	27.2	65.194	1.77329	0.07093	0.004624
2.5	267.2	298.2	31	65.703	2.03681	0.08147	0.005353
2.5	278.7	307.1	28.4	63.374	1.79981	0.07199	0.004562
2.5	288.9	316.1	27.2	61.342	1.66851	0.06674	0.004094
2.5	259.5	285.5	26	68.113	1.77093	0.07084	0.004825
2.5	283.9	312.6	28.7	62.235	1.78613	0.07145	0.004446
2.5	271.9	299.2	27.3	65.001	1.77452	0.07098	0.004614
2.5	311.3	344.9	33.6	56.590	1.90143	0.07606	0.004304
2.5	272.3	299.9	27.6	64.878	1.79064	0.07163	0.004647
2.5	316.4	350.9	34.5	55.652	1.91998	0.07680	0.004274
					Average =	0.07289	0.004574
				Standard Deviation =		0.00412	0.000348
				90% confidence =		0.00214	0.000181
				95% confidence =		0.00256	0.000216

Table 4.1 Calculation sheet for the 10v50mer AC +300/-50V, 4Hz experiments.

Experimental Results

The pulsatile flow oscillated about the mean steady flow voltage of +125V. The first pulsatile flow scenario was the +300/-50V, 4Hz since the controller in the high voltage power supply had a minimum ±45V limit. The subsequent pulsatile flow voltages had an addition of 50V added to the amplitude of the oscillations. Both the 10mer vs 50mer trials and the 10mer vs 100mer trials were ran using the same voltage combinations to allow for the opportunity to directly compare the separation patterns. A 90% confidence interval was calculated for the separation per distance and the separation per distance per residence time data sets and was applied to the graphical representations found in Figures 4.3 to 4.6. Appendix C shows the graphs with a 95% confidence interval and further statistical analysis of the separation data can be found later in this chapter and in Appendix D.

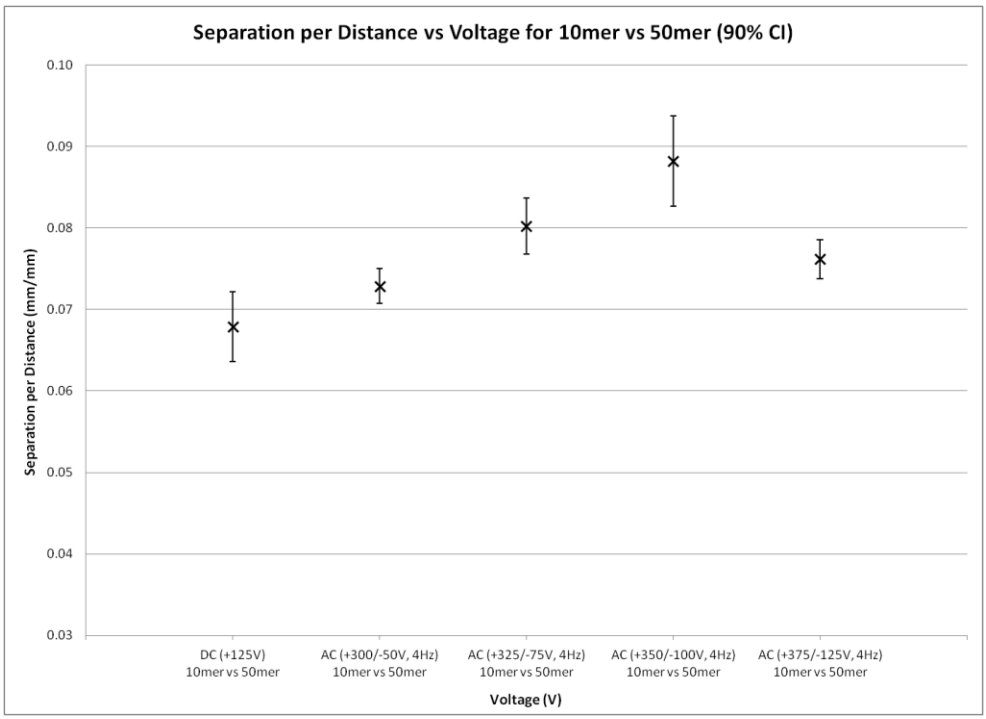

Figure 4.3 Separation per distance for 10v50mer trails plotted against the steady and pulsatile voltages with 90% confidence intervals.

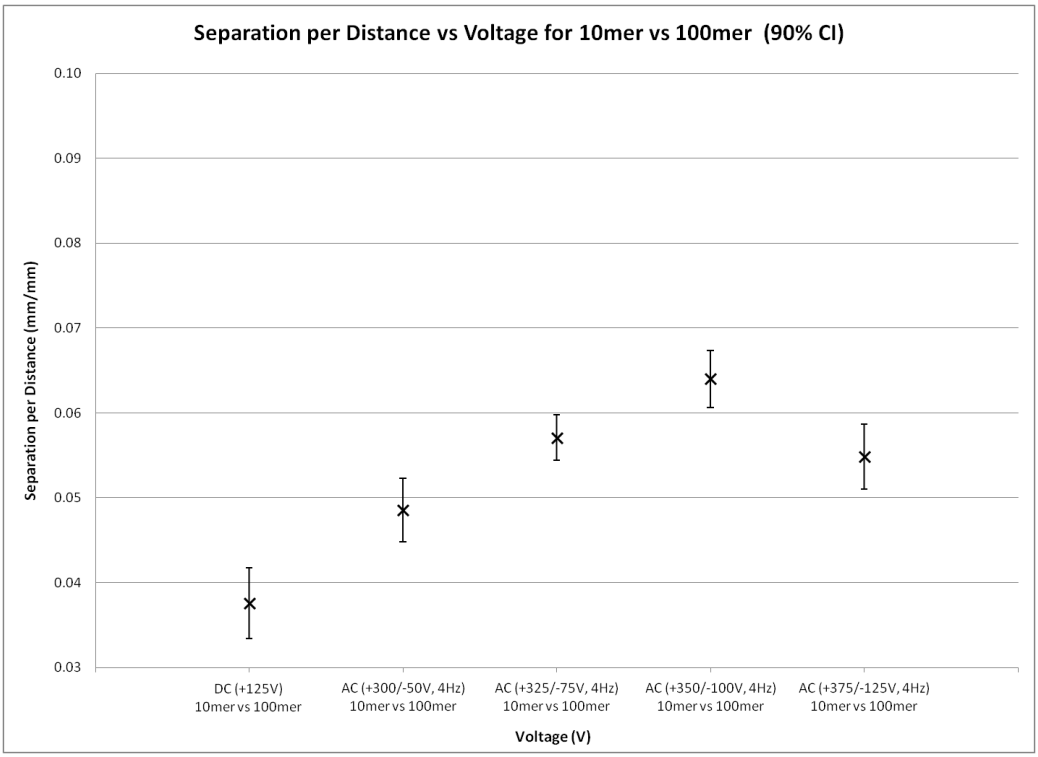

Figure 4.4 Separation per distance for 10v100mer trails plotted against the steady and pulsatile voltages with 90% confidence intervals.

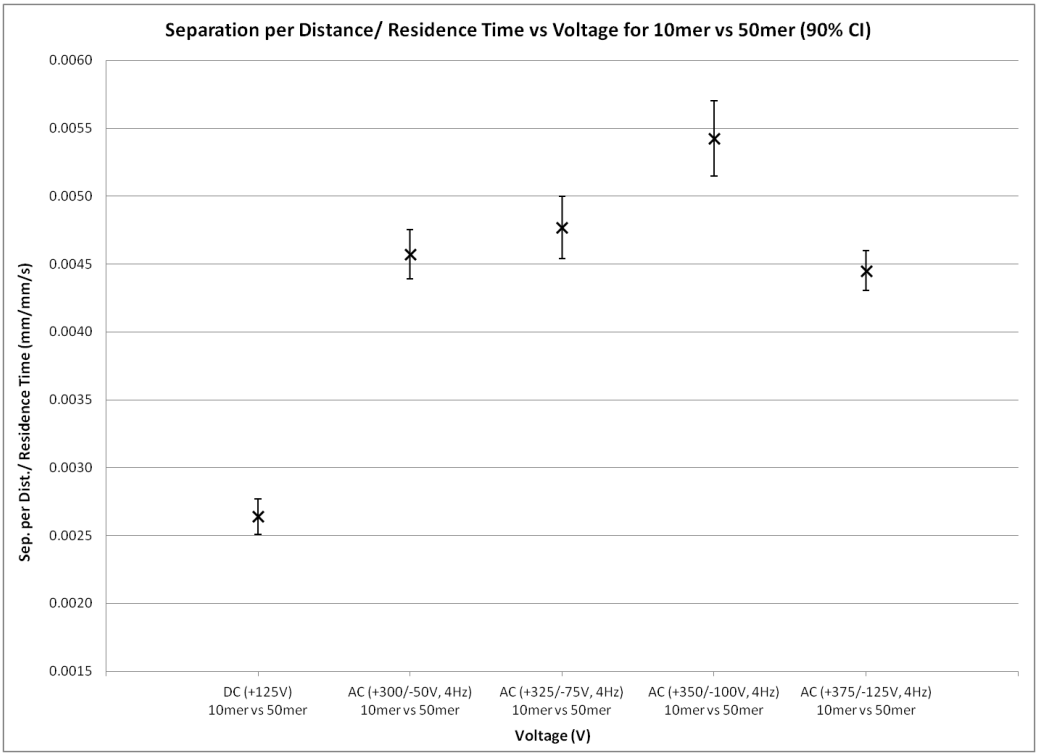

Figure 4.5 Separation per distance per residence time for 10v50mer trails plotted against the steady and pulsatile voltages with 90% confidence intervals.

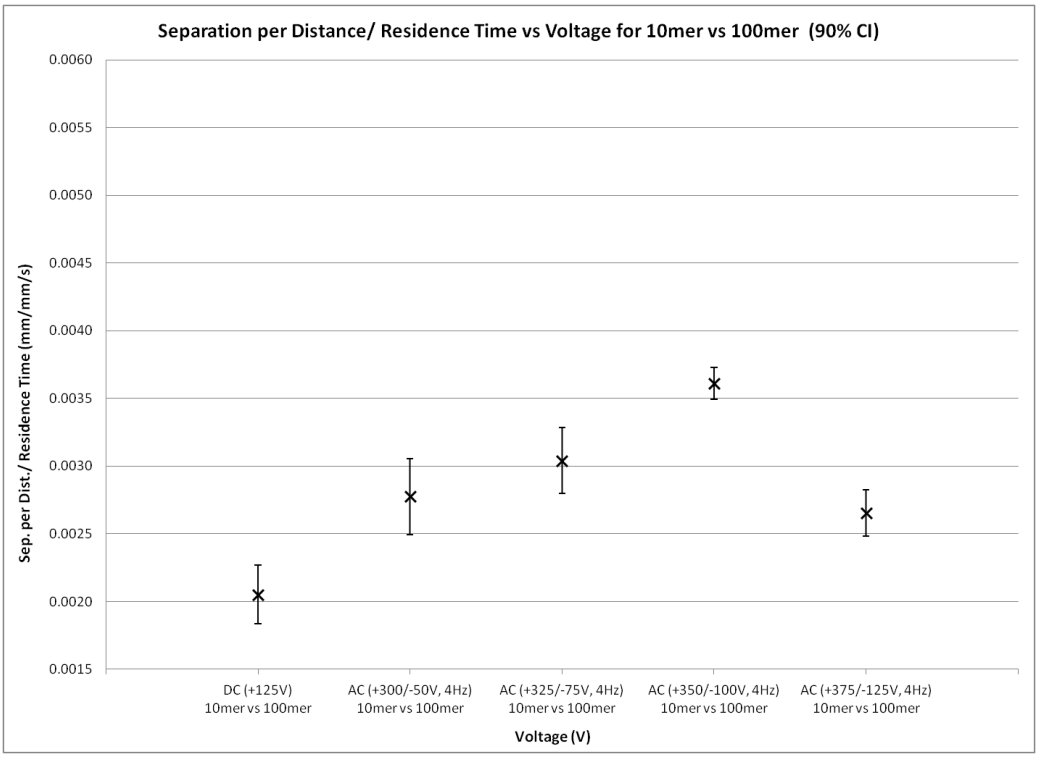

Figure 4.6 Separation per distance per residence time for 10v100mer trails plotted against the steady and pulsatile voltages with 90% confidence intervals.

After observation of the results in Figures 4.3 to 4.6, the trends shown in the separation pattern are nearly identical for the 10mer vs 50mer and the 10mer vs 100mer trials. The main difference between the two sets of data is that the 10mer vs 100mer trials resulted in a lower separation efficacy than that of the 10mer vs 50mer trials. This shows that although there is a larger dissimilarity in the size of the species, this disparity will not necessarily lead to an inherent increase in the mass transfer difference between the species. Instead the electric potential, or rather the changes in the electric potential, which directly affects the migration speed of the species and the structure of the electrical double layer, is shown to be the driving force for the consistency in the results. An example of this trend can be seen when the voltage was increased from +300/-50V, 4Hz to +325/-75V, 4Hz and there was an increase in the separation per distance per residence time by a value of $2x10^{-4}$ mm/mm/s in the 10mer vs 50mer trials as well as the 10mer vs 100mer trials.

Referring back to Figures 4.1 and 4.2, which illustrated the experimental output of a steady flow experiment and a pulsatile flow experiment respectively, also support the results of the pulsatile flow situation demonstrating an enhanced mass transfer. In the steady flow situation, the separation process took roughly 575s to reach the 2.5 cm detection point and the pulsatile flow took roughly 375s. The increase in the migration speed alone, even if the separation distance had been the same, indicates that there is an enhanced mass transfer in the species as it moves down the channel faster. The trend was consistent for essentially all of the steady flow situations compared to that of the pulsatile flow situations which can be seen in the raw data in Appendix B.

Another reason that the 10mer vs 100mer trials had a lower separation efficacy may be that the 100mer was long enough to cause an entanglement issue which led to more of a sieving mechanism for the 10mer to filter through. Therefore, the 10mer had to first travel through the large 100mer strands thus slowing it down and hindering its movement. This would give rise to a lower separation although there is a greater size disparity between the two strands.

The lowest average separation per distance and separation per distance per residence time for both the 10mer vs 50mer and the 10mer vs 100mer was found to be the steady flow situation. Therefore, the difference in mass transfer is seen to be lower than in the oscillatory flow case. Furthermore, as the amplitude of the oscillations increased, a noticeable enhancement of separation occurred until the +375/-125V, 4Hz trials. At this point, the separation efficacy saw a dramatic regression to the level that was consistent with the smallest oscillatory amplitude.

The reduction of the separation can possibly be due to the fact that at larger oscillation amplitudes, the axial and radial movements of the species are stronger which leads to an increase in dispersion. Another possibility is that once the amplitude of the oscillations reaches a specific negative or positive potential, the oscillations are so large that it begins to

promote a mixing of the species. Further testing was conducted for possible confirmation of this theory and is discussed in the following subchapter.

Amplitude Threshold Results

It has been mentioned that large amplitude oscillations will begin to promote the mixing of the species at a certain value which will decreases the separation. A secondary set of testing was conducted using the 10mer vs 50mer setup but with two new combinations of the positive and negative electric potentials to find when the process reaches a “danger zone” or “threshold limit”.

The first electric potential tested was +375/-100V, 4Hz which was compared to the previously observed +350/-100V, 4Hz, a +25V difference, in order to confirm if the positive potential was the limiting factor in the separation. The second electric potential was +350/-125V, 4Hz, a -25V difference, to confirm if the negative potential was causing a decrease in the separation. The results can be seen in Figures 4.7 and 4.8 which depict the separation per distance and the separation per distance per residence time respectively.

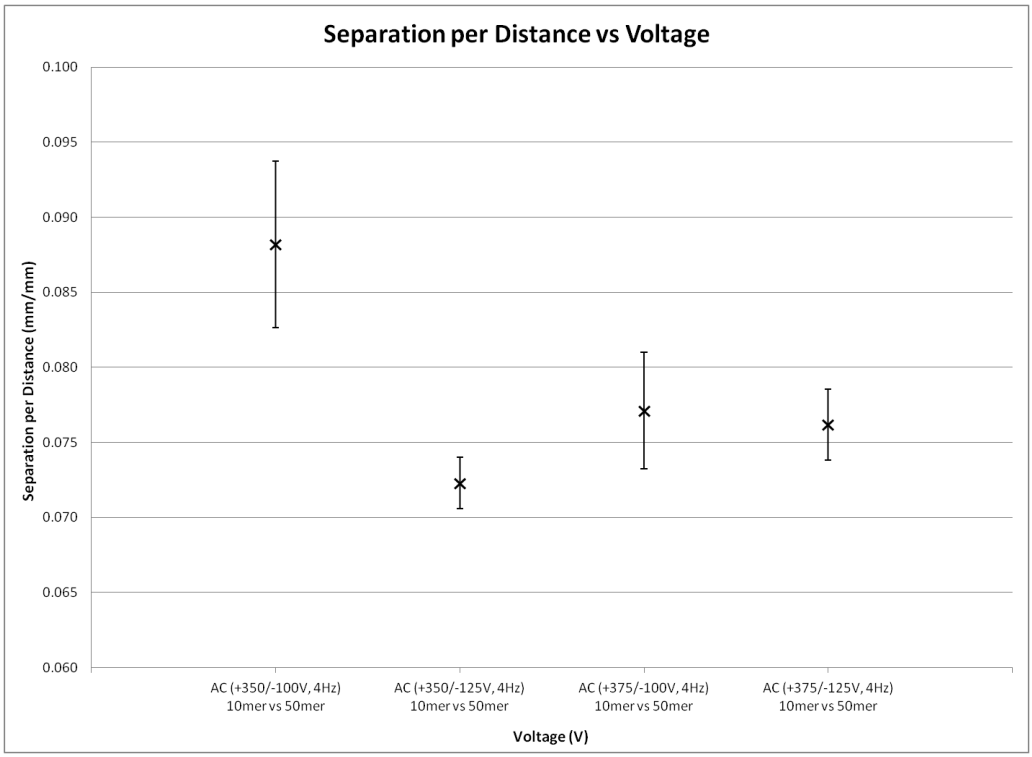

Figure 4.7 Separation per distance for 10v50mer threshold limit trails with 90% confidence intervals.

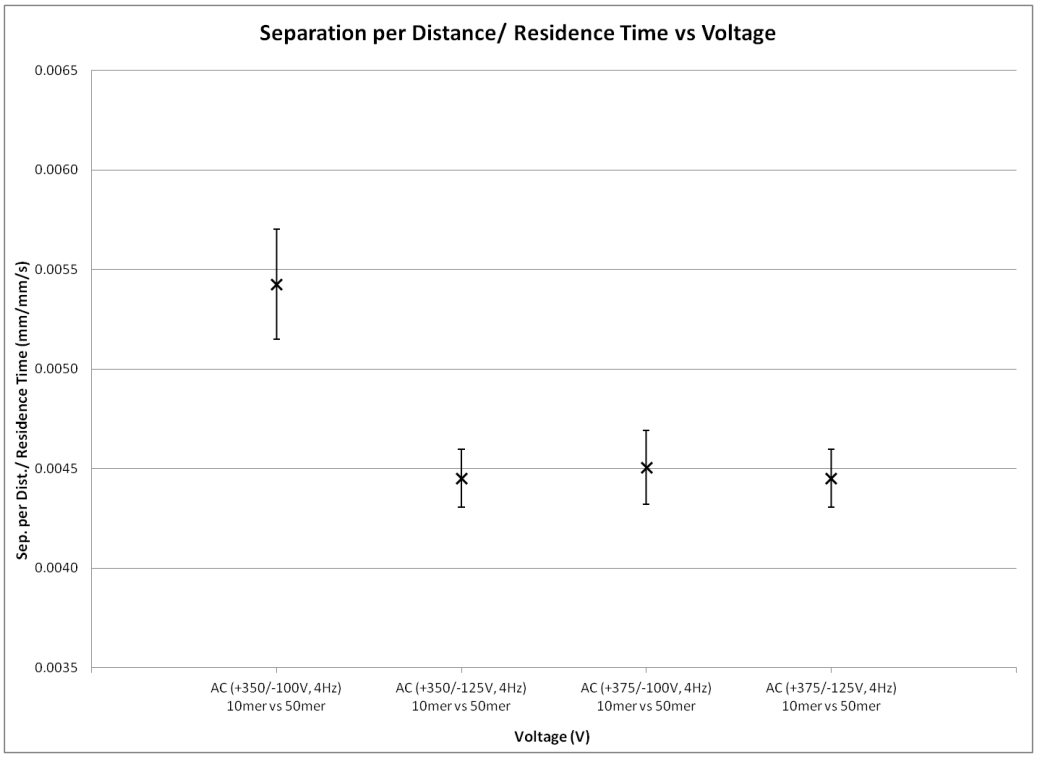

Figure 4.8 Separation per distance per residence time for 10v50mer threshold limit trails with 90% confidence intervals.

The +350/-125V, 4Hz electric potential demonstrated a decrease in the separation from the +350/-100V, 4Hz data set which therefore shows that the negative potential is a limiting threshold. In addition, the +375V/-100V, 4Hz electric potential demonstrated a decrease in the separation which gives evidence that the positive potential is a limiting threshold as well. The evidence supports the theory that there is a threshold at which the separation efficacy is found to regress, these limits being a negative potential of -125V and a positive potential of +375V.

Size Dependent Variability

Although the separations showed similar trends for the 10mer vs 50mer trials and the 10mer vs 100mer trials, there was one significant variation between the two: the order of appearance. During the 10mer vs 100mer trials, the first dsDNA to appear in the observation point was the 10mer which was then quickly followed by the 100mer. This is to be expected since the mobility of the 10mer is greater than that of the 100mer which is large enough to possibly become entangled within itself. However, upon observation of the 10mer vs 50mer trials, the 50mer was the first to appear in the observation point and was then followed by the 10mer, therefore showing that the order of migrating species is not necessarily exclusively dependent on the mobility of the species. Instead, the order of appearance is theorized to be dependent on the width the diffuse layer in contrast to the dimensions of the microchannel and the space concentrations of the species. In the work by Mr. Subramanian, who tested for the separation of ssDNA using a 10mer and 50mer, the first species to appear was the 10mer and was followed by the 50mer. The only disparity between his ssDNA trials and these dsDNA trials were the concentrations of the species, which was a 1:1 ratio, and the dimensions of his microchannels, which were 50 microns wider and 10 microns deeper on average.

Referring back to the works of Thomas and Narayanan [40-43], another possible explanation to this abnormality is that at certain values of dimensionless groups, there is a crossover

effect when the species with a lesser diffusivity develops a greater mass transfer than the faster diffusing species. However, this would extend to properties that are consistent with the steady and pulsatile flows since the order of appearance was constant throughout each mixture of dsDNA that was tested. Another theory may be that either steric hindrances or the species ability to enter certain velocity regions attributed to flow restrictions. In the case of the 10mer and 50mer trials, they were free to interact with the varying flow field, the Stern and diffuse layers, but when the 100mer was analyzed with the 10mer it may have been too bulky to interact in the regions or entered the various flow fields at a slower rate than that of the smaller species. A species ability to remain in faster moving flow regions as the fluid oscillates back and forth will affect its overall mass transfer and ultimately separation between species.

Comparison of Numerical Model and Experimental Results

As was predicted in the numerical model, the increase in the amplitude of the oscillations resulted in the enhancement of the overall mass transfer. However, simulations were not performed for the higher amplitudes where the effect was seen to have decreased the mass transfer from the previous amplitude. It was also unfortunate that the simulation was not able to be run past the 350s time step which would have helped to further characterize the effects of the pulsatile flow once the species reaches the analytical point in the channel. Another adverse factor that was in the simulations was that the mobilities of the dsDNA species were calculated from experimental observations due to the dearth of papers having these literature values. However, the simulations did demonstrate the expected trend in mass transfer which was observed in the experimental data. The numerical model seen in Chapter 2 seems to be an appropriate starting point for the visualization of the velocity, concentration, and mass transfer profiles for a system utilizing steady and pulsatile electroosmotic flow for the separation of biomolecules.

Experimental Variations

There were several variations in the experimental process, the first being the width of the microchannels. The fabrication process associated with each microchannel can result in width variations on the order of ±20 microns as compared to 60 microns which is the average width of the microchannels. The dimensions and geometry of the microchannel can have a significant effect on the electroosmotic flow and can consequently alter the migration time of the species. In order to minimize the error that could be associated with the process, the width of the microchannels were compared to one another under a microscope and if the variation was greater than ±5 microns, the channels were recast.

Another variable process was the plug formation. Since the formation of the plug initially relied on a pressure gradient to force the dsDNA into the main channel, there is a small degree of error associated with the magnitude of the pressure gradient and its reproducibility. A small change in the pressure head in the top well could cause the dsDNA to flow and disperse, instead of forming the plug. Reducing the effect of this limitation was accomplished by managing the thickness of the PDMS during the casting process. Typically this problem arises due to a slightly uneven drying surface causing one end of the microchannel to be thicker than the other. Simply ensuring the even distribution of the PDMS lessened the reoccurrence of this inconsistency.

The third irregularity was the alteration of the PDMS surface chemistry. As previously mentioned, PDMS is inherently hydrophobic and in order to render it temporarily hydrophilic, the microchannels were plasma cleaned. However, the hydrophilic effect is temporary. It was observed by Mr. Neil Sing [47] that 30 minutes after plasma cleaning, the velocity of the plug was nearly half than that of a plug in a microchannel immediately after plasma cleaning. This phenomenon was addressed by minimizing the time that elapses between the preparation of the microchannel and the running of the experiment.

The final challenge in the experimentation was the issue of photobleaching the dsDNA. In order to observe the formation of the plug, the lasers need to be illuminating the intersection of the microchannel, therefore fluorescing the dsDNA. However, if the dsDNA was illuminated for an extensive amount of time (which varies based on the laser power and the half-life associated with the dye), the fluorescent effect was no longer discernible and prevents the spectrophotometer from observing the dsDNA. For the 10mer and 50mer, the problem was almost negligible, but the 100mer was only able to exhibit its luminous effect for several seconds. In order to conserve the fluorescent ability of the dsDNA, the lasers were essentially flashed on the intersection for a very brief amount of time until it was observed that the formation of the plug was ensured. However, in future experiments, it is recommended that a different dye be used for the dsDNA instead of the Cy5 dye which was selected for its particular wavelength and availability.

Statistical Confirmations

The experimental variations discussed in the previous subchapter resulted in deviations around the mean separation values which were seen in Figures 4.3 to 4.8 (which were plotted with 90% confidence intervals). It is essential to confirm whether or not the separation is indeed statistically greater for the pulsatile electroosmotic flow than that of the steady flow condition. Therefore, a standard student t-test was used to compare the samples and statistically justify the results.

The t-test starts with the null hypothesis and the alternative hypothesis. The null hypothesis assumes that the separation of the dsDNA is the same for both the pulsatile and steady flows where as the alternative hypothesis assumes that they are different. A secondary set of hypotheses was created so that the secondary null hypothesis assumes that an increase in the amplitude of the pulsatile flow would not increase separation where as the alternative assumes that increasing the amplitude would increase the separation. The calculations of the t-test are shown in Appendix D. It was seen that when the mean of the steady flow for both separation parameters (separation per distance and separation per distance per

residence time) were less than that of any of the pulsatile flow situations with confidence intervals of 90%, 95%, and 99.5%. It was also confirmed that the increase in the amplitude of the oscillations, the separation was increased until the potentials reached the aforementioned threshold limits which resulted in the failure to reject the null hypothesis which means that the separation was not statistically greater than the contrasting data set. However, the flow oscillations were confirmed to indeed give rise to greater separations than the steady flow DC field.

Chapter 5: Conclusions & Recommendations

The effects of steady and pulsatile electroosmotic flow as a separation mechanism for biomolecules was examined as a potential viable separation method in microchannels. Experiments were performed with two mixtures of dsDNA; a 10mer labeled with Alexa Fluor 405 and a 50mer labeled with Alexa Fluor 532, the other mixture also used the 10mer but was combined with a 100mer labeled with Cy5. A numerical model was generated to depict the velocity profile and the progression of the dsDNA through the experiment to provide a sense of what should be observed experimentally. Although the numerical model only demonstrated the comparison of three simulations, one steady flow and two oscillatory flows, it accurately demonstrated the increase in the mass transfer from a steady flow to an oscillatory AC field and the separation was even greater upon the increase in the amplitude of the oscillations.

Alterations to prior methods used by Mr. Subramanian such as the shape of the microchannel resulted in a reduction in the amount of dsDNA wasted in each experiment. Another change was the implementation of the spectrophotometer apparatus to allow for more accurate measurements of the migration and separation of the dsDNA. The custom built apparatus was a major accomplishment in this study as it allowed real-time measurements of the migration of the dsDNA as well as more accurate measurements of the amount of separation achieved. The COMSOL numerical model also agreed with the theoretical model that Mr. Subramanian generated although the numerical model was simulated for a specific situations instead of using dimensionless parameters for various situations.

Conclusions

The separation of the dsDNA in steady flow demonstrated the expected electroosmotic-electrophoretic force interactions with the electroosmotic force, exhibiting a greater magnitude of effect since the flow migrated towards the cathode. The pulsatile flow showed an increase in both separation characteristics (separation per distance and the separation

per distance per residence time), which was statistically confirmed via a standard student t-test. It was also observed that the separation patterns for both sets of dsDNA mixtures exhibited identical trends in the separation parameters suggesting that the difference in the ratio of species size does not affect separation efficacy as strongly as the electric potential.

The separation efficacy increased as the magnitude of the oscillations increased until the threshold limit which was later identified to be at a positive potential of +375V and at a negative potential of -125V. At these points, the process started to demonstrate what is suggested to be a remixing of the dsDNA. The pulsatile electroosmotic flow proved to be the more viable method for the efficient separation of biomolecules such as dsDNA on 'lab-on-a-chip' devices over that of the steady flow, even once the threshold limit has been reached for the pulsatile flow.

Pulsatile electroosmotic flow has proven to be a viable method for the separation of dsDNA on 'lab-on-a-chip' devices due to the enhancement in the separation efficacy of the species. The concept of a threshold limit was discovered at certain positive and negative electric potentials that resulted in the inflection of the separation trend. The success of developing a numerical model was significant enough to be included in the study of the fluid progression of an analyte mixture.

Future Work

One of the most interesting observations made during the course of this thesis was the threshold limit at certain negative and positive electric potentials. However, since there was such a short allotment of time for the collection of data, there is still a multitude of other voltage combinations that can be performed to further explore if this phenomenon. Also, some measure of the variability of the threshold limit at other frequencies would be beneficial. Further understanding of a possible voltage limit would aid in establishing an optimal range for the separation of the biomolecules.

Another intriguing aspect of these experiments was the order of appearance of the species. It is not fully understood why one species migrates faster than the other. The only potential factors that were found may be the ratio of the species concentrations and the dimensions of the microchannels. Testing at other concentration ratios and other geometric variations of the microchannels would yield further insight into the reason as to why a larger species may migrate faster than the other or vice versa.

Although there was some testing of variously sized dsDNA, this variable can also be further explored. The mixture with the 100mer was seen to have a lesser separation efficacy than the mixture with the 50mer. Analyzing the same size ratio (the 10mer vs 50mer or a possible 50mer vs 250mer mixture) would also assist in understanding the trends associated with the varying base pair combinations.

The replacement of the dsDNA with proteins could be the next natural progression for this course of study [50,51]. However, the absorbance of the proteins into the surface of PDMS has been known to occur [52]. Alterations to the PDMS can be made to reduce these effects, as seen in the methods of Makamba et al [53]. Another was to possible counteract these effects is to simply change the material used to cast the microchannels. One alternative is polymethylmethacrylate (PMMA), which has been used in protein separations in capillary electrophoresis [54]. Another possibility for the evolution of this project is to separate a mixture of ssDNA and dsDNA. Separating oligonucleotides of the same length may help contrast the difference in mobilities while maintaining the consistency of other properties.

The numerical model, however helpful in the visualization of the project, could still be improved upon. The model was not fully executed due to the long simulation time associated with each run, even with the abundance of available computing power. Optimizing the simulation process may allow for a complete model of the pulsatile electroosmotic flow situations.

The final suggestion for improvement is to possible find a new polymer for the casting of the microchannels or a means to prolong the hydrophilic interactions. The depreciation of the phenomenon is rapid enough to possibly affect the consistency of the experiments. A surfactant such as polyethyleneimine (PEI) or polyethylene oxide (PEO) could be pumped through the PDMS microchannel and provide a possible solution to this limitation [52,55]. The prospect of fabricating a microchannel that could be used for several trials rather than just one would also be within the realm of possibility if such a surfactant were to be used.

References

[1] R Zengerle, P Kotlay, J Ducree “Microfluidics: An Enabling Technology for the Life Sciences” *Micro-Nanomechatronics and Human Science*, 2004, pp. 1-6

[2] S Sia, G Whitesides, “Microfluidic device fabricated in poly(dimethylsiloxane) for biological studies” *Electrophoresis*, 2003, 24, pp. 3563-3576

[3] T Chovan, A Guttman, “Microfabricated devices in biotechnology and biochemical processing” *TRENDS in Biotechnolgy*, 2002, 20, pp. 116-122

[4] E Verpoorte, N De Rooji, “Microfluidics meets MEMS” *Proceedings of the IEEE*, 2003, 91, pp. 930-948

[5] G Hetsroni, A Mosyak, E Pogrebnyak, L P Yarin, “Fluid flow in microchannels” *Int. Journal of Heat and Mass Transfer*, 2005, 48, pp. 1982-1998

[6] C H Mastangelo, “DNA analysis on a chip” *Adv. Sci. and Technology*, 1999, 26, pp. 465

[7] R C McGlennen, “Miniaturization Technologies for Molecular Diagnostics” *Clinical Chemistry*, 2001, 47, pp. 393-402

[8] A Offenhausser, R Rinaldi, “Nanobioelectronics – for Electronics, Biology, and Medicine” *Springer*, 2009

[9] H A Stone, S Kim, “Microfluidics: Basic Issues, Application, and Challenges” *AIChE Journal*, 2001, 47, pp. 1250- 1254

[10] M Wang, J Wang, S Chen, N Pan, “Electrokinetic pumping effects of charged porous media in microchannels using the lattice Poisson-Boltzmann method” *Journal of Colloid and Interface Science*, 2006, 304, 246-253

[11] Y Sato, K Hishida, “Electrokinetic effects on motion of submicron particles in microchannel” *Fluid Dynamics Research*, 2006, 38, pp. 787-802

[12] R Probstein, “Physicochemical hydrodynamics: an introduction” *John Wiley & Sons*, 2005

[13] S Chakraborty, “Microfluidics and Microfabrication” *Springer*, 2010

[14] D Grahame, “The Electric Double Layer and the Theory of Electrocapillarity” *Chem. Rev.*, 1947, 41, pp. 441-501

[15] KL Yang, “Electrical Double-Layer Formation at the Nanoscale” *School of Civil and Envn. Eng. Georgia Inst. Of Tech.*, 2003

[16] FF Reuss, *Memoires de la Societe Imperiale des Natualistes de Moscou*, 1809, 2, pp. 327

[17] G Wiedemann, *Pogg. Ann.*, 1852, 87, pp. 321

[18] H Helmholtz, “Studies of electric boundary layers” *Annals Physik*, 1879, 7, pp. 337-382

[19] L Gouy, *Journal of Physics*, 1910, 9, pp. 456

[20] P Debye, E Hückel, “The theory of electrolytes: lowering of freezing point and related phenomena” *Physikalische Zeitschrift*, 1923, 24, pp. 185-206

[21] O Stern, *Z. Elektrochem.*, 1924, 30, pp. 508

[22] C Ng, Q Zhou, “Dispersion due to electroosmotic flow in a circular microchannel with slowly varying wall potential and hydrodynamic slippage” *Physics of Fluids*, 2012, 24, pp. 112002

[23] Z Chen, S Ghosal, “Electromigration dispersion in capillary electrophoresis” *Bull Math Biol.*, 2012, 74, pp. 346-355

[24] R Aris, “On the dispersion of a solute in a fluid flowing in a tube” *Proc. R. Soc. Lond. A*, 1956, 235, pp. 67-77

[25] G Taylor, “Dispersion of soluble matter in solvent flowing slowly through a tube” *Proc. R. Soc. Lond. A*, 1953, 219, pp. 186-203

[26] G Taylor, “Conditions under which dispersion of a solute in a stream of solvent can be used to measure molecular diffusion” *Proc. R. Soc. Lond. A*, 1954, 225, pp. 473-477

[27] G Taylor, “The dispersion of matter in turbulent flow through a pipe” *Proc. R. Soc. Lond. A*, 1954, 223, pp. 446-468

[28] DSW Lim, JS Kuo, DT Chiu, “Parametric investigation on the effect of channel topologies on electrophoretic separations” *J. Chrommatogr.*, 2004, 1027, pp. 237-244

[29] K Swinney, DJ Bornhop, “Quantification and evaluation of Joule heating in on-chip capillary electrophoresis” *Electrophoresis*, 2002, 23, pp. 613-620

[30] J Koo, C Kleinstreuer, “Viscous dissipation effects in microtubes and microchannels” *Int. J. Heat Mass Transfer*, 2004, 47, pp. 3159-3169

[31] D Maynes, BW Webb, “The effect of viscous dissipation in thermally fully developed electroosmotic hear transfer in microchannels” *Int. J. Heat Mass Transfer*, 2004, 47, pp. 987-999

[32] H Bayley, “Sequencing single molecules of DNA” *Chemical Biology*, 2006, 10, pp. 628-637

[33] D Ling, X Ling, “On the distribution of DNA translocation times in solid state nanopores: an analysis using Schrodinger’s first passage time theory” *J. Phys. Condens. Matter*, 2013, 25, pp. 375102

[34] TT Duong, G Kim, R Ros, M Streek, F Schmid, J Brugger, D Anselmetti, A Ros, “Size dependent free solution DNA electrophoresis in structured microfluidic systems” *Microelectron. Eng.*, 2003, 67, pp. 905-912

[35] S Allison, C Chen, D Stigter, “The length dependence of translational diffusion, free solution electrophoretic mobility, and electrophoretic tether force of rigid rod-like model duplex DNA” *Biophysical Journal*, 2001, 81, pp. 2558-2568

[36] BR McCord, E Buel, “Capillary electrophoresis in forensic genetics” *Encyclopedia of Forensic Sciences*, 2013, pp. 394-401

[37] S Paliwal, B Hwang, K Tsai, S Mitragotri, “Diagnostic opportunities based on skin biomarkers” *European Journal of Pharmaceutical Sciences*, 2013, 50, pp. 546-556

[38] H Harris, S Goren, “Axial diffusion in a cylinder with pulsed flow” *Chemical Eng. Science*, 1967, 22, pp. 1571-1576

[39] UH Kurzweg, MJ Jaeger, “Diffusional separation of gases by sinusoidal oscillations” *Physics of Fluids*, 1987, 30, pp. 1023-1025

[40] A Thomas, “Mass transfer and separation of species in oscillating flows” *University of Florida*, 2001

[41] A Thomas, “Unusual effects of oscillating flows in an annulus on mass transfer and separation” *Advances in Space Research*, 2003, 32, pp. 279-285

[42] A Thomas, R Narayanan, “A comparison between the enhanced mass transfer in boundary and pressure driven oscillatory flow” *Int. J. Heat Mass Transfer*, 2002, 45, pp. 4057-4062

[43] A Thomas, R Narayanan, “Physics of oscillatory flow and its effect on the mass transfer and separation of species” *Physics of Fluids*, 2001, 13, pp. 859-866

[44] YL Chen, MD Graham, JJ de Pablo, K Jo, DC Schwartz, “DNA molecules in microfluidic oscillatory flow” *Macromolecules*, 2005, 38, pp. 6680-6687

[45] D Erickson, D Li, “Analysis of alternating current electroosmotic flows in a rectangular microchannel” *Langmuir*, 2003, 19, pp. 5421-5430

[46] G Ramon, Y Agnon, C Dosoretz, “Solute dispersion in oscillating electroosmotic flow with boundary mass exchange” *Microfluidics and Nanofluidics*, 2011, 10, pp. 97-106

[47] T Aldridge, “Oscillating electroosmotic flow in microchannels” *University of Idaho*, 2007

[48] P Subramanian, “Separation of single stranded DNA by steady and pulsed electroosmotic flows in a microchannel” *University of Idaho*, 2011

[49] S M Hong, S H Kim, J H Kim, J I Hwang, “Hydrophilic Surface Modification of PDMS Using Atmospheric RF Plasma” *Journal of Physics*, 2006, 34, pp. 656-661

[50] H Nagata, M Tabuchi, K Hirano, Y Baba, “Microchip electrophoretic protein separation using electroosmotic flow induced by dynamic sodium dodecyl sulfate-coating of uncoated plastic chips” *Electrophoresis*, 2005, 26, pp. 2247-2253

[51] D Petsev, G Lopez, C Ivory, S Sibbett, “Microchannel protein separation by electric field gradient focusing” *Lab Chip*, 2005, 5, pp. 587-597

[52] I Wong, C Ho, “Surface molecular property modifications for PDMS based microfluidic devices” *Microfluid Nanofluidics*, 2009, 7, pp.291-306

[53] H Makamba, JH Kim, K Lim, N Park, JH Hahn, “Surface modification of polydimethylsiloxane microchannels” *Electrophoresis*, 2003, 24, pp. 3607-3619

[54] Y Huang, M Uppalapati, W Hancock, T Jackson, “Microtubule transport, concentration and alignment in enclosed microfluidic channels” *Biomed Microdevices*, 2007, 9, pp. 175-184

[55] M Yao, J Fang, “Hydrophilic PEO-PDMS for microfluidic applications” *J. Micromech. Microeng.*, 2012, 22, pp. 025012

Appendix A: Sample Plots of Experimental Data

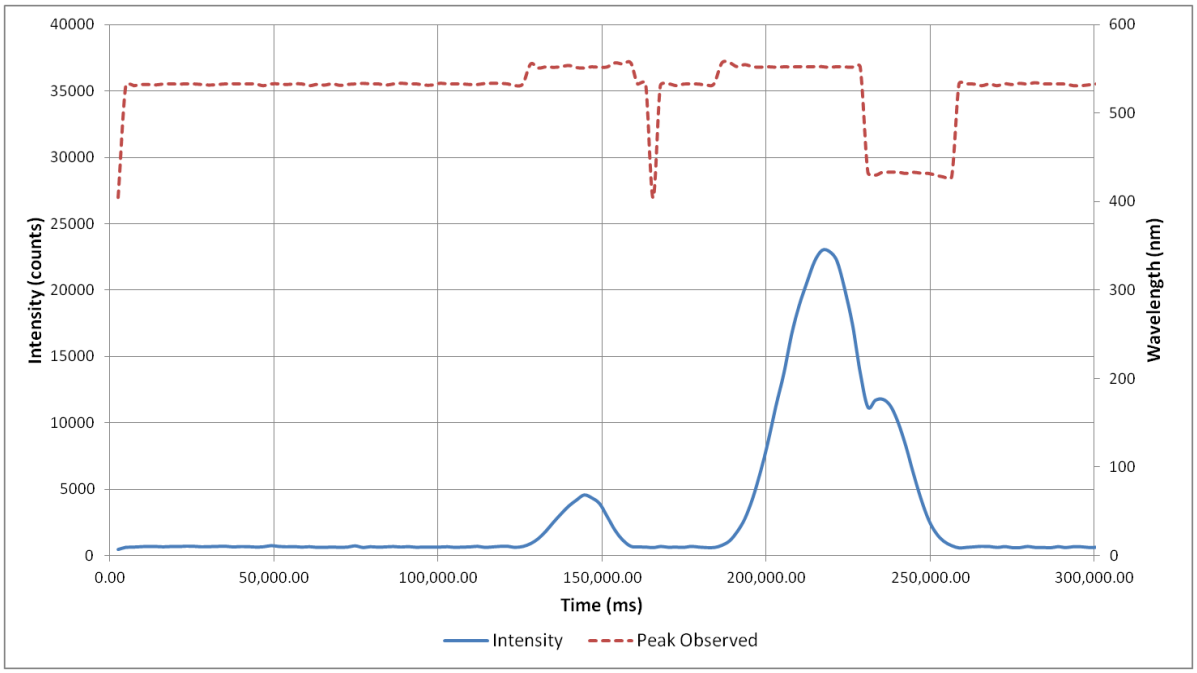

Figure A.1 Avasoft data from a 10v50mer steady flow experiment at a voltage of +125V.

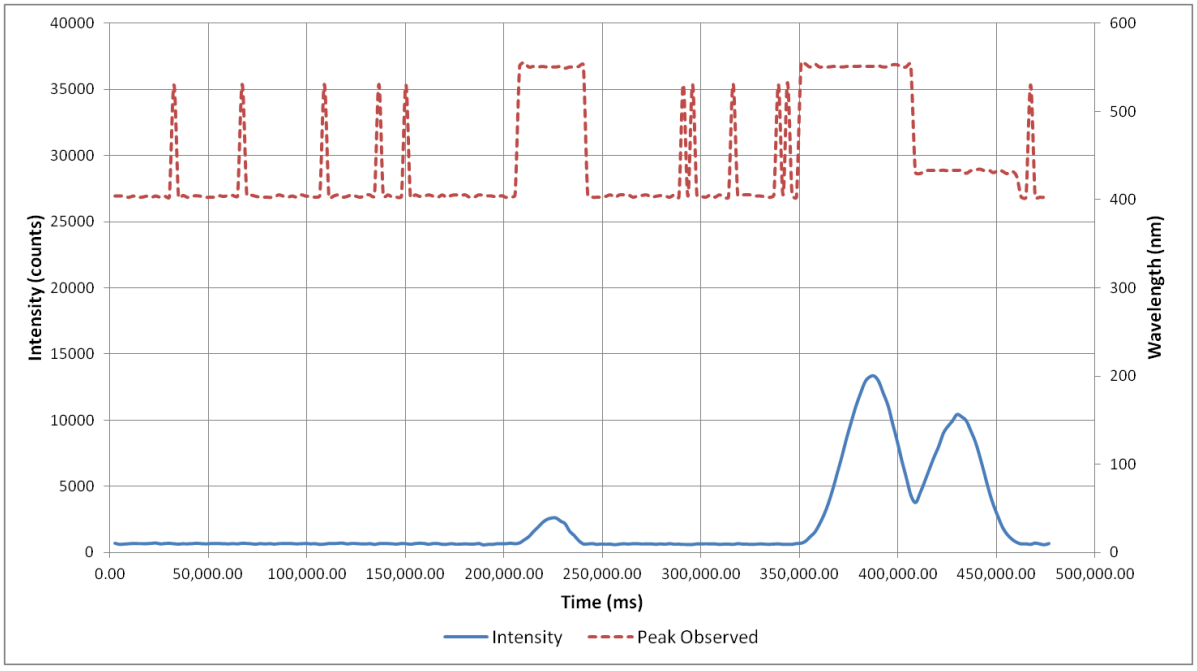

Figure A.2 Avasoft data from a 10v50mer steady flow experiment at a voltage of +125V.

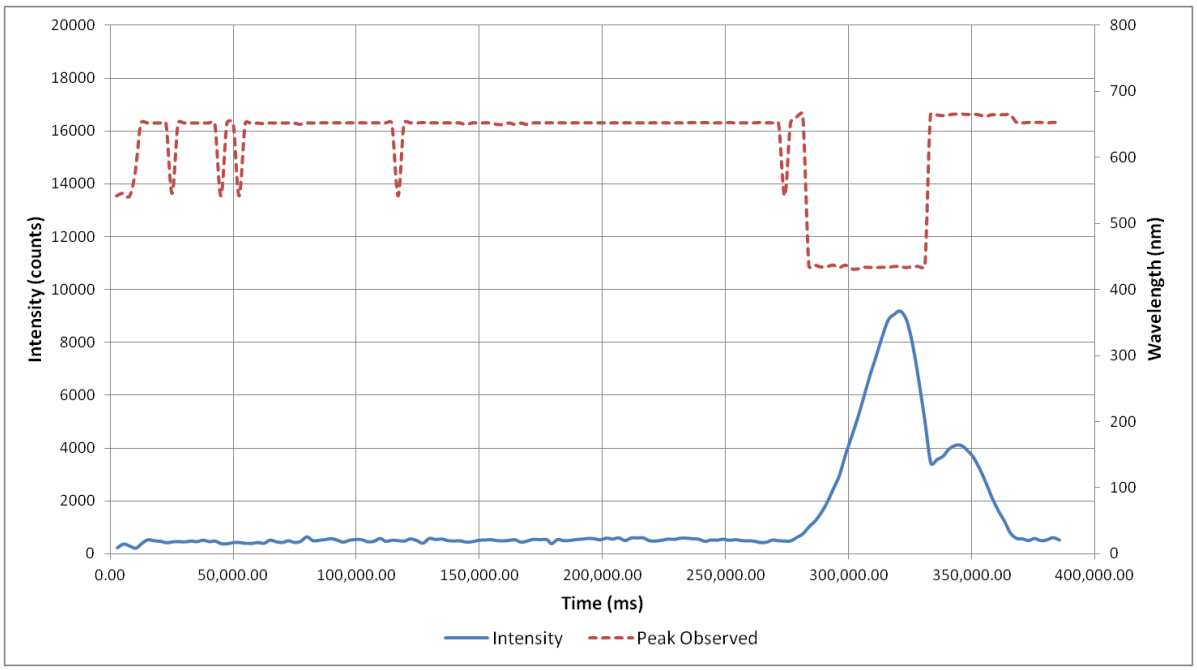

Figure A.3 Avasoft data from a 10v100mer steady flow experiment at a voltage of +125V.

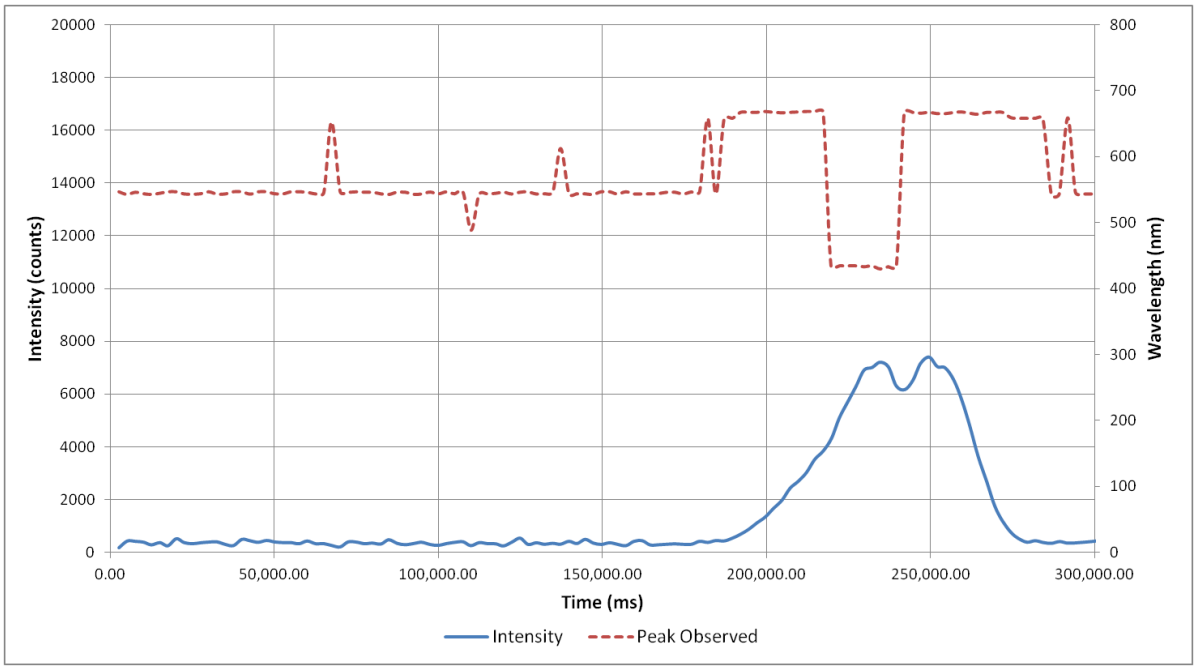

Figure A.4 Avasoft data from a 10v100mer steady flow experiment at a voltage of +125V.

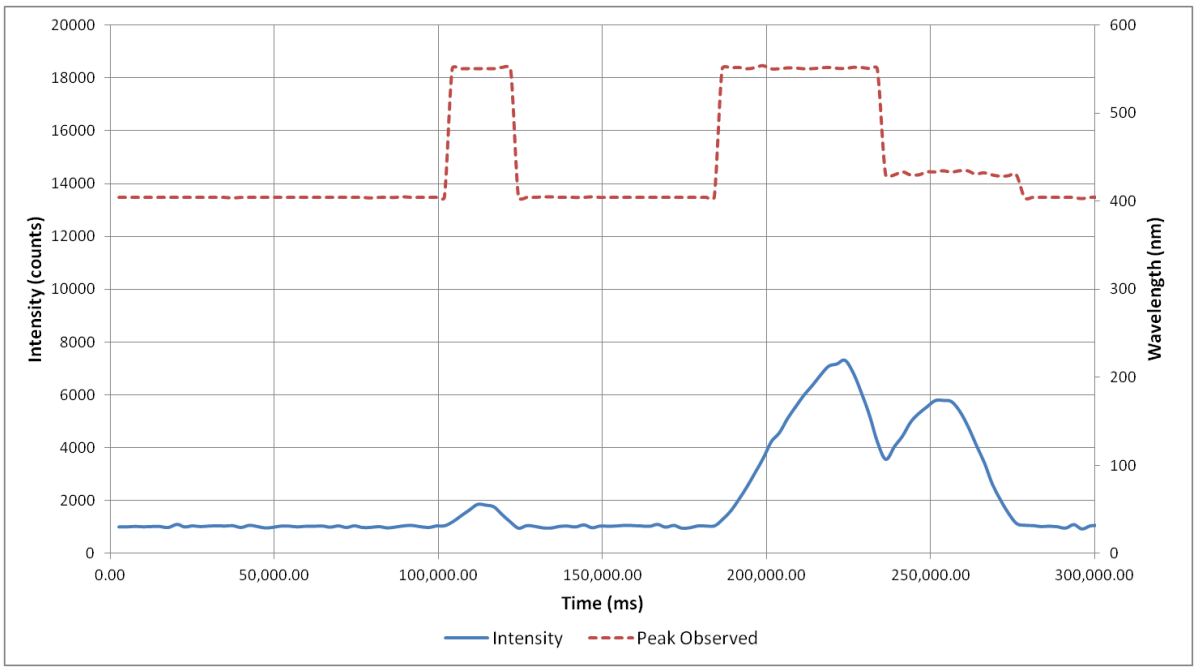

Figure A.5 Avasoft data from a 10v50mer pulsatile flow experiment at a voltage of +300/-50V, 4Hz.

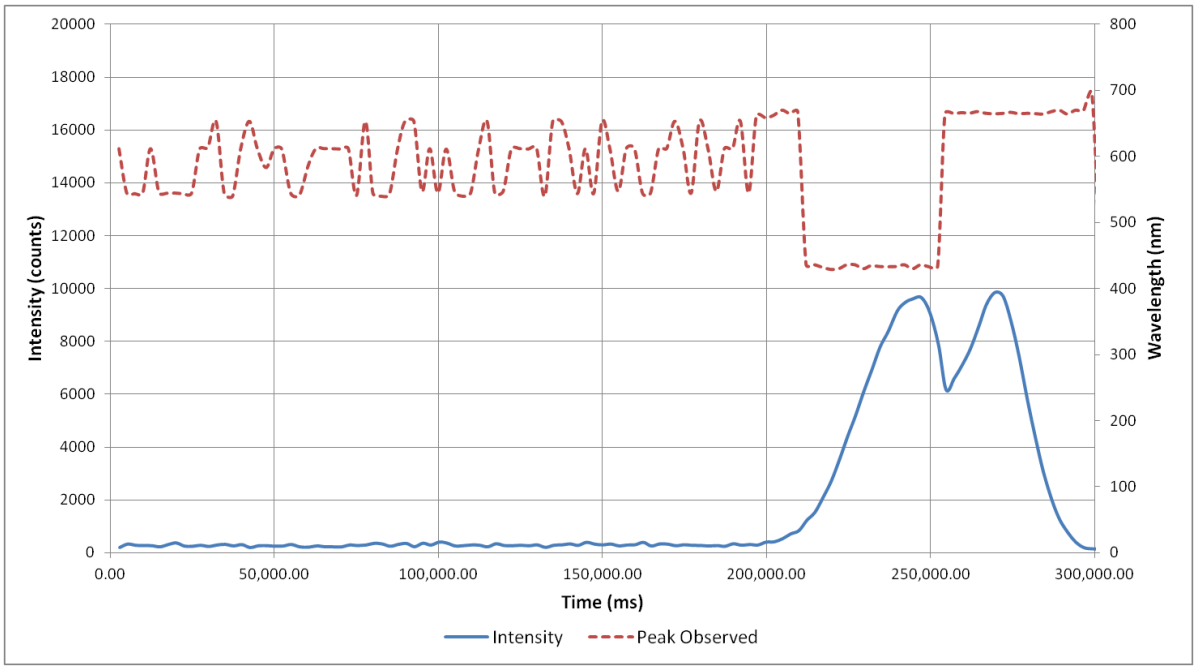

Figure A.6 Avasoft data from a 10v100mer pulsatile flow experiment at a voltage of +300/-50V, 4Hz.

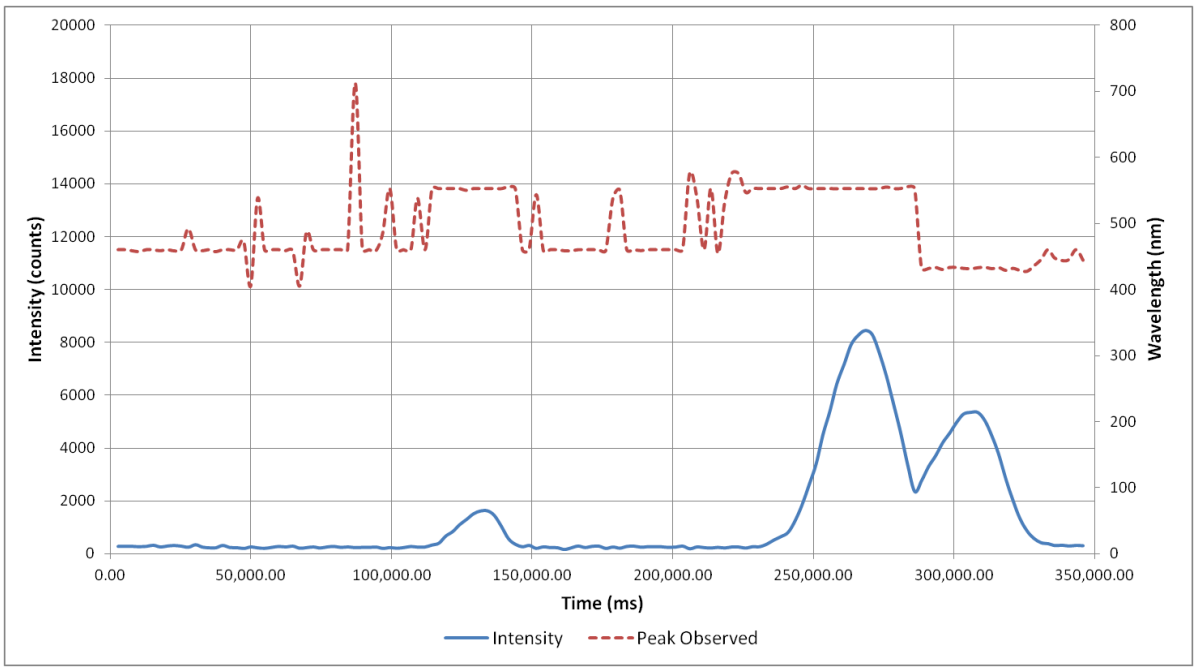

Figure A.7 Avasoft data from a 10v50mer pulsatile flow experiment at a voltage of +325/-75V, 4Hz.

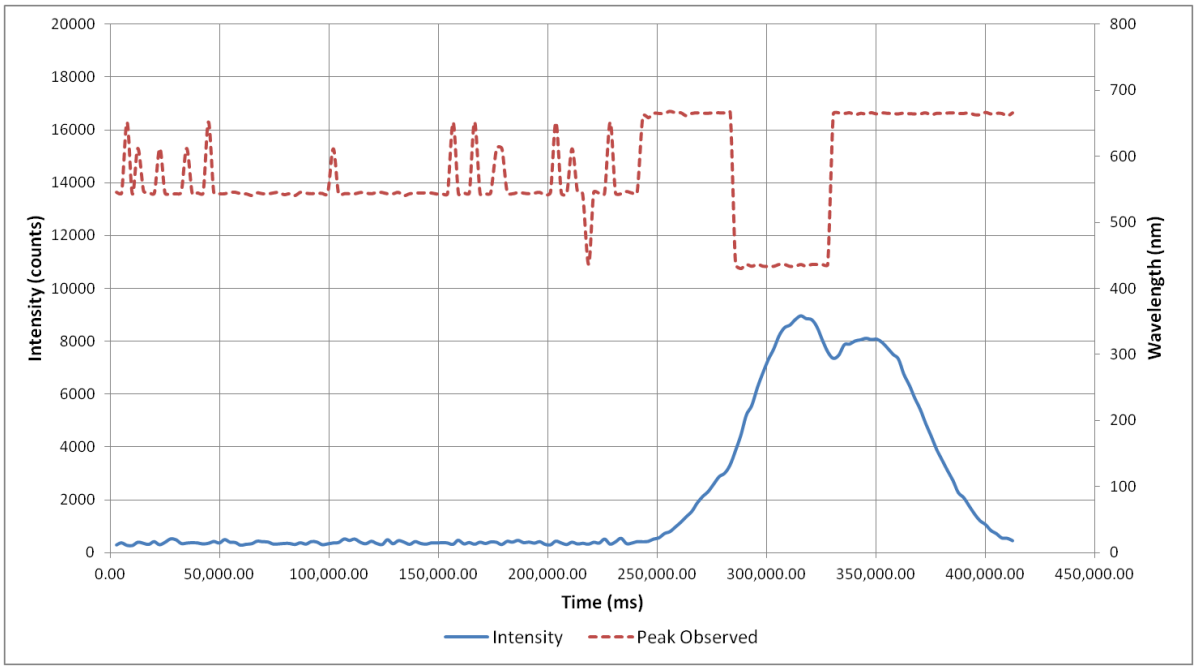

Figure A.8 Avasoft data from a 10v100mer pulsatile flow experiment at a voltage of +325/-75V, 4Hz.

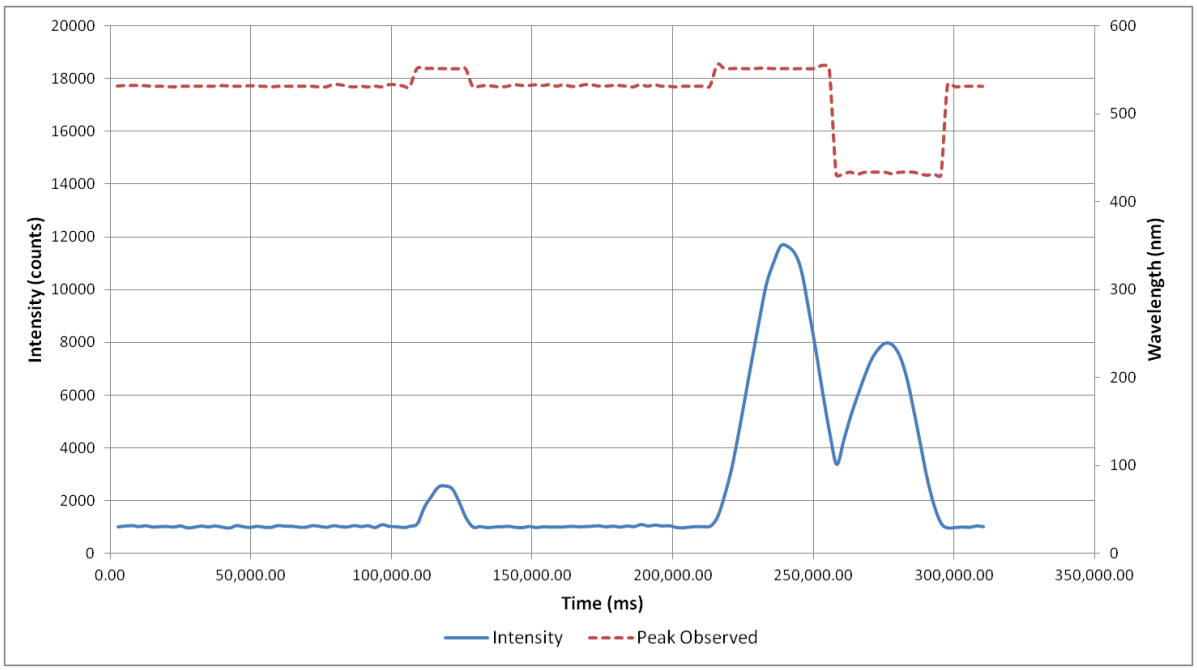

Figure A.9 Avasoft data from a 10v50mer pulsatile flow experiment at a voltage of +350/-100V, 4Hz.

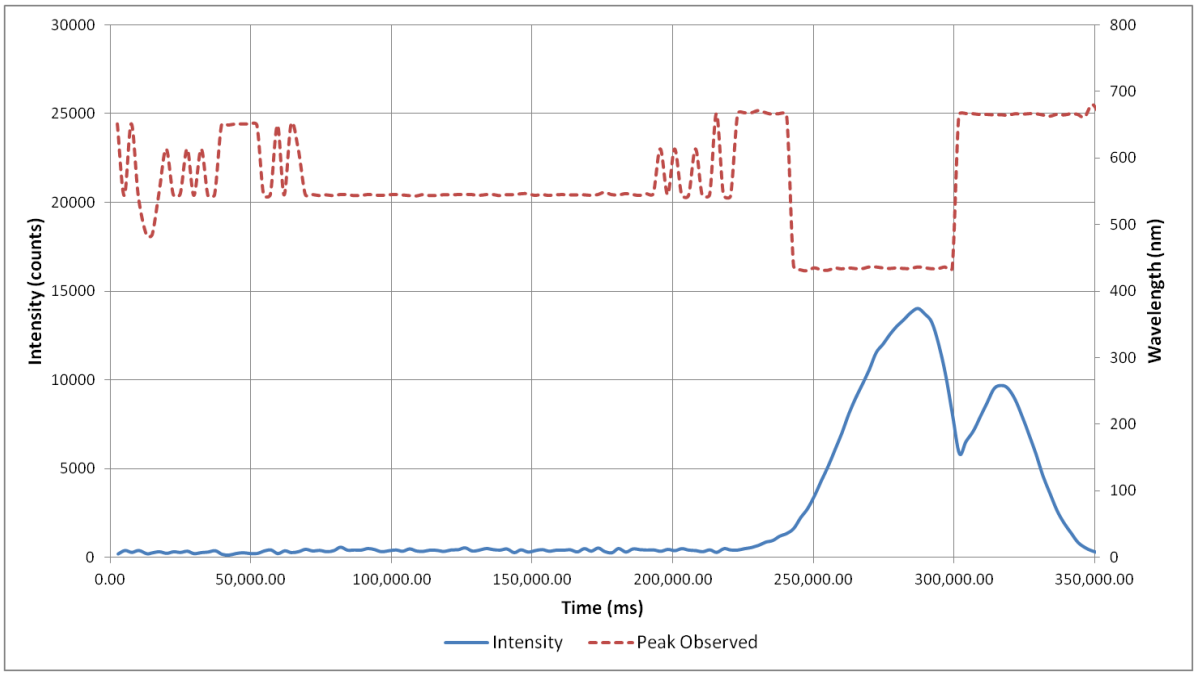

Figure A.10 Avasoft data from a 10v100mer pulsatile flow experiment at a voltage of +350/-100V, 4Hz.

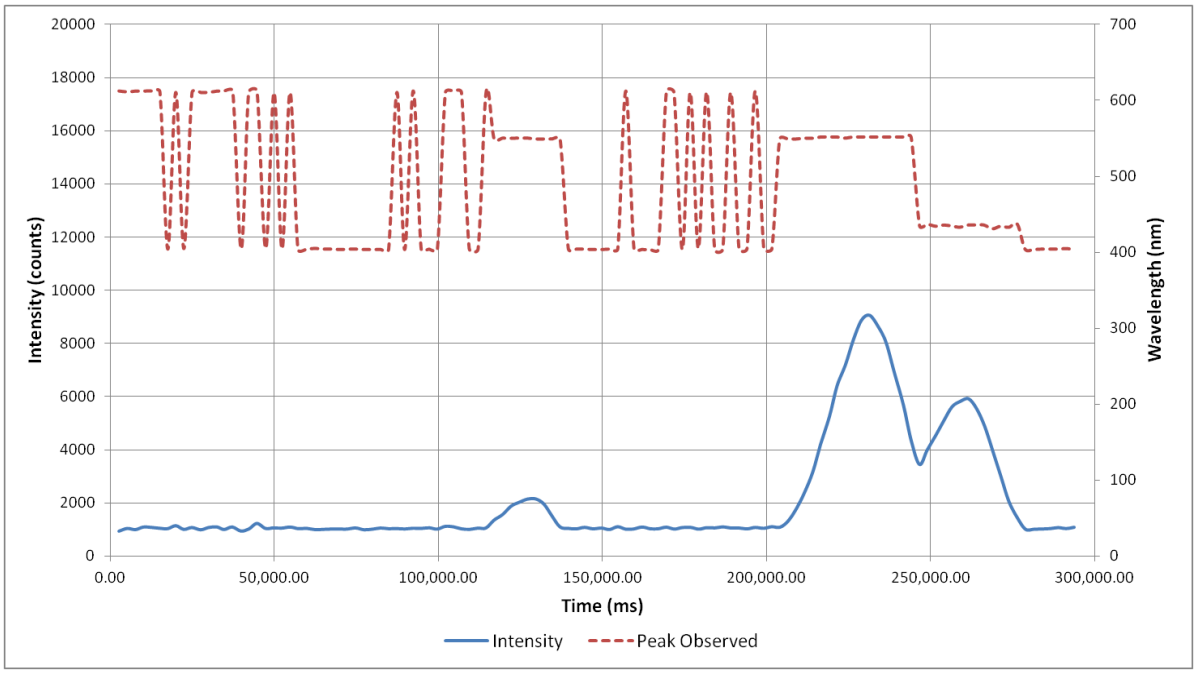

Figure A.11 Avasoft data from a 10v50mer pulsatile flow experiment at a voltage of +375/-125V, 4Hz.

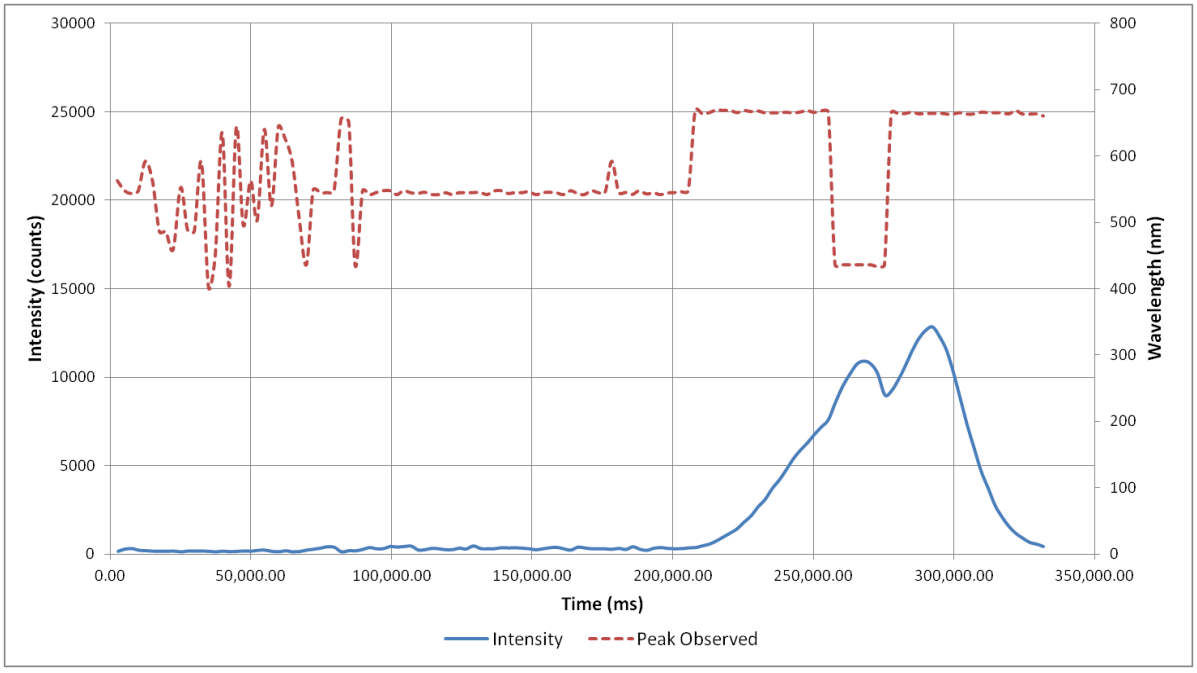

Figure A.12 Avasoft data from a 10v100mer pulsatile flow experiment at a voltage of +375/-125V, 4Hz.

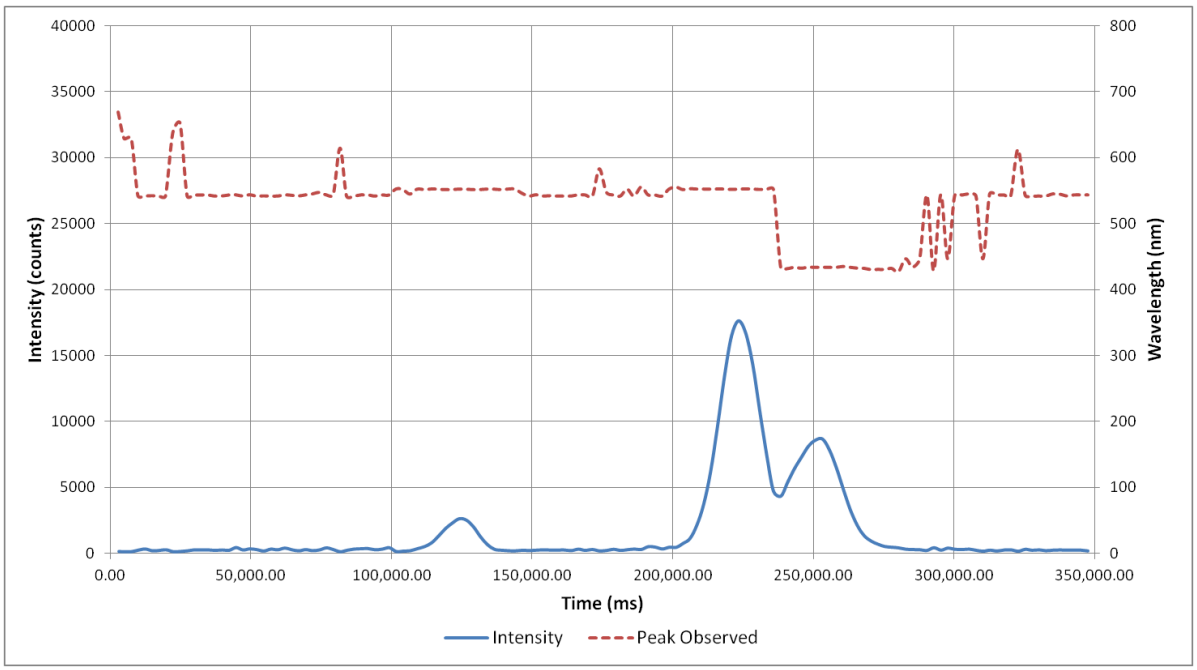

Figure A.13 Avasoft data from a 10v50mer pulsatile flow experiment at a voltage of +350/-125V, 4Hz.

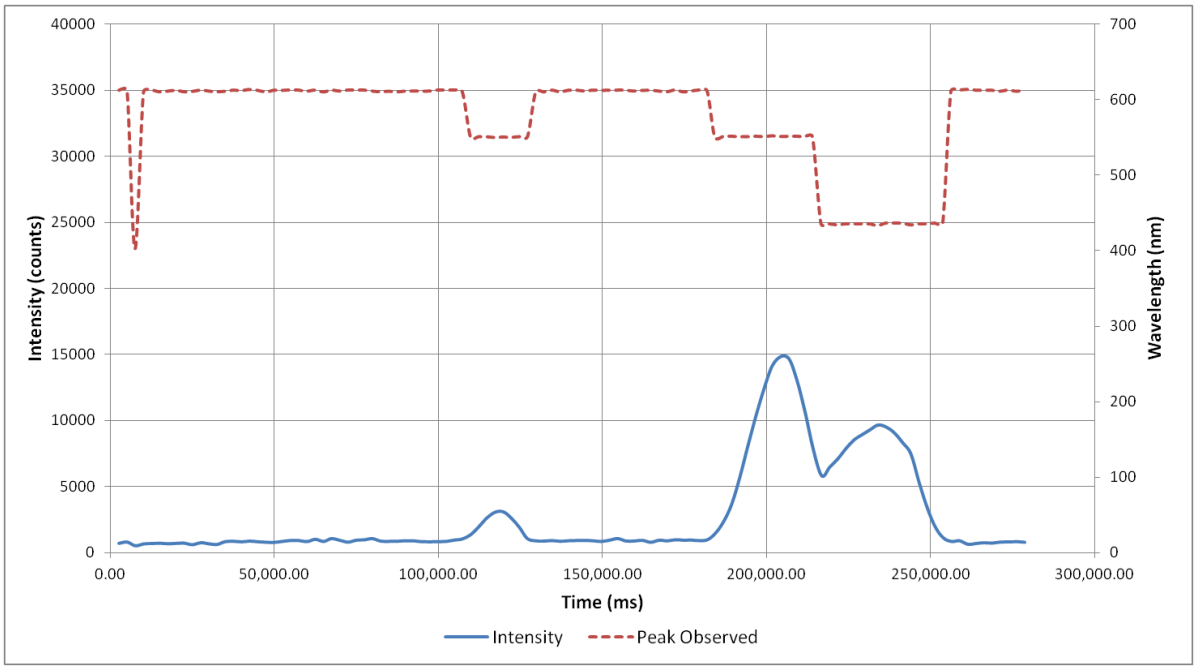

Figure A.14 Avasoft data from a 10v50mer pulsatile flow experiment at a voltage of +375/-100V, 4Hz.

Appendix B: Raw Data

Distance from Intersct. (cm)	AF 532 Peak (s)	AF 405 Peak (s)	Inter-Peak Distance (s)	Averaged speed (microns/s)	Separation Distance (mm)	Separation per Distance (mm/mm)	Sep. Dist./ Residence Time
2.5	519.4	575.3	55.9	33.921	1.89621	0.07585	0.002573
2.5	495.9	540.3	44.4	35.809	1.58991	0.06360	0.002277
2.5	488.5	533.1	44.6	36.323	1.62001	0.06480	0.002354
2.5	504.7	555.7	51	35.008	1.78543	0.07142	0.002500
2.5	425.9	467.8	41.9	41.534	1.74026	0.06961	0.002891
2.5	473.6	520.4	46.8	37.343	1.74767	0.06991	0.002611
2.5	524.8	582.8	58	33.531	1.94479	0.07779	0.002608
2.5	277	295.6	18.6	64.751	1.20436	0.04817	0.003119
2.5	442.5	487	44.5	39.938	1.77723	0.07109	0.002839
2.5	447.9	490	42.1	39.569	1.66586	0.06663	0.002637
					Average =	0.06789	0.002641
					Standard Deviation =	0.00823	0.000252
					90% confidence =	0.00428	0.000131
					95% confidence =	0.00510	0.000156

Table B.1 Calculation sheet for the 10v50mer DC +125V experiments.

Distance from Intersct. (cm)	AF 405 Peak (s)	Cy5 Peak (s)	Inter-Peak Distance (s)	Averaged speed (microns/s)	Separation Distance (mm)	Separation per Distance (mm/mm)	Sep. Dist./ Residence Time
2.5	449.9	475.8	25.9	40.041	1.03706	0.04148	0.001661
2.5	302	309.4	7.4	60.586	0.44834	0.01793	0.001087
2.5	268.5	281.1	12.6	67.425	0.84955	0.03398	0.002291
2.5	363.9	385	21.1	49.495	1.04433	0.04177	0.002068
2.5	276.3	291.2	14.9	65.309	0.97310	0.03892	0.002542
2.5	321.9	338.1	16.2	56.151	0.90964	0.03639	0.002043
2.5	317.1	335.7	18.6	56.782	1.05614	0.04225	0.002399
2.5	294.5	309.5	15	61.357	0.92036	0.03681	0.002259
2.5	362.8	383.8	21	49.647	1.04258	0.04170	0.002070
2.5	381	404.6	23.6	47.187	1.11362	0.04454	0.002102
					Average =	0.03758	0.002052
					Standard Deviation =	0.00795	0.000415
					90% confidence =	0.00414	0.000216
					95% confidence =	0.00493	0.000257

Table B.2 Calculation sheet for the 10v100mer DC +125V experiments.

Distance from Intersct. (cm)	AF 532 Peak (s)	AF 405 Peak (s)	Inter-Peak Distance (s)	Averaged speed (microns/s)	Separation Distance (mm)	Separation per Distance (mm/mm)	Sep. Dist./ Residence Time
2.5	271.1	298.3	27.2	65.194	1.77329	0.07093	0.004624
2.5	267.2	298.2	31	65.703	2.03681	0.08147	0.005353
2.5	278.7	307.1	28.4	63.374	1.79981	0.07199	0.004562
2.5	288.9	316.1	27.2	61.342	1.66851	0.06674	0.004094
2.5	259.5	285.5	26	68.113	1.77093	0.07084	0.004825
2.5	283.9	312.6	28.7	62.235	1.78613	0.07145	0.004446
2.5	271.9	299.2	27.3	65.001	1.77452	0.07098	0.004614
2.5	311.3	344.9	33.6	56.590	1.90143	0.07606	0.004304
2.5	272.3	299.9	27.6	64.878	1.79064	0.07163	0.004647
2.5	316.4	350.9	34.5	55.652	1.91998	0.07680	0.004274
					Average =	0.07289	0.004574
				Standard Deviation =		0.00412	0.000348
				90% confidence =		0.00214	0.000181
				95% confidence =		0.00256	0.000216

Table B.3 Calculation sheet for the 10v50mer AC +300/-50V, 4Hz experiments.

Distance from Intersct. (cm)	AF 532 Peak (s)	AF 405 Peak (s)	Inter-Peak Distance (s)	Averaged speed (microns/s)	Separation Distance (mm)	Separation per Distance (mm/mm)	Sep. Dist./ Residence Time
2.5	262.1	274.5	12.4	69.059	0.85633	0.03425	0.002365
2.5	329	353.8	24.8	54.315	1.34700	0.05388	0.002926
2.5	269	284	15	67.024	1.00536	0.04021	0.002695
2.5	558.2	594.5	36.3	32.163	1.16750	0.04670	0.001502
2.5	271.7	291.5	19.8	65.843	1.30369	0.05215	0.003434
2.5	311.7	331.6	19.9	57.629	1.14681	0.04587	0.002644
2.5	289.1	308.9	19.8	62.003	1.22766	0.04911	0.003045
2.5	307.1	329.6	22.5	58.243	1.31047	0.05242	0.003053
2.5	360.9	390.9	30	49.343	1.48029	0.05921	0.002922
2.5	291.7	312.7	21	61.353	1.28841	0.05154	0.003162
					Average =	0.04853	0.002775
				Standard Deviation =		0.00718	0.000536
				90% confidence =		0.00373	0.000279
				95% confidence =		0.00445	0.000332

Table B.4 Calculation sheet for the 10v100mer AC +300/-50V, 4Hz experiments.

Distance from Intersct. (cm)	AF 532 Peak (s)	AF 405 Peak (s)	Inter-Peak Distance (s)	Averaged speed (microns/s)	Separation Distance (mm)	Separation per Distance (mm/mm)	Sep. Dist./ Residence Time
2.5	288.8	323.5	34.7	60.683	2.10571	0.08423	0.005111
2.5	328.5	366.1	37.6	53.478	2.01078	0.08043	0.004301
2.5	303.6	335.7	32.1	58.080	1.86437	0.07457	0.004331
2.5	234	256.3	22.3	75.696	1.68802	0.06752	0.005111
2.5	368.2	412.7	44.5	47.583	2.11745	0.08470	0.004030
2.5	271.1	303.4	32.3	64.673	2.08893	0.08356	0.005404
2.5	308.5	348.2	39.7	56.606	2.24724	0.08989	0.005088
2.5	285.3	317.5	32.2	61.617	1.98408	0.07936	0.004890
2.5	284.3	314	29.7	62.057	1.84308	0.07372	0.004575
2.5	305.7	342.6	36.9	57.315	2.11493	0.08460	0.004849
					Average =	0.08026	0.004769
					Standard Deviation =	0.00663	0.000441
					90% confidence =	0.00345	0.000230
					95% confidence =	0.00411	0.000274

Table B.5 Calculation sheet for the 10v50mer AC +325/-75V, 4Hz experiments.

Distance from Intersct. (cm)	AF 532 Peak (s)	AF 405 Peak (s)	Inter-Peak Distance (s)	Averaged speed (microns/s)	Separation Distance (mm)	Separation per Distance (mm/mm)	Sep. Dist./ Residence Time
2.5	420.8	453.5	32.7	42.421	1.38718	0.05549	0.002354
2.5	291.8	316.4	24.6	60.996	1.50050	0.06002	0.003661
2.5	359.1	385.1	26	49.828	1.29554	0.05182	0.002582
2.5	375.7	405.5	29.8	47.480	1.41489	0.05660	0.002687
2.5	366.3	399.7	33.4	48.443	1.61801	0.06472	0.003135
2.5	316.4	341.4	25	56.386	1.40965	0.05639	0.003179
2.5	283.9	304.2	20.3	63.053	1.27997	0.05120	0.003228
2.5	300.2	327.3	27.1	59.133	1.60252	0.06410	0.003790
2.5	408.8	443.5	34.7	43.528	1.51041	0.06042	0.002630
2.5	283.3	303.1	19.8	63.232	1.25200	0.05008	0.003167
					Average =	0.05708	0.003041
					Standard Deviation =	0.00518	0.000472
					90% confidence =	0.00270	0.000245
					95% confidence =	0.00321	0.000292

Table B.6 Calculation sheet for the 10v100mer AC +325/-75V, 4Hz experiments.

Distance from Intersct. (cm)	AF 532 Peak (s)	AF 405 Peak (s)	Inter-Peak Distance (s)	Averaged speed (microns/s)	Separation Distance (mm)	Separation per Distance (mm/mm)	Sep. Dist./ Residence Time
2.5	262.9	290.3	27.4	67.115	1.83896	0.07356	0.004937
2.5	281	322.8	41.8	61.635	2.57636	0.10305	0.006352
2.5	269.5	301.9	32.4	65.027	2.10688	0.08428	0.005480
2.5	299.6	335.6	36	58.496	2.10584	0.08423	0.004927
2.5	298.1	340.4	42.3	58.262	2.46448	0.09858	0.005743
2.5	298.4	344	45.6	57.946	2.64234	0.10569	0.006125
2.5	281.4	316.3	34.9	62.178	2.17001	0.08680	0.005397
2.5	263.8	293.6	29.8	66.637	1.98577	0.07943	0.005293
2.5	323.5	363.4	39.9	54.102	2.15866	0.08635	0.004671
2.5	263.4	293.4	30	66.711	2.00134	0.08005	0.005340
					Average =	0.08820	0.005427
					Standard Deviation =	0.01069	0.000530
					90% confidence =	0.00556	0.000276
					95% confidence =	0.00663	0.000329

Table B.7 Calculation sheet for the 10v50mer AC +350/-100V, 4Hz experiments.

Distance from Intersct. (cm)	AF 532 Peak (s)	AF 405 Peak (s)	Inter-Peak Distance (s)	Averaged speed (microns/s)	Separation Distance (mm)	Separation per Distance (mm/mm)	Sep. Dist./ Residence Time
2.5	281.1	303.3	22.2	63.468	1.40898	0.05636	0.003577
2.5	302.2	330.5	28.3	58.655	1.65995	0.06640	0.003895
2.5	340.4	372.7	32.3	52.045	1.68105	0.06724	0.003500
2.5	356.3	393.6	37.3	49.512	1.84679	0.07387	0.003658
2.5	270.3	292.6	22.3	65.900	1.46958	0.05878	0.003874
2.5	331.4	361.1	29.7	53.582	1.59137	0.06365	0.003411
2.5	273.3	295.5	22.2	65.214	1.44774	0.05791	0.003777
2.5	295.2	320	24.8	60.301	1.49547	0.05982	0.003607
2.5	347.3	377.2	29.9	51.208	1.53112	0.06124	0.003136
2.5	357.6	395.5	37.9	49.304	1.86863	0.07475	0.003685
					Average =	0.06400	0.003612
					Standard Deviation =	0.00647	0.000227
					90% confidence =	0.00337	0.000118
					95% confidence =	0.00401	0.000141

Table B.8 Calculation sheet for the 10v100mer AC +350/-100V, 4Hz experiments.

Distance from Intersct. (cm)	AF 532 Peak (s)	AF 405 Peak (s)	Inter-Peak Distance (s)	Averaged speed (microns/s)	Separation Distance (mm)	Separation per Distance (mm/mm)	Sep. Dist./ Residence Time
2.5	298.2	327.9	29.7	59.289	1.76087	0.07043	0.004176
2.5	308.2	338.1	29.9	57.429	1.71713	0.06869	0.003945
2.5	313.8	348.6	34.8	56.068	1.95117	0.07805	0.004376
2.5	291.4	321.6	30.2	60.566	1.82910	0.07316	0.004431
2.5	338.8	378.2	39.4	51.812	2.04139	0.08166	0.004231
2.5	301.2	335.9	34.7	58.307	2.02324	0.08093	0.004719
2.5	298.3	331.8	33.5	58.946	1.97470	0.07899	0.004656
2.5	289.2	321.7	32.5	60.799	1.97597	0.07904	0.004805
2.5	290.9	323.3	32.4	60.470	1.95921	0.07837	0.004739
2.5	288.9	318.6	29.7	61.112	1.81504	0.07260	0.004437
					Average =	0.07619	0.004451
					Standard Deviation =	0.00457	0.000281
					90% confidence =	0.00238	0.000146
					95% confidence =	0.00283	0.000174

Table B.9 Calculation sheet for the 10v50mer AC +375/-125V, 4Hz experiments.

Distance from Intersct. (cm)	AF 532 Peak (s)	AF 405 Peak (s)	Inter-Peak Distance (s)	Averaged speed (microns/s)	Separation Distance (mm)	Separation per Distance (mm/mm)	Sep. Dist./ Residence Time
2.5	421	460.3	39.3	42.109	1.65489	0.06620	0.002787
2.5	352.3	373.4	21.1	51.079	1.07778	0.04311	0.002202
2.5	439.4	474	34.6	40.607	1.40500	0.05620	0.002282
2.5	404.6	436.9	32.3	44.078	1.42372	0.05695	0.002510
2.5	328	352.5	24.5	54.497	1.33517	0.05341	0.002911
2.5	325.9	346.1	20.2	55.164	1.11432	0.04457	0.002459
2.5	328.8	353.6	24.8	54.346	1.34779	0.05391	0.002930
2.5	357.8	385.1	27.3	49.922	1.36287	0.05451	0.002721
2.5	391.2	420.9	29.7	45.668	1.35633	0.05425	0.002478
2.5	354.5	387.1	32.6	50.039	1.63126	0.06525	0.003265
					Average =	0.05484	0.002655
					Standard Deviation =	0.00738	0.000328
					90% confidence =	0.00384	0.000171
					95% confidence =	0.00457	0.000203

Table B.10 Calculation sheet for the 10v100mer AC +375/-125V, 4Hz experiments.

Distance from Intersct. (cm)	AF 532 Peak (s)	AF 405 Peak (s)	Inter-Peak Distance (s)	Averaged speed (microns/s)	Separation Distance (mm)	Separation per Distance (mm/mm)	Sep. Dist./ Residence Time
2.5	278.7	306.2	27.5	63.462	1.74521	0.06981	0.004430
2.5	261.5	286.3	24.8	67.749	1.68018	0.06721	0.004553
2.5	301.5	331.4	29.9	58.650	1.75365	0.07015	0.004114
2.5	281.1	310.9	29.8	62.721	1.86910	0.07476	0.004689
2.5	325.9	359.6	33.7	54.160	1.82520	0.07301	0.003954
2.5	283.4	313.2	29.8	62.235	1.85462	0.07418	0.004617
2.5	261.4	286.5	25.1	67.740	1.70028	0.06801	0.004607
2.5	286	315.9	29.9	61.686	1.84440	0.07378	0.004551
2.5	277.5	307.4	29.9	63.488	1.89829	0.07593	0.004821
2.5	321.7	356.5	34.8	54.755	1.90547	0.07622	0.004173
					Average =	0.07231	0.004451
					Standard Deviation =	0.00327	0.000280
					90% confidence =	0.00170	0.000145
					95% confidence =	0.00202	0.000173

Table B.11 Calculation sheet for the 10v50mer AC +350/-125V, 4Hz experiments.

Distance from Intersct. (cm)	AF 532 Peak (s)	AF 405 Peak (s)	Inter-Peak Distance (s)	Averaged speed (microns/s)	Separation Distance (mm)	Separation per Distance (mm/mm)	Sep. Dist./ Residence Time
2.5	348.6	388.2	39.6	50.413	1.99636	0.07985	0.004026
2.5	286.6	313.9	27.3	61.805	1.68727	0.06749	0.004171
2.5	320.3	357.4	37.1	54.815	2.03365	0.08135	0.004459
2.5	264.4	294	29.6	66.514	1.96881	0.07875	0.005238
2.5	300.3	336.6	36.3	58.342	2.11780	0.08471	0.004942
2.5	291.6	321.5	29.9	60.553	1.81055	0.07242	0.004385
2.5	338.2	380.4	42.2	51.719	2.18254	0.08730	0.004515
2.5	315.4	352.6	37.2	55.617	2.06896	0.08276	0.004603
2.5	286.7	315.2	28.5	61.672	1.75765	0.07031	0.004336
2.5	266.7	291.6	24.9	66.471	1.65513	0.06621	0.004401
					Average =	0.07711	0.004508
					Standard Deviation =	0.00746	0.000355
					90% confidence =	0.00388	0.000185
					95% confidence =	0.00463	0.000220

Table B.12 Calculation sheet for the 10v50mer AC +375/-100V, 4Hz experiments.

Appendix C: Separation Plots

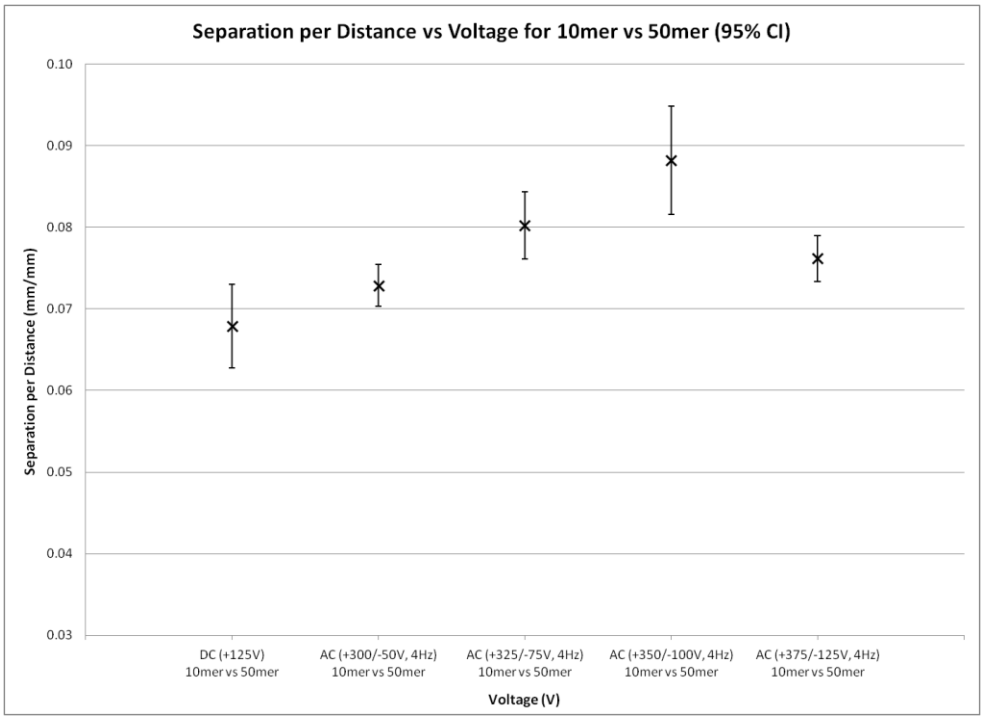

Figure C. 1 Separation per distance for 10v50mer trails plotted against the steady and pulsatile voltages with 95% confidence intervals.

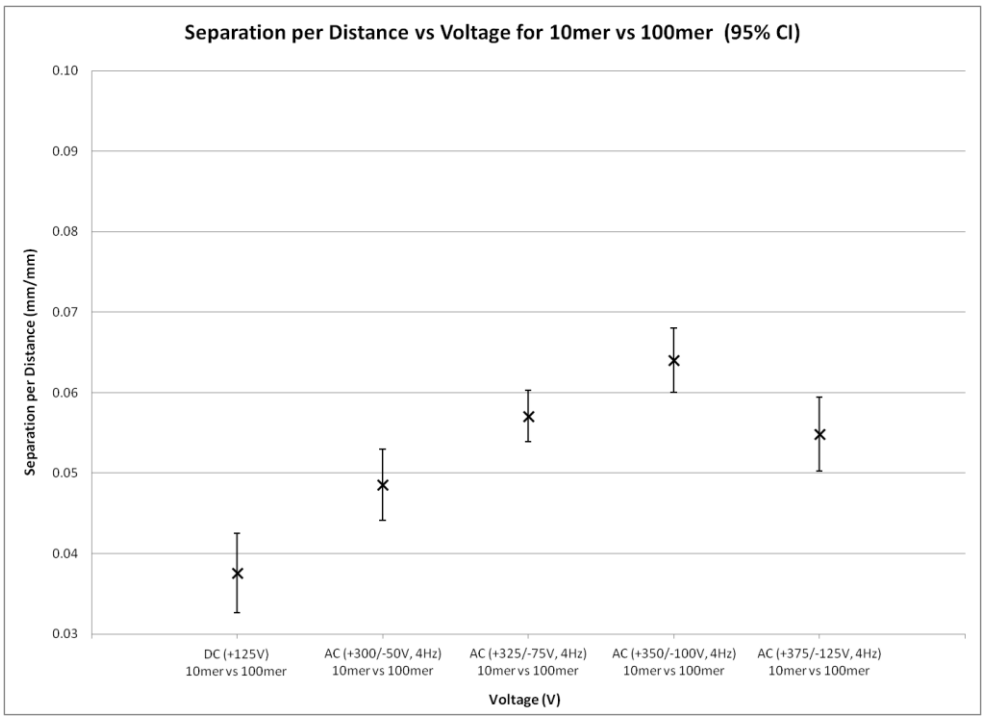

Figure C. 2 Separation per distance for 10v100mer trails plotted against the steady and pulsatile voltages with 95% confidence intervals.

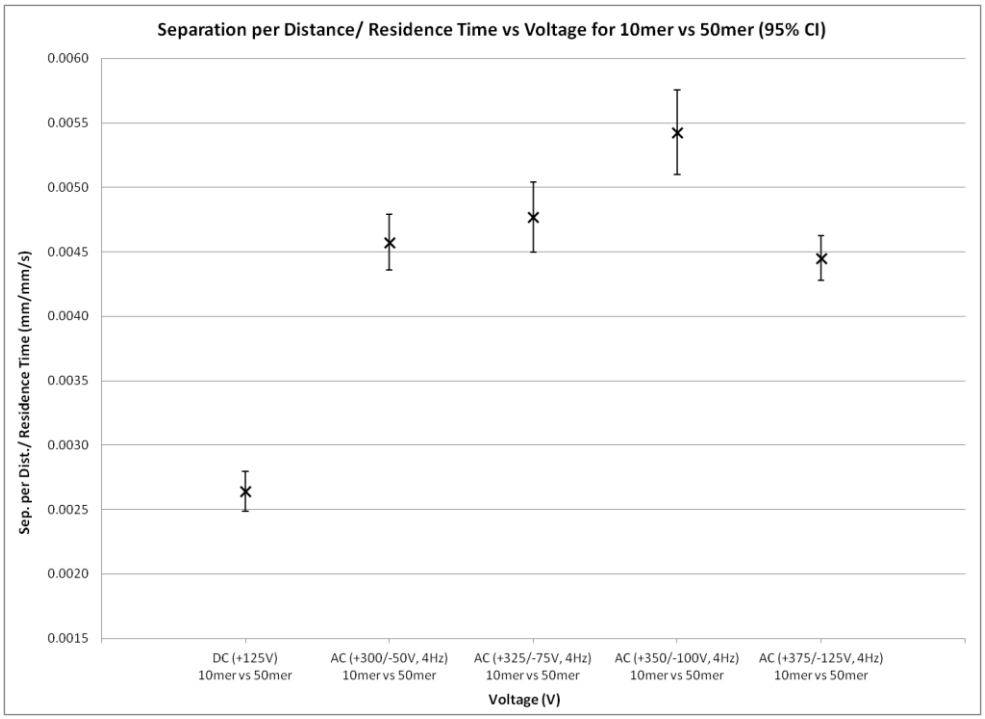

Figure C. 3 Separation per distance per residence time for 10v50mer trails plotted against the steady and pulsatile voltages with 95% confidence intervals.

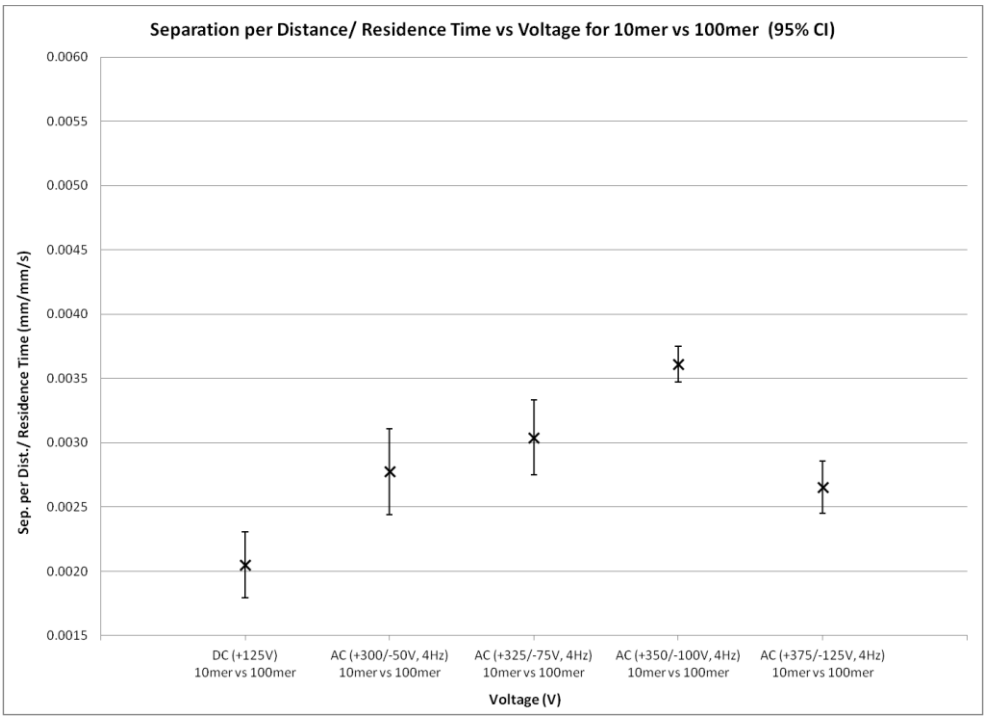

Figure C. 4 Separation per distance per residence time for 10v100mer trails plotted against the steady and pulsatile voltages with 95% confidence intervals.

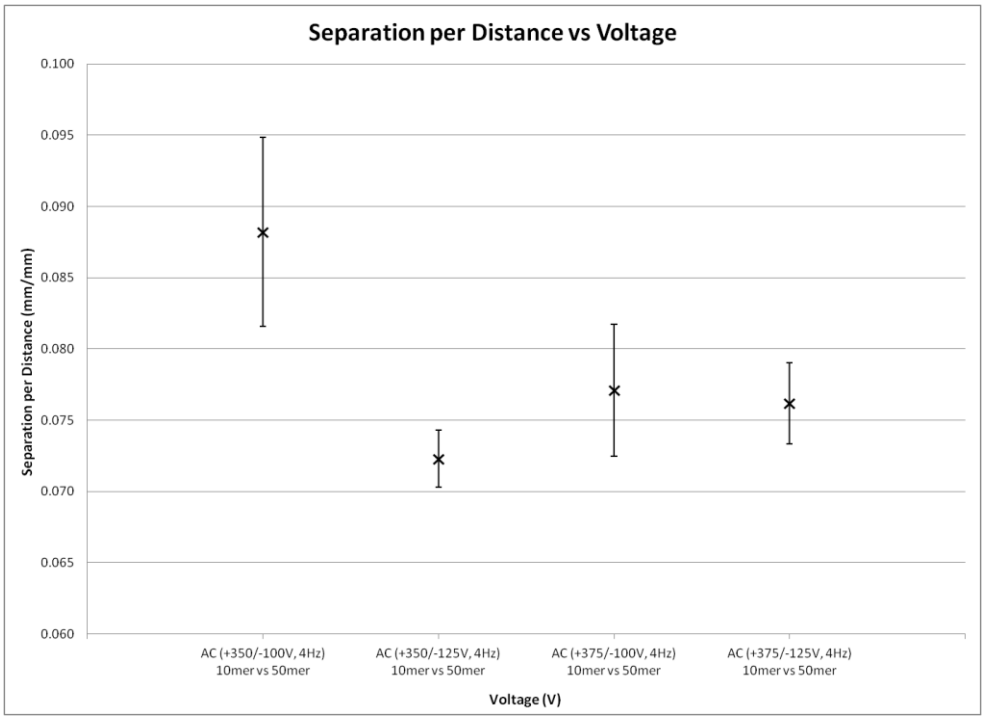

Figure C. 5 Separation per distance for 10v50mer threshold limit trails with 95% confidence intervals.

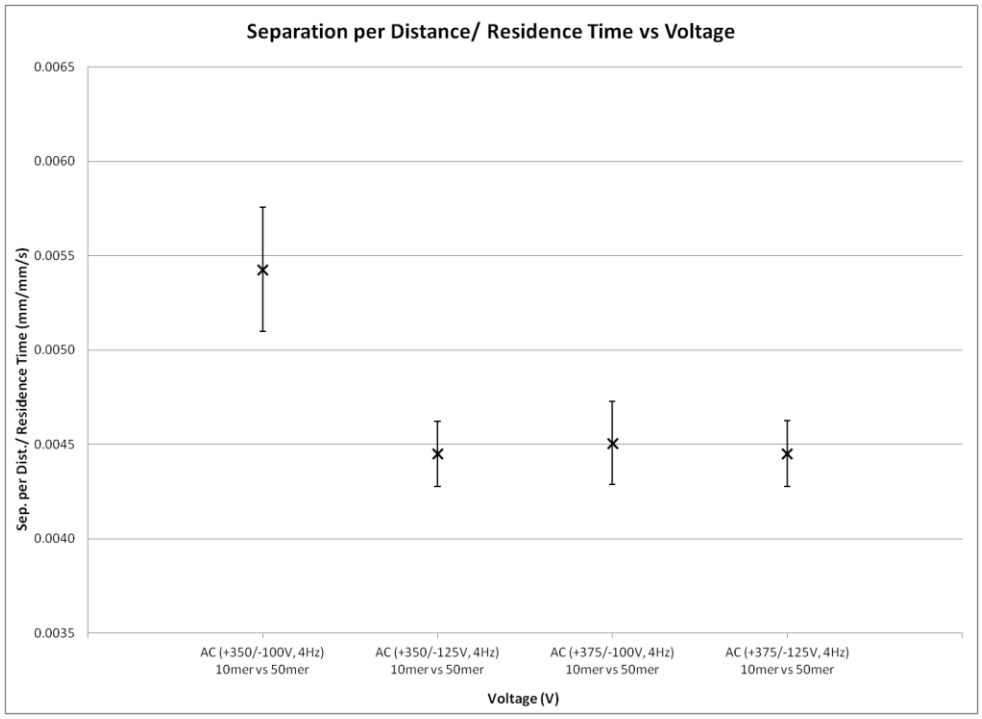

Figure C. 6 Separation per distance per residence time for 10v50mer threshold limit trails with 95% confidence intervals.

Appendix D: Statistical Calculations

The means of the pulsed flows(X_p) with the varying voltage combinations but all with a frequency of 4Hz are compared to the mean steady voltage values(X_s) at (+125V). There is also a comparison of the pulsed flows to characterize the trends as the oscillations increase as well as the "threshold limit" trials. By utilizing the standard deviations of the steady flows(σ_s) and the pulsed flows(σ_p) the critical t-value can be found which corresponds to the needed t-value in order to reject the null hypothesis. The t-value is also dependent on the confidence interval $(CI = 100\% \times (1 - \alpha))$ where α is the total area under the standard distribution curve. The null hypothesis assumes that the means of the two data sets are not significantly different. If the null hypothesis is rejected, it means that the latter data set is significantly greater than the preceding data set. For example, in Table 7.21 the null hypothesis was rejected since the mean values for the AC (+350/-100V, 4Hz) data set was significantly larger than that of the AC (+350/125-V, 4Hz) data set. It should also be noted that there was a sample size of 10 for each data set.

		Separation per Distance	Separation per Distance/Residence Time
X_s	=	0.067887	0.002641
X_p	=	0.072888	0.004574
σ_s	=	0.008228	0.000252
σ_p	=	0.004123	0.000348
α	=	0.1	0.005
t-value for α	=	1.35017	2.92078
t-value for data	=	1.71843	14.23289
Reject null hypothesis	=	Yes	Yes

Table D. 1 Statistical analysis of 10mer/50mer at DC +125V vs AC +300/-50V, 4Hz.

		Separation per Distance	Separation per Distance/Residence Time
X_s	=	0.067887	0.002641
X_p	=	0.080258	0.004769
σ_s	=	0.008228	0.000252
σ_p	=	0.006633	0.000441
α	=	0.005	0.005
t-value for α	=	2.89823	2.97684
t-value for data	=	3.70151	13.23861
Reject null hypothesis	=	Yes	Yes

Table D. 2 Statistical analysis of 10mer/50mer at DC +125V vs AC +325/-75V, 4Hz.

		Separation per Distance	Separation per Distance/Residence Time
X_s	=	0.067887	0.002641
X_p	=	0.088203	0.005427
σ_s	=	0.008228	0.000252
σ_p	=	0.010691	0.000530
α	=	0.005	0.005
t-value for α	=	2.92078	3.05454
t-value for data	=	4.76214	15.00066
Reject null hypothesis	=	Yes	Yes

Table D. 3 Statistical analysis of 10mer/50mer at DC +125V vs AC +350/-100V, 4Hz.

		Separation per Distance	Separation per Distance/Residence Time
X_s	=	0.067887	0.002641
X_p	=	0.076191	0.004451
σ_s	=	0.008228	0.000252
σ_p	=	0.004570	0.000281
α	=	0.05	0.005
t-value for α	=	1.76131	2.89823
t-value for data	=	2.79009	15.17548
Reject null hypothesis	=	Yes	Yes

Table D. 4 Statistical analysis of 10mer/50mer at DC +125V vs AC +375/-125V, 4Hz.

		Separation per Distance	Separation per Distance/Residence Time
X_s	=	0.037579	0.002052
X_p	=	0.048534	0.002775
σ_s	=	0.007952	0.000415
σ_p	=	0.007178	0.000536
α	=	0.005	0.005
t-value for α	=	2.89823	2.92078
t-value for data	=	3.23387	3.36897
Reject null hypothesis	=	Yes	Yes

Table D. 5 Statistical analysis of 10mer/100mer at DC +125V vs AC +300/-50V, 4Hz.

		Separation per Distance	Separation per Distance/Residence Time
X_s	=	0.037579	0.002052
X_p	=	0.057083	0.003041
σ_s	=	0.007952	0.000415
σ_p	=	0.005185	0.000472
α	=	0.005	0.005
t-value for α	=	2.94671	2.89823
t-value for data	=	6.49686	4.97884
Reject null hypothesis	=	Yes	Yes

Table D. 6 Statistical analysis of 10mer/100mer at DC +125V vs AC +325/-75V, 4Hz.

		Separation per Distance	Separation per Distance/Residence Time
X_s	=	0.037579	0.002052
X_p	=	0.064003	0.003612
σ_s	=	0.007952	0.000415
σ_p	=	0.006473	0.000227
α	=	0.005	0.005
t-value for α	=	2.89823	3.01228
t-value for data	=	8.14939	10.42479
Reject null hypothesis	=	Yes	Yes

Table D. 7 Statistical analysis of 10mer/100mer at DC +125V vs AC +350/-100V, 4Hz.

		Separation per Distance	Separation per Distance/Residence Time
X_s	=	0.037579	0.002052
X_p	=	0.054837	0.002655
σ_s	=	0.007952	0.000415
σ_p	=	0.007378	0.000328
α	=	0.005	0.005
t-value for α	=	2.89823	2.89823
t-value for data	=	5.03070	3.59917
Reject null hypothesis	=	Yes	Yes

Table D. 8 Statistical analysis of 10mer/100mer at DC +125V vs AC +375/-125V, 4Hz.

		Separation per Distance	Separation per Distance/Residence Time
$X_{(+350/-125V,\ 4Hz)}$	=	0.072306	0.004451
$X_{(+350/-100V,\ 4Hz)}$	=	0.088203	0.005427
$\sigma_{(+350/-125V,\ 4Hz)}$	=	0.007378	0.000328
$\sigma_{(+350/-100V,\ 4Hz)}$	=	0.010691	0.000530
α	=	0.005	0.005
t-value for α	=	3.16927	3.01228
t-value for data	=	4.49710	5.14541
Reject null hypothesis	=	Yes	Yes

Table D. 9 Statistical analysis of 10mer/50mer at AC +350/-125V, 4Hz vs AC +375/-125V, 4Hz.

		Separation per Distance	Separation per Distance/Residence Time
$X_{(+375/-100V,\ 4Hz)}$	=	0.077115	0.004508
$X_{(+350/-100V,\ 4Hz)}$	=	0.088203	0.005427
$\sigma_{(+375/-100V,\ 4Hz)}$	=	0.007464	0.000355
$\sigma_{(+350/-100V,\ 4Hz)}$	=	0.010691	0.000530
α	=	0.05	0.005
t-value for α	=	1.74588	2.94671
t-value for data	=	2.68913	4.55268
Reject null hypothesis	=	Yes	Yes

Table D. 10 Statistical analysis of 10mer/50mer at AC +350/-125V, 4Hz vs AC +375/-100V, 4Hz.

		Separation per Distance	Separation per Distance/Residence Time
$X_{(+375/-125V, 4Hz)}$	=	0.076191	0.004451
$X_{(+375/-100V, 4Hz)}$	=	0.077115	0.004508
$\sigma_{(+375/-125V, 4Hz)}$	=	0.004570	0.000281
$\sigma_{(+375/-100V, 4Hz)}$	=	0.007464	0.000355
α	=	0.1	0.1
t-value for α	=	1.34503	1.33338
t-value for data	=	-0.33368	-0.39240
Reject null hypothesis	=	No	No

Table D. 11 Statistical analysis of 10mer/50mer at AC +375/-125V, 4Hz vs AC +375/-100V, 4Hz.

		Separation per Distance	Separation per Distance/Residence Time
$X_{(+300/-50V, 4Hz)}$	=	0.072888	0.004574
$X_{(+325/-75V, 4Hz)}$	=	0.080258	0.004769
$\sigma_{(+300/-50V, 4Hz)}$	=	0.004123	0.000348
$\sigma_{(+325/-75V, 4Hz)}$	=	0.006633	0.000441
α	=	0.1	0.1
t-value for α	=	1.34061	1.33338
t-value for data	=	2.98413	1.09564
Reject null hypothesis	=	Yes	No

Table D. 12 Statistical analysis of 10mer/50mer at AC +300/-50V, 4Hz vs AC +325/-75V, 4Hz.

		Separation per Distance	Separation per Distance/Residence Time
$X_{(+325/-75V, 4Hz)}$	=	0.080258	0.004769
$X_{(+350/-100V, 4Hz)}$	=	0.088203	0.005427
$\sigma_{(+325/-75V, 4Hz)}$	=	0.006633	0.000441
$\sigma_{(+350/-100V, 4Hz)}$	=	0.010691	0.000530
α	=	0.05	0.05
t-value for α	=	1.75305	1.73961
t-value for data	=	1.99673	3.01300
Reject null hypothesis	=	Yes	Yes

Table D. 13 Statistical analysis of 10mer/50mer at AC +325/-75V, 4Hz vs AC +350/-100V, 4Hz.

		Separation per Distance	Separation per Distance/Residence Time
$X_{(+350/-100V,\ 4Hz)}$	=	0.088203	0.005427
$X_{(+375/-125V,\ 4Hz)}$	=	0.076191	0.004451
$\sigma_{(+350/-100V,\ 4Hz)}$	=	0.010691	0.000530
$\sigma_{(+375/-125V,\ 4Hz)}$	=	0.004570	0.000281
α	=	0.1	0.1
t-value for α	=	1.35622	1.35017
t-value for data	=	-3.26696	-5.13875
Reject null hypothesis	=	No	No

Table D. 14 Statistical analysis of 10mer/50mer at AC +350/-100V, 4Hz vs AC +375/-125V, 4Hz.

		Separation per Distance	Separation per Distance/Residence Time
$X_{(+300/-50V,\ 4Hz)}$	=	0.048534	0.002775
$X_{(+325/-75V,\ 4Hz)}$	=	0.057083	0.003041
$\sigma_{(+300/-50V,\ 4Hz)}$	=	0.007178	0.000536
$\sigma_{(+325/-75V,\ 4Hz)}$	=	0.005185	0.000472
α	=	0.1	0.1
t-value for α	=	1.33676	1.33338
t-value for data	=	3.05296	1.18034
Reject null hypothesis	=	Yes	No

Table D. 15 Statistical analysis of 10mer/100mer at AC +300/-50V, 4Hz vs AC +325/-75V, 4Hz.

		Separation per Distance	Separation per Distance/Residence Time
$X_{(+325/-75V,\ 4Hz)}$	=	0.057083	0.003041
$X_{(+350/-100V,\ 4Hz)}$	=	0.064003	0.003612
$\sigma_{(+325/-75V,\ 4Hz)}$	=	0.005185	0.000472
$\sigma_{(+350/-100V,\ 4Hz)}$	=	0.006473	0.000227
α	=	0.05	0.05
t-value for α	=	1.73961	1.78229
t-value for data	=	2.63875	3.44646
Reject null hypothesis	=	Yes	Yes

Table D. 16 Statistical analysis of 10mer/100mer at AC +325/-75V, 4Hz vs AC +350/-100V, 4Hz.

		Separation per Distance	Separation per Distance/Residence Time
$X_{(+350/-100V,\ 4Hz)}$	=	0.064003	0.003612
$X_{(+375/-125V,\ 4Hz)}$	=	0.054837	0.002655
$\sigma_{(+350/-100V,\ 4Hz)}$	=	0.006473	0.000227
$\sigma_{(+375/-125V,\ 4Hz)}$	=	0.007378	0.000328
α	=	0.1	0.1
t-value for α	=	1.33338	1.33676
t-value for data	=	-2.95322	-7.58474
Reject null hypothesis	=	No	No

Table D. 17 Statistical analysis of 10mer/100mer at AC +350/-100V, 4Hz vs AC +375/-125V, 4Hz.

Appendix E: Experimental Procedure

1) Preparing the Silicon Wafer Templates for Microchannels
    a) Cleaning the wafer
        i) Put the wafer in a glass tray in a hood.
        ii) Pour 30mL of concentrated sulfuric acid over it carefully.
        iii) Add 10mL anhydrous hydrogen peroxide. Do this slowly and watch for the amount of fumes being produced as this step runs the risk of a violent reaction.
        iv) Tilt the tray back and forth to mix the solution and ensure that the wafer is completely immersed in the solution.
        v) Wait a minimum of 1 hour.
        vi) Remove tray from hood and place it in a sink.
        vii) Dilute the solution in the tray with copious amounts of Di water, allowing the diluted solution to wash down the drain until it has been diluted enough that the wafer can be safely picked up with gloved hands.
        viii) Rinse the wafer surface thoroughly with a stream of DI water.
        ix) Use an air hose with air flowing at a moderate speed to dry the wafer; do this be driving the water off of the wafer surface as much as possible because if water is left on the surface and evaporates, it has the potential to leave behind residue.
        x) Wafer should now be clean and the surface should be “mirror-like” with no obvious residue or impurities on its surface.
    b) Using Photolithography to Etch Pattern on to Wafer (MUST BE DONE UNDER DARKROOM CONDITIONS) (*Notes: Steps v-viii are very time dependent and temperature dependent and should be done with care and attention to detail.*)
        i) Take the clean wafer and set it, shiny side upward, on the chock of the spin coater. The spin coater should be set up in a darkroom with light sources that will not interact with the photoresist that will be used. Turn the normal lights off so the photoresist can be handled without complications and preheat the oven to 70^{o}C.

ii) Plug in the vacuum pump and turn on the air flow to start the spin coater and initialize it.

iii) Pour ~3mL of liquid photoresist on to the center of the wafer.

iv) Center the wafer on the chock and put the lid over the spin coater.

v) Select “Recipe 3” on the spin coater’s control display; this will spin up to 500RPM for ~15 seconds to spread the photoresist, then up to 3000RPM for ~45 seconds to throw off any excess and bring the photoresist to the corresponding height.

vi) Place the coated wafer in the oven; set it on top of a Petri dish to prevent the wafer from sticking to the oven surface. It is very important that the oven be very close to 70^{o}C to get the right amount of evaporation. Bake the wafer for 10 minutes at 70^{o}C.

vii) Remove the wafer from the oven and let it cool for 5 minutes. Place the photomask over the wafer as centered as possible and set a glass slide over the pattern on the photomask. Then place the wafer under a UV lamp for 6 minutes.

viii) After the 6 minutes, turn off the lamp and remove the glass slides and photomask from the wafer and place the wafer back in the oven at 70^{o}C for 10 minutes.

ix) After the 10 minutes is up, remove the wafer from the oven and let it cool for 5 minutes. Put the wafer back in the spin coater for developing. Center the wafer back on the chock and coat it liberally with developer solution so long as the developer does not pool over the sides of the wafer.

x) Put the lid on the spin coater and run “Recipe 3” again to remove the developer and the dissolved photoresist from the wafer surface. There may be multicolored streaks on the wafer afterwards; this indicates that the soluble photoresist has not been completely removed from the surface. In this case, pour more developer solution on to the wafer and repeat the spinning process. It may be necessary to clean the wafer 2 to 3 times to remove all of the soluble

photoresist. When the wafer is clean, it should be a uniform, shiny, black with the pattern from the photomask etched on to the surface with clearly visible thin lines with no discontinuities.

2) Casting and Preparation of PDMS for Electroosmosis Experiment
    a) Casting PDMS Microchannels on the Wafers (*Notes: It is easier to prepare the PDMS for the experiment in part b of this section if you do it immediately after the procedure in part a but it is not crucial. Also, for steps iii and iv, it is not crucial to have the exact amounts of elastomer and curing agent so long as they are in the general vicinity of one another.*)
        i) Preheat the oven to 100^{o}C.
        ii) Place a plastic cup on the scale and tare it.
        iii) Pour 9 grams of elastomer (PDMS) into the cup.
        iv) Pour 0.9 grams of curing agent into the cup.
        v) Stir the mixture vigorously for 60-90 seconds. After this, it should have lots of small bubbles giving it a milky white color.
        vi) Set the wafer on a Petri dish and pour the mixture on tot the center of a (clean) wafer template and let it pool out over the surface.
        vii) (If necessary) pick up the wafer and tilt it back and forth in a rolling motion until the polymer coats the wafer evenly. This coating does not have to reach the very edge but should leave plenty of coated space all around the etched pattern on the wafer template.
        viii) Set the wafer back on the Petri dish and give it 10-20 minutes for the bubbles to work their way out of the polymer.
        ix) Once the microchannel itself and the area immediately around it is clear of bubbles, put the wafer (on top of the Petri dish) into the oven to bake. The PDMS should bake for at least 45 minutes (maximum 60 minutes) at 100^{o}C. If the temperature is a little low when you put it in the oven, you can just leave it in a little longer. This step is not as sensitive to changes as the developing process.

x) After an hour, take the wafer (with the PDMS layer on top) out of the oven and set it to the side to cool.

b) Preparing PDMS microchannels for the Electroosmosis Experiment (*Notes: Once you start step vii, the microchannel has a shelf life of only 30 minutes, so only one at a time, run through the preparation fairly quickly and perform the electroosmosis DNA separation experiment immediately after preparing the microchannel. Microchannels prepared up through step vi can be left that way without harming them and should be stored in a container to protect against dust. While is it important to perform steps xii-xiv carefully, it is also helpful to get them done as quickly as possible. There are only a few seconds after the PDMS comes out of the plasma cleaner when it will truly and strongly bond to the glass. Try to align it and lower it quickly, allowing the microchannel to make contact first, but then get the corners down so that they can seal or they will tend to pop up later when you put the slide in the holder.*)

i) Take the wafer with a baked (polymerized) PDMS layer on top of it. Use a razor blade to lift the edge of the PDMS away from the silicon wafer.

ii) Gently pull the PDMS upwards, away from the wafer while holding the wafer with moderate, evenly distributed pressure. (The wafer is fragile and can break in this step). Peel the PDMS off, carefully using the razor blade to work any tears or stuck spots off of the wafer without tearing through the microchannel. Set the wafer aside once the PDMS has been separated.

iii) Cut the PDMS between the channels to separate into two. Place the other aside for later use.

iv) Use the hole punch to punch out the wells at each of the channel ends.

v) Place a glass slide over the microchannel to protect it from dust or physical damage.

vi) Use a razor blade to trim away the excess PDMS on the sides of the microchannel so it will fit easily into the vacuum chamber of the plasma cleaner.

vii) Take the microchannel to the plasma cleaner. Take the plasma (vacuum) chamber out and separate the glass slide form the PDMS microchannel. Place both in the

vacuum chamber so that they are lying on the ridges in the glass. The PDMS should have the microchannel side pointing upwards and you should check that it is loosely contacting the ridges only and is not sealed to the glass of the vacuum chamber anywhere. It may be necessary to leave a little bit of PDMS hanging over the edge of the vacuum chamber to get it to stay loose. If you do not do this, it will bond covalently and will be useless.

viii) Replace the vacuum chamber (now containing the PDMS and the glass slide) in the plasma cleaner. Hold it in so that the gasket seals.

ix) Turn on the vacuum pump and close the air inflow valve to the side of the plasma cleaner. Pull gently on the vacuum chamber to make sure it is actually sealed. If it is, close the plasma cleaner.

x) Push the button “Add 30 Seconds” and wait until the chamber lights up with a purplish glow. Once that happens, wait an additional 4 seconds for the plasma to affect the PDMS, then hit stop or cancel. The time in the plasma cleaner may vary based on the power output of the device. Adjust accordingly. (If power is 50%, plasma effect should be 4-5 seconds or if power is 25%, plasma effect should be 12-13 seconds).

xi) Turn off the vacuum pump and open the valve. When you do this, make sure your hand is placed behind the vacuum chamber so it will not pop out and break. Once the seal releases (you can tell when this happens because the chamber will shift more or slide out slightly) pull the vacuum chamber out.

xii) Take the glass slide out and place it over the template.

xiii) Take the PDMS out and orient it so that the microchannel side is facing downward and the microchannel is placed over the slide as indicated by the template.

xiv) Lower the PDMS on to the glass slide. It will bond covalently when it makes contact so be careful to keep it aligned.

xv) Use a metal stirring stick to carefully work out any air bubbles. It is crucial to work any air bubbles away from the microchannel so that it can seal, and you must do

it gently so as not to collapse the microchannel. Air bubbles that are away from the microchannel and wells are not particularly important.

xvi) Trim away all excess PDMS. Then apparatus exactly fits a glass slide so the PDMS needs to be trimmed all the way to the very edge of the slide. Excess cutting also creates PDMS dust which can get on the surface and obscure the microchannel, so try to do this with as few careful strokes as you can manage.

3) Running the Electroosmotic Separation Experiment and Preparation of DNA Solution

a) Electroosmotic Separation Experiment (*Notes: Seen in Chapter 2, a schematic of the microchannel is shown with the nomenclature from this section labeled. The DNA sample solution is made by taking 100µM stock solution of each DNA and combining it in the mixture designated in Chapter 3. Turn on the power supply box, then open "shortcut to hvwaveform" on the computer; select the voltage/pattern needed and click "set". The power supply box MUST be on before opening "hvwaveform" otherwise error messages will prevent the program from working and the USB connection will need to be unplugged and plugged back in order to reset the program.*)

i) Open the Avasoft software and setup the "dark" and "reference" spectrums.

ii) In the Avasoft program, open two "Time Series" applications. Under the first time series, select the function "Peak Intensity" and under the second time series, select the function "Peak Tracking".

iii) Prepare a microchannel as described in Section 2-b; once you do that you will have 30 minutes to complete the experiment.

iv) Mark the microchannel (if not previously marked) at 2.5cm from the intersection with a pen or marker.

v) Place the microchannel in the slide depression on the apparatus. (Do this so that the intersection is on the left side of the glass slide).

vi) Examine the length of the microchannel for flaws, collapses, or blockage using the camera display on the computer screen. Once you are sure the microchannel is in order, continue.

vii) Turn on the LED lamp and center the camera display on the intersection.

viii) Pipette 2.5µL of 1x TE buffer into the bottom well. Watch the intersection for the buffer to wet the entire microchannel.

ix) Add 2.5µL of the 1x TE buffer to the top well also. This will create a slight pressure head from the top well which is essential for the remaining steps in the experiment.

x) Once the buffer has spread throughout the entire microchannel, add 2.7µL of the DNA sample solution to the sample well. Turn on either laser to illuminate the intersection. When the sample reaches the intersection, it will appear as a bright blue, yellow, or red color on the camera screen.

xi) Wait for the DNA plug to form in the main channel. Intermittently turn the laser on and off to check on the progress of the DNA. It is best not to leave the laser on because the light can photo-bleach the dyes attached to the DNA over prolonged periods and lessen the intensity of the peaks.

xii) Once the plug is sufficiently formed, add an additional 1.6µL of 1x TE buffer to the top well. This will flush the excess sample back towards the sample well and pushes the plug slightly down the channel.

xiii) Once the pressure head has equilibrated (~10 seconds) apply the electrodes to the top and bottom wells to start the electroosmotic process. Record the starting time.

xiv) Observe the plug briefly to make sure it is moving and that it has started separating. If it separating, you should see the leading edge of the plug produce a solitary color rather than two.

xv) Turn on both lasers if not done so already.

xvi) Move the viewing field to the 2.5cm mark and start the Avasoft software on the computer. Record the starting time and observe the DNA separation at the point.